AD-A241 988

DTIC
ELECTE
OCT 28 1991
S D
D

THERMO-MECHANICAL FATIGUE OF A FIBER REINFORCED TITANIUM ALUMINIDE COMPOSITE

Thesis

Mark A. Bates
AFIT/GAE/ENY/91S-1

This document has been approved for public release and sale; its distribution is unlimited.

91-14126

DEPARTMENT OF THE AIR FORCE
AIR UNIVERSITY
AIR FORCE INSTITUTE OF TECHNOLOGY

Wright-Patterson Air Force Base, Ohio

91 10 25 038

1

DTIC
ELECTE
OCT 28 1991
S D
D

THERMO-MECHANICAL FATIGUE OF A FIBER REINFORCED TITANIUM ALUMINIDE COMPOSITE

Thesis

Mark A. Bates
AFIT/GAE/ENY/91S-1

This document has been approved for public release and sale; its distribution is unlimited.

Accesion For
NTIS CRA&I
DTIC TAB
Unannounced
Justification
By
Distribution /
Availability Codes
Dist
A-1

REPORT DOCUMENTATION PAGE

Form Approved
OMB No. [illegible]

1. AGENCY USE ONLY (Leave blank)	2. REPORT DATE	3. REPORT TYPE AND DATES COVERED
	March 1991	Thesis, Final

4. TITLE AND SUBTITLE

Thermo-Mechanical Fatigue of a Fiber Reinforced Titanium Aluminide Composite

5. FUNDING NUMBERS

6. AUTHOR(S)

Mark A. Bates

7. PERFORMING ORGANIZATION NAME(S) AND ADDRESS(ES)

School of Engineering
Air Force Institute of Technology
Wright-Patterson AFB OH 45433

8. PERFORMING ORGANIZATION REPORT NUMBER

AFIT/GAE/ENY/91S-1

9. SPONSORING/MONITORING AGENCY NAME(S) AND ADDRESS(ES)

Dr Ted Nicholas
WL/MLLN
Wright-Patterson AFB OH 45433

10. SPONSORING/MONITORING AGENCY REPORT NUMBER

11. SUPPLEMENTARY NOTES

12a. DISTRIBUTION/AVAILABILITY STATEMENT

Approved for public release; distribution unlimited

12b. DISTRIBUTION CODE

13. ABSTRACT (Maximum 200 words)

The thermo-mechanical fatigue behavior of a specific unidirectional fiber reinforced titanium aluminide composite was investigated. Three test specimens were subjected to in-phase thermo-mechanical cycling and four to out-of-phase thermo-mechanical cycling. The applied maximum mechanical stresses ranged from 500-800 MPa. The stress ratio of 0.1 was used for all tests. The temperature range was from 150-650°C and the resulting fatigue lives were in the 58-1487 cycles range. The test results were analyzed using a simple micromechanics analysis and compared. The fracture surfaces from both test conditions were investigated using the scanning electron microscope. Additionally the test specimens were sectioned and the fatigue damage was studied in regions away from the fracture surface. The stresses that occurred throughout the test cycles were analyzed and related to the observed fatigue damage. The results were compared to the existing failure model for composite materials. Additionally, the results from the in-phase and out-of-phase tests were compared to isothermal and constant load test results.

14. SUBJECT TERMS

Thermo-Mechanical Fatigue, Metal Matrix Composite, Fracture Characteristics, Stress Analysis

15. NUMBER OF PAGES

123

16. PRICE CODE

17. SECURITY CLASSIFICATION OF REPORT	18. SECURITY CLASSIFICATION OF THIS PAGE	19. SECURITY CLASSIFICATION OF ABSTRACT	20. LIMITATION OF ABSTRACT
Unclassified	Unclassified	Unclassified	UL

NSN 7540-01-280-5500 Standard Form 298 (Rev. 2-89)

AFIT/GAE/ENY/91S-1

THERMO-MECHANICAL FATIGUE OF A FIBER REINFORCED TITANIUM ALUMINIDE COMPOSITE

THESIS

Presented to the Faculty of the School of Engineering

of the Air Force Institute of Technology

Air University

in Partial Fulfillment of the

Requirements for the Degree of

Master of Science in Aeronautical Engineering

Mark A. Bates, B.S.

March 1991

Approved for public release; distribution unlimited

Preface

I would like to thank my advisor Dr. S. Mall of the Air Force Institute of Technology and Dr. T. Nicholas of the Air Force Wright Research and Development Center at Wright-Patterson AFB, Ohio, for their timely guidance essential to the completion of this project. Deep gratitude is also expressed to Steve Russ for his technical assistance with the test equipment and the scanning electron microscope and to Bob Lewis for his assistance with the metallography.

Mark A. Bates

List of Figures

Figure		Page
1	Example In-Phase Thermo-mechanical Load Profile	9
2	Example Out-of-Phase Thermo-mechanical Load Profile	10
3	Test Equipment	14
4	Mounted Test Specimen	15
5	Four Zone Temperature Control	17
6	Test Specimen	18
7A	In-Phase and Out-of-Phase Thermo-mechanical Fatigue Life Results (linear)	26
7B	In-Phase and Out-of-Phase Thermo-mechanical Fatigue Life Results (semi-log)	27
8	Typical In-Phase Fracture Surface	31
9	Typical Out-of-Phase Fracture Surface	33
10	Typical Longitudinal Cracking	36
11	Typical Transverse Cracking	37
12	Typical Broken Fibers	38
13	Typical Out-of-Phase Surface Damage	39
14	Typical Fiber Breakage and Pullout Along Exposed Edges	42
15	Typical Broken Fibers Along Exposed Edges	43
16	Typical Surface After In-Phase Test	44
17	Typical Out-of-Phase Test Specimen Surface Cracking	45
18	Typical Stress-Strain Response	47
19	Typical Change in Maximum and Minimum Strain During In-Phase Thermo-mechanical	

Fatigue Testing 49

20 Typical Change in Maximum and Minimum Strain During Out-of-Phase Thermo-mechanical Fatigue Testing 51

21 Out-of-Phase Test Showing Change in Secant Modulus 53

22 Subregions Used to Model the Variation in Constituent Properties 58

23 Residual Stresses Due to Cool-Down from Processing Temperature 60

24 Stresses Throughout One In-Phase Cycle 62

25 Stresses Throughout One Out-of-Phase Cycle 63

26 Comparison of Sigma 11 (in matrix) Between In-Phase and Out-of-Phase Cycles 66

27 Comparison of Sigma 11 (in fiber) Between In-Phase and Out-of-Phase Cycles 67

28A Sigma 11 Maximum (in matrix) Versus Number of Cycles to Failure from In-Phase and Out-of-Phase Test Conditions (linear).....68

28B Sigma 11 Maximum (in matrix) Versus Number of Cycles to Failure from In-Phase and Out-of-Phase Test Conditions (semi-log).....69

29A Change in Sigma 11 (in matrix) Versus Number of Cycles to Failure from In-Phase and Out-of-Phase Test Conditions (linear).....70

29B Change in Sigma 11 (in matrix) Versus Number of Cycles to Failure from In-Phase and Out-of-Phase Test Conditions (semi-log).....71

30A Sigma 11 Maximum (in fiber) Versus Number of Cycles to Failure from In-Phase and Out-of-Phase Test Conditions (linear).....73

30B Sigma 11 Maximum (in fiber) Versus Number of Cycles to Failure from In-Phase and Out-of-Phase Test Conditions (semi-log).....74

31A Change in Sigma 11 (in fiber) Versus Number of Cycles to Failure from In-Phase and Out-of-Phase Test Conditions (linear).....75

31B Change in Sigma 11 (in fiber) Versus Number of Cycles to Failure from In-Phase and Out-of-Phase Test Conditions (semi-log).....76

32 Empirical Fatigue Life Diagram 78

33A Possible Fiber Dominated Region for In-Phase and Out-of-Phase Test Conditions (linear).....80

33B Possible Fiber Dominated Region for In-Phase and Out-of-Phase (semi-log).....81

34A Possible Matrix Dominated Region for In-Phase and Out-of-Phase Test Conditions (linear).....82

34B Possible Matrix Dominated Region for In-Phase and Out-of-Phase Test Conditions (semi-log).....83

35 Summary of Various Test Conditions.....85

36A Thermo-mechanical Fatigue Life Results from Various Test Conditions (linear).....87

36B Thermo-mechanical Fatigue Life Results from Various Test Conditions (semi-log).....88

37A Sigma 11 Maximum (in matrix) Versus Number of Cycles to Failure from Various Test Conditions (linear).....90

37B Sigma 11 Maximum (in matrix) Versus Number of Cycles to Failure from Various Test Conditions (semi-log).....91

38A Change in Sigma 11 (in matrix) Versus Number of Cycles to Failure from Various Test Conditions (linear).....93

38B Change in Sigma 11 (in matrix) Versus Number of Cycles to Failure from Various Test Conditions (semi-log).....94

39A Sigma 11 Maximum (in fiber) Versus Number of Cycles to Failure from Various Test Conditions (linear).....95

39B Sigma 11 Maximum (in fiber) Versus Number of Cycles to Failure from Various Test Conditions (semi-log).....96

40A Change in Sigma 11 (in fiber) Versus Number of Cycles to Failure from Various Test Conditions (linear).....97

40B Change in Sigma 11 (in fiber) Versus Number of Cycles to Failure from Various Test Conditions (semi-log).....98

41A Possible Fiber Dominated Region for Various Test Conditions (linear).....99

41B Possible Fiber Dominated Region for Various Test Conditions (semi-log).....100

42A Possible Matrix Dominated Region for Various Test Conditions (linear).....101

42B Possible Matrix Dominated Region for Various Test Conditions (semi-log).....102

List of Tables

Table		Page
I.	Material Properties of Ti-24Al-11Nb/SCS-6	8
II.	Test Matrix	12
III.	Longitudinal Static Strength Properties for SCS-6/Ti-24Al-11Nb	13
IV.	Thermo-mechanical Fatigue Life Results	28
V	Maximum Total Strain Response During Testing	55
VI.	Thermo-mechanical Fatigue Life Results from Various Test Conditions	89

Abstract

The thermo-mechanical fatigue behavior of a specific unidirectional fiber reinforced titanium aluminide composite was investigated. Three test specimens were subjected to in-phase thermo-mechanical cycling and four to out-of-phase thermo-mechanical cycling. The applied maximum mechanical stresses ranged from 500-800 MPa. The stress ratio of 0.1 was used for all tests. The temperature range was from 150 - 650 °C and the resulting fatigue lives were in the 58 - 1487 cycles range. The out-of-phase test specimens failed sooner compared to their respective in-phase counterparts. In order to find out why, the test results were analyzed using a simple micromechanics analysis and compared. The fracture surfaces from both test conditions were investigated using the scanning electron microscope. Additionally, the test specimens were sectioned and the fatigue damage was studied in regions away from the fracture surface using a high power optical microscope and metallography. The stresses that occurred throughout the test cycles were analyzed and related to the observed fatigue damage. The results were compared to the existing failure model for composite materials. Additionally, the results from the in-phase and out-of-phase tests were compared to isothermal and constant load test results.

Table of Contents

	Page
Preface	ii
List of Figures	iii
List of Tables	vii
Abstract	viii
I. Introduction	1
Background	1
Scope	5
Sequence of Presentation	6
II. Equipment and Test Procedures	7
Test Material	7
Specimen Preparation	7
Test Conditions	8
Test Equipment	11
Test Set-up Procedures	16
III. Results and Discussion	25
Fatigue Life Curves	25
Scanning Electron Microscope Fractography	29
Optical Micrography	34
Surface Damage	41
Stress-Strain Response	46
Damage Summary	56
Stress Analysis	57
Residual Stresses	59
Thermo-mechanical Stresses	61
Thermo-mechanical Stresses Related to Fatigue Life	65
Comparison to Existing Theory	72
Comparison to Other Thermo-mechanical Fatigue Data	84
IV. Conclusions and Recommendations	103
Conclusions	103
Recommendations	106
Appendix A: Computer Program	107

Bibliography 110

Vita 111

THERMO-MECHANICAL FATIGUE OF A FIBER REINFORCED TITANIUM ALUMINIDE COMPOSITE

I. Introduction

Background

Advanced military aerospace systems of the future will require aircraft and engine components constructed from new materials. These materials must be capable of operating at higher temperatures with increased strength and lower weight. For example, the Integrated High Performance Turbine Engine Technologies initiative was formed by the United States Air Force to identify advanced fighter engine concepts for the future. One of the basic goals of the initiative is to develop and demonstrate engine concepts that have a thrust-to-weight ratio at twice the current levels (5:4). In order to meet this goal the development of new high temperature, high strength, and low density materials is required.

Metal matrix composites offer one potential solution to this demand for greater performance. In particular, titanium aluminide metal matrix composites reinforced with silicon carbide fibers provide the improved strength, density, and high temperature capability required. However,

before titanium aluminides can be safely implemented, it is essential to understand their fatigue and fracture characteristics.

Metal matrix composites for high temperature applications are new and investigations into their fatigue and fracture characteristics are just beginning. In fact, a review of the available literature revealed that only few studies have been conducted, all of which were finished within the last couple of years.

Bartolotta, Castelli, and Ellis studied the effects of thermo-mechanical cycling on SCS-6/Ti-15V-3Cr-3Al-3Sn (1:1-18) and found that specimens subjected to out-of-phase test conditions failed sooner than their respective in-phase counterparts. During in-phase test conditions the sinusoidal thermal and mechanical loads were employed zero degrees apart while during out-of phase conditions they were shifted by 180 degrees. They found that the only fatigue damage in the in-phase test specimens was in the form of broken fibers. This was attributed to the higher longitudinal stress in the fiber that occurs during in-phase test conditions. The fatigue damage in the out-of-phase test specimens was limited to surface cracks in the matrix perpendicular to the fibers. These cracks grew inward as the test progressed. No broken fibers were found. This was attributed to the higher longitudinal stress that occurs in the matrix during out-of-phase test conditions.

Gabb, Gayda, and MacKay at NASA Lewis also investigated the isothermal and nonisothermal behavior of SIC/Ti-15V-3Cr-3Al-3Sn (4:1-24). During isothermal testing the temperature was held constant while a complex mechanical load was varied. In nonisothermal testing both a complex temperature and mechanical load were varied. They found that the nonisothermal test conditions reduced the fatigue life when compared to isothermal conditions. Isothermal fatigue cracks initiated at fiber-matrix interfaces and at foil lamination lines throughout the specimen crossection. This is in contrast to the nonisothermal fatigue cracks which initiated at the test specimen surface or at near surface fiber-matrix interfaces.

Additionally, Johnson, Lubowinski, and Highsmith tested SCS-6/Ti-15V-3Cr-3Al-3Sn, in five different lay-ups at room temperature, in order to determine their static and fatigue strengths as well as their basic mechanical properties (6:1-14). Typical fatigue damage was fiber/matrix separation at the fiber/matrix interface.

Majumdar, and Newaz at Battelle Memorial Institute also investigated the isothermal and in-phase thermo-mechanical fatigue properties of SCS-6/Ti-15V-3Cr-3Al-3Sn (7:1-21). On a stress basis the thermo-mechanical test specimens had a significantly shorter life than the isothermal test specimens. In both the isothermal and thermo-mechanical test specimens most of the fatigue damage

was in the form of cracks in the matrix that were perpendicular to the fiber originating at the fiber/matrix interface. They suggested that the local strain in this region may control the fatigue life. Negligible inter-ply delamination was observed in the isothermal test specimens. However, specimens that were thermo-mechanically cycled showed significant delamination cracking between plies.

Gambone at Allison Gas Turbine Division of General Motors Corporation (5:52-68) has done the only investigation into the fracture and fatigue characteristics of SCS-6/Ti-24Al-11Nb to date. This material is a candidate for use in rotating engine compressor structures. Gambone found that test specimens subjected to out-of-phase thermo-mechanical test conditions failed sooner than their respective in-phase counterparts. Additionally, he found that fatigue damage initiated as surface cracking and progressed as these cracks grew larger in from the surface.

Due to the limited amount of information currently available and because of the importance of metal matrix composites to advanced Air Force weapon systems of the future, the Air Force Wright Research and Development Center has begun its own investigation into the fatigue characteristics of metal matrix composites. The existing studies at the material laboratories at the Wright Research and Development Center have already looked into the isothermal and constant load thermo-mechanical fatigue

behavior of SCS-6/Ti-24Al-11Nb. The purpose of this investigation was to investigate both the in-phase and out-of-phase thermo-mechanical fatigue behavior of the same material.

Scope

The test material chosen was eight ply, unidirectional, SCS-6/Ti-24Al-11Nb. In order to evaluate the effects of thermo-mechanical cycling, seven rectangular test specimens were tested in a specially designed test apparatus. The investigation was limited to seven test specimens due to the availability of the material.

Three specimens were tested with the thermo-mechanical cycling in-phase and four specimens were tested with the thermo-mechanical cycles out-of-phase. All cycles were six minutes long with a temperature range of 150 - 650°C. Both the thermal and mechanical load profiles were triangular. An in-phase test applied the maximum mechanical load at the maximum temperature and an out-of-phase test applied the maximum mechanical load at the minimum temperature. A stress ratio of 0.1 was used for all tests. The fracture surfaces from both test conditions were studied using the scanning electron microscope. Additionally, the test specimens were sectioned and the fatigue damage was studied in regions away from the fracture surface using a high power optical microscope and metallography. A micromechanics

analysis was conducted for all tested specimens to determine the stresses in the fibers, matrix, and fiber matrix interfaces and these stresses were related to the observed fatigue damage mechanism. The results from the in-phase and out-of-phase thermo-mechanical fatigue tests were also compared to the results already in the data base from the isothermal and constant load tests. Additionally, the results from all four tests were compared to existing failure theory.

Sequence of Presentation

The test equipment and procedures are described in Chapter II. In Chapter III the test results are presented and discussed. Conclusions and recommendations are made in Chapter IV.

II. Equipment and Test Procedures

In order to evaluate the effects of thermo-mechanical cycling, rectangular tensile specimens were subjected to thermo-mechanical cycling in a specially designed test apparatus. The purpose of this chapter is to discuss the following: the material used, specimen preparation, test conditions, test equipment, and test procedures.

Test Material

The material used for this investigation was SCS-6/Ti-24Al-11Nb. The composite was made by hot pressing unidirectional tapes of silicon carbide fibers designated as SCS-6 between foils of Ti-24Al-11Nb. Panels having eight plies of zero degree fibers were supplied by Allison Gas Turbine Division of General Motors Corporation. The individual plies were approximately 0.25625 mm thick with a fiber volume fraction of 0.35. The individual fibers were 0.14224 mm in diameter. The fiber and matrix material properties used for micromechanics analysis are given in Table 1. The properties listed are functions of temperature and the values given correspond to the average temperature that occurred during the thermal test cycle (400 °C).

Specimen Preparation

All test specimens were nominally 102.00 mm long x 6.36 mm wide x 2.05 mm thick. The specimen edges were

Table 1 Material Properties of Ti-24Al-11Nb/SCS-6

	Matrix	Fiber
Young's Modulus	80 GPa	414 GPa
CTE	1.3×10^{-5} / °C	4.86×10^{-6} / °C
Poisson's Ratio	0.3	0.3

polished by wet grinding with progressively finer grades of silicon carbide paper. The polishing removed any damage caused by machining from which unwanted cracks might initiate during testing. A smooth surface was also provided by polishing on which surface cracking might be replicated using replication tape.

Test Conditions

To evaluate the effects of thermo-mechanical cycling, seven rectangular tensile specimens were tested. Three specimens were tested with the thermo-mechanical cycling in-phase and four specimens were tested with the thermo-mechanical cycles 180 degrees out-of-phase. All cycles were six minutes long with a temperature range of 150 - 650 °C. Both the thermal and mechanical load profiles were triangular as shown in Figures 1 and 2. As shown, an in-phase test applied the maximum mechanical load at the maximum temperature and an out-of-phase test applied the maximum mechanical load at the minimum temperature. A stress ratio of 0.1 was used for all tests. The stress

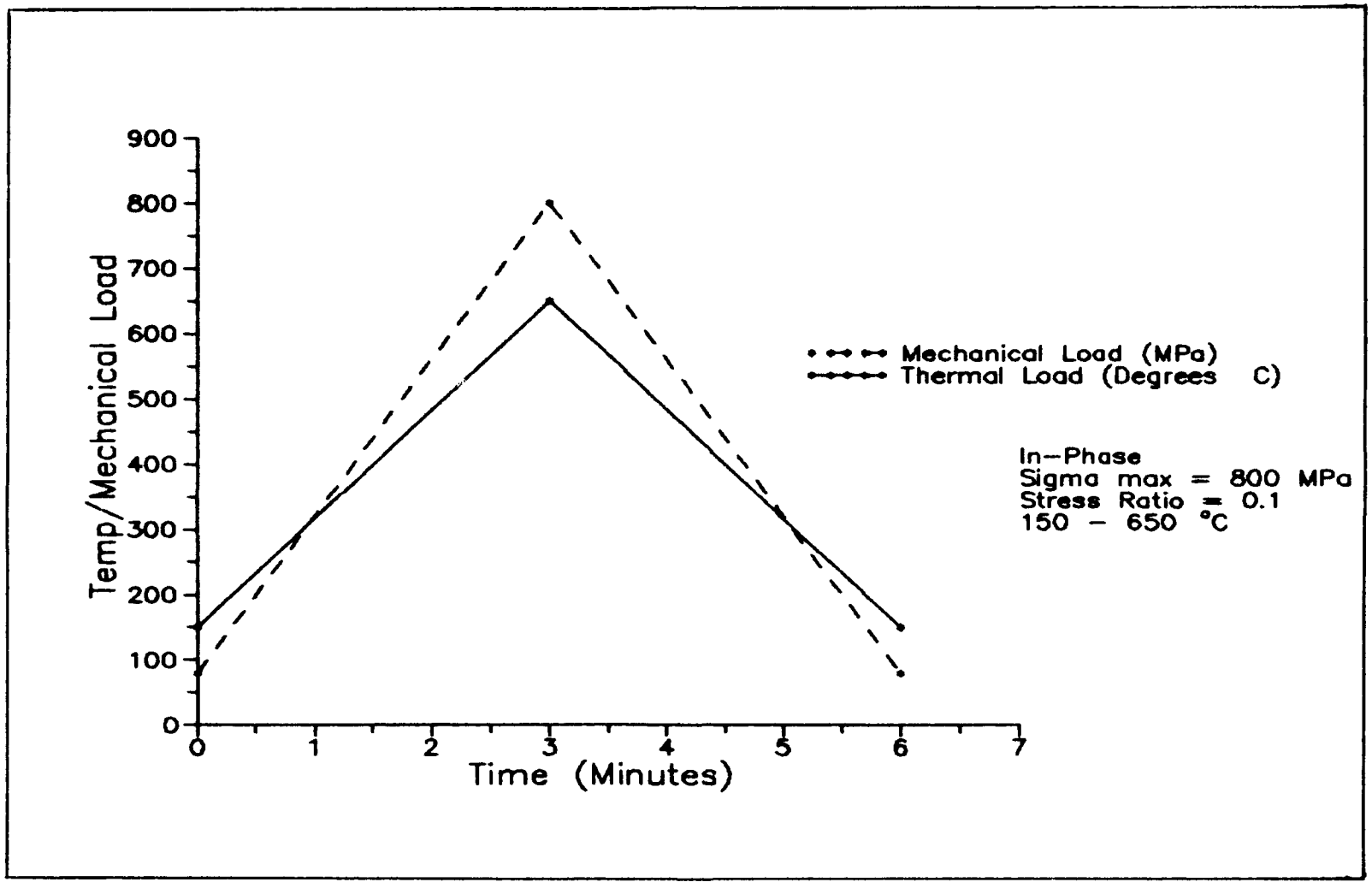

Figure 1 Example In-Phase Thermo-mechanical Load Profile

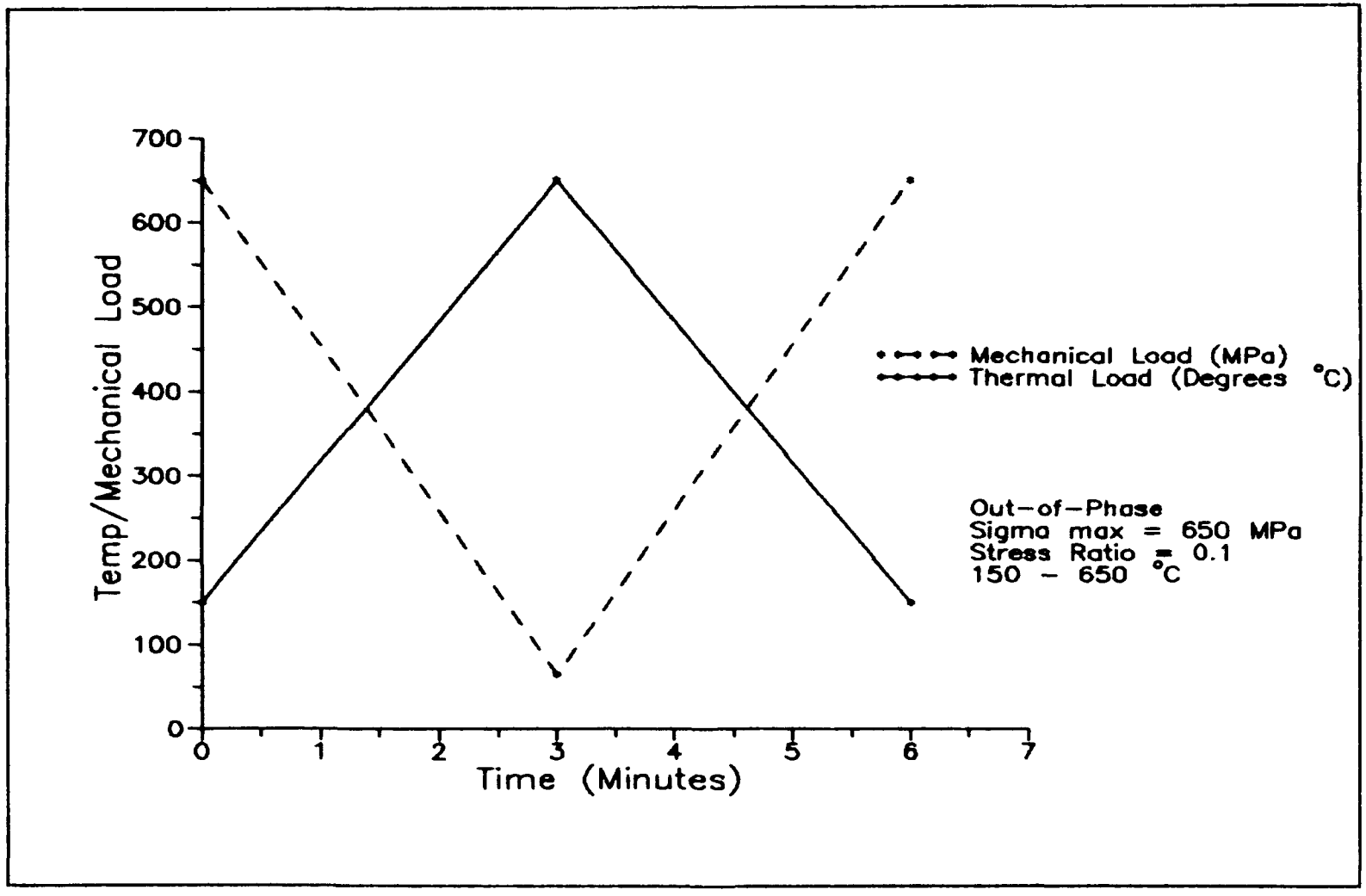

Figure 2 Example Out-of-Phase Thermo-mechanical Load Profile

ratio is the minimum mechanical stress divided by the maximum mechanical stress. Table II shows the temperature and mechanical stress range utilized for each test. In Table III the longitudinal static strength at various temperatures found by Gambone at Allison (5:10) is given.

Test Equipment

The thermo-mechanical fatigue experiments were conducted using a Schenck type machine that was specially modified to do the task by the Wright Research and Development Center and the University of Dayton Research Institute. Using a waveform generator and the Schenck, an arbitrary load with respect to time can be applied to a test specimen. The load can be either thermal, mechanical, or some combination of both. Additionally, the thermal and mechanical loads can be either constant, in-phase, or out-of-phase. A picture of the Schenck is shown in Figure 3.

To apply the mechanical load using the Schenck, the test specimen was held in tension between two hydraulically controlled friction grips. A test specimen mounted and ready for testing is shown in Figure 4. The mechanical load was applied by pulling on one of the grips using a pneumatic piston and cylinder arrangement with an actuator. The piston and cylinder arrangement was connected to the friction grips through a large spring. The mechanical stress level was controlled by a computer system and

Table II. Test Matrix

Test Matrix			
Specimen Number	Temperature (Degrees °C)	Maximum Stress (MPa)	Stress Ratio
90-052	150 - 650	800 (in-phase)	0.1
90-054	150 - 650	750 (in-phase)	0.1
90-053	150 - 650	700 (in-phase)	0.1
90-058	150 - 650	650 (out-of-phase)	0.1
90-055	150 - 650	600 (out-of-phase)	0.1
90-056	150 - 650	550 (out-of-phase)	0.1
90-057	150 - 650	500 (out-of-phase)	0.1

Table III. Longitudinal Static Strength Properties for SCS-6/Ti-24Al-11Nb

Test Temperature (°C)	Ultimate Tensile Strength (MPa)	Percent Total Strain
26	1442	1.07
26	1494	1.09
26	1495	1.085
316	1299	0.98
316	1330	0.95
538	1152	0.86
538	1185	0.868
649	1136	0.84
649	1201	0.895
649	1165	0.85
760	1055	0.805
760	1079	0.79

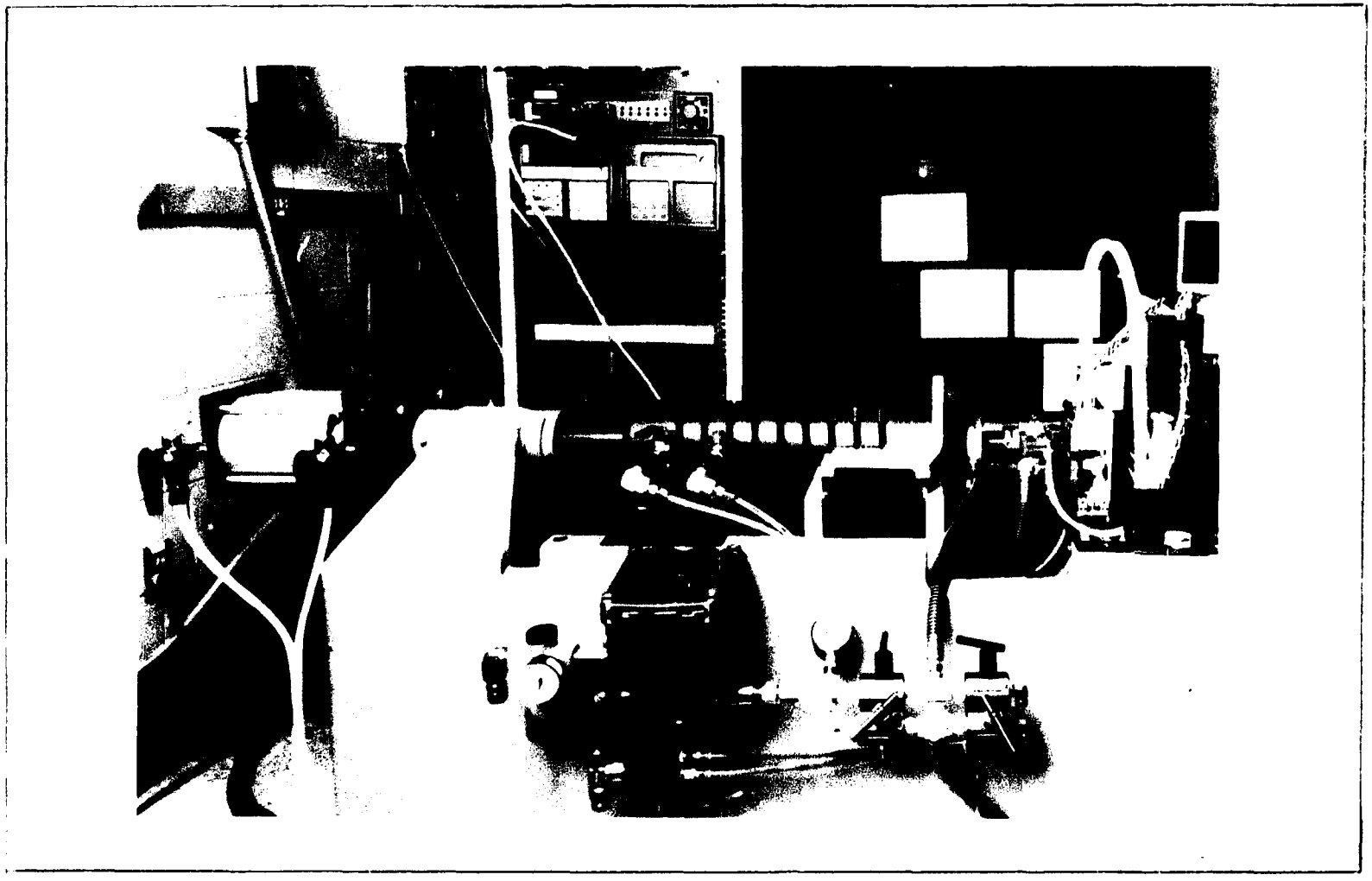

Figure 3 Test Equipment

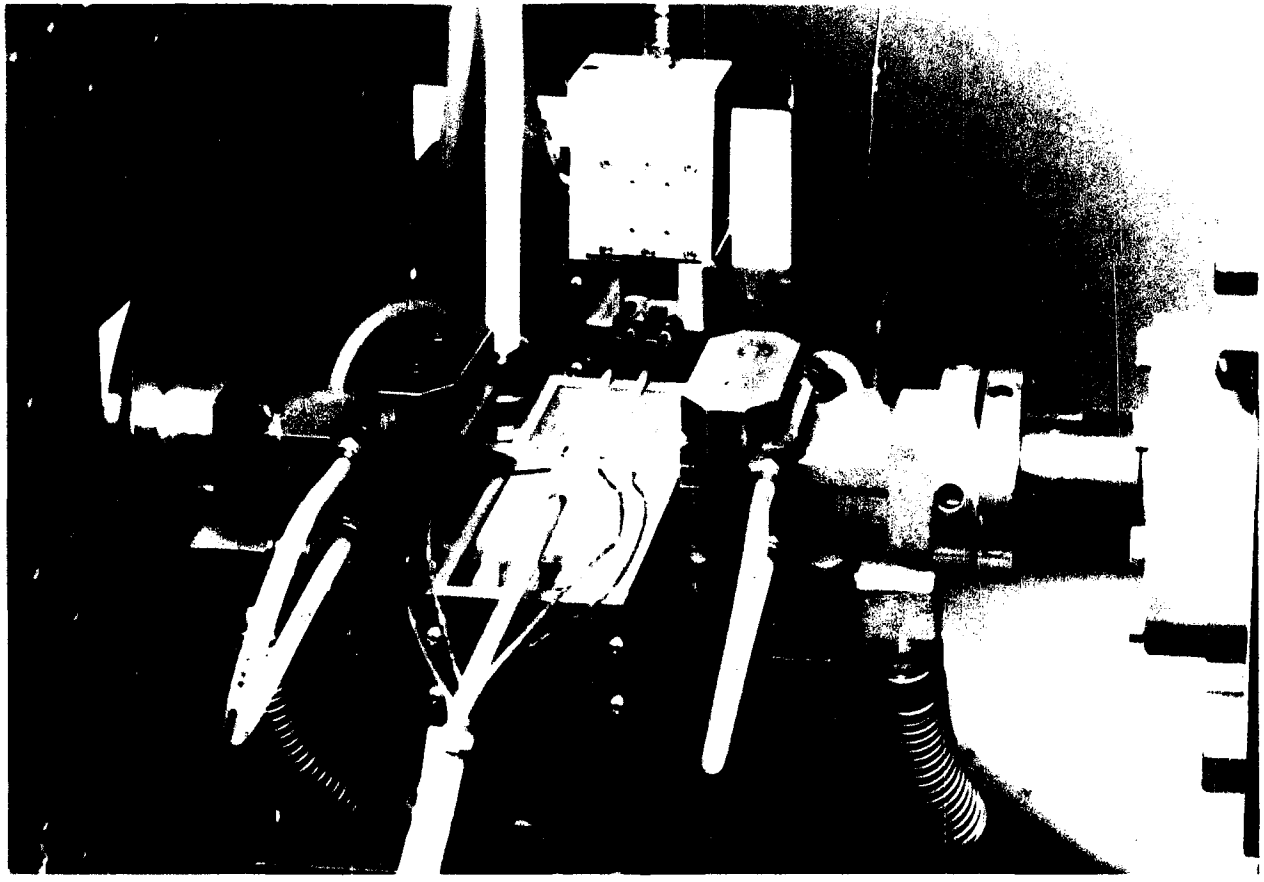

Figure 4 Mounted Test Specimen

measured using a pressure transducer with an electrical interface located behind one of the grips.

The thermal load was applied using the heat from two sets of quartz induction lamps as shown in Figure 4. In the figure the upper lamp assembly has been removed for clarity. Each set consisted of a bank of four lamps. The upper lamp assembly was placed 7 mm directly above the specimen and the lower assembly 7 mm below. The specimen was divided into the four zones for temperature control shown in Figure 5. A type K thermocouple, spot-welded to the test specimen in each zone, was used to measure and feedback temperature readings to the computer system. The computer system controlled the temperature by adjusting the electrical power input to the lamps in each zone. Additionally, forced convective cooling was required to reduce the specimen temperature to the desired level during cycling. This was accomplished using a manually regulated jet of compressed air.

Test Set-up Procedures

Before the test specimen was mounted and aligned it was measured and marked as shown in Figure 6. Then, the temperature zone 4 thermocouple was spot-welded underneath on the specimen in the position shown. Zone 4 was done first. This was because the thermocouple was located on the specimen's underside and the specimen could not be turned

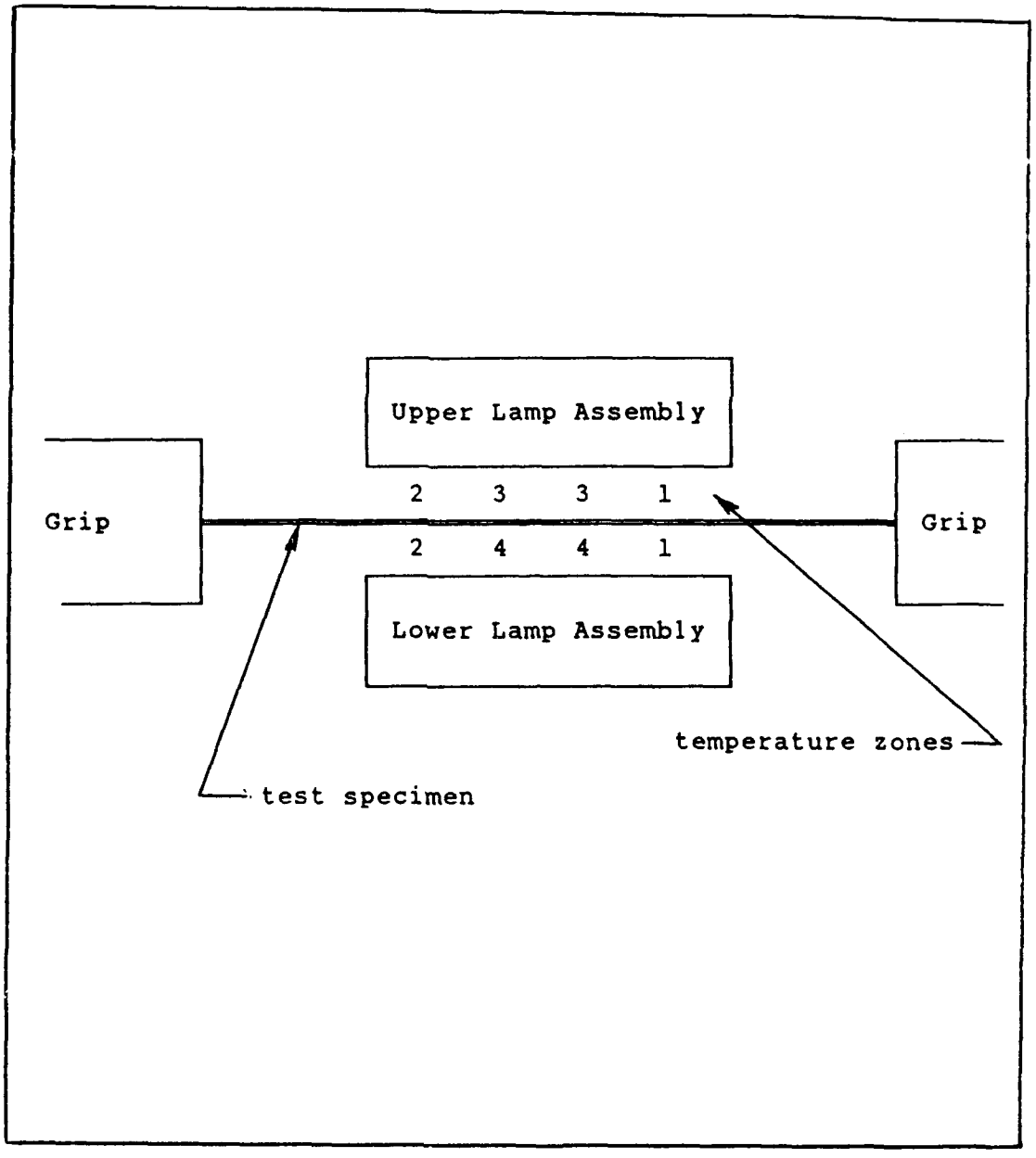

Figure 5 Four Zone Temperature Control

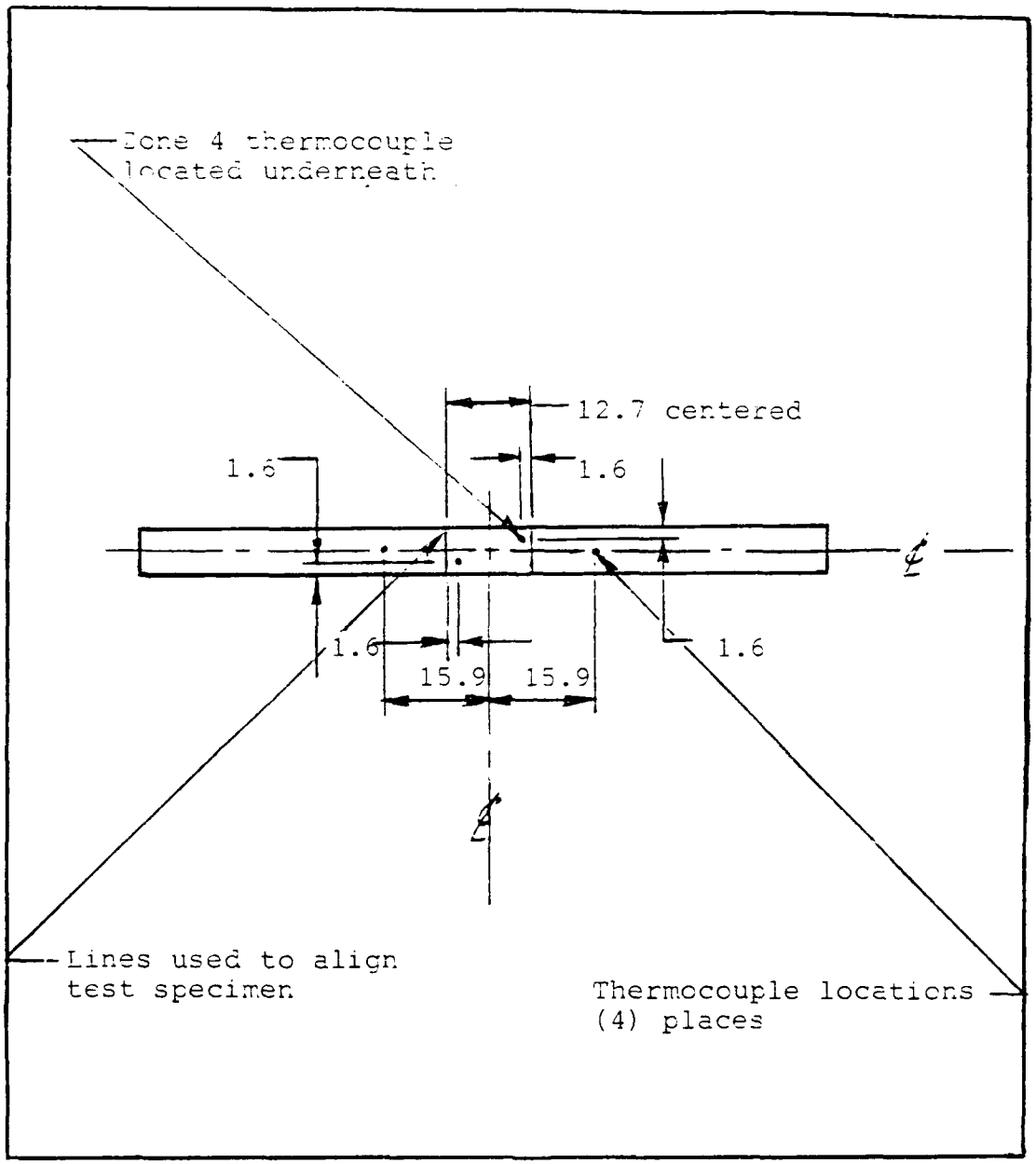

Figure 6 Test Specimen

over after the thermocouples for zones 1-3 (located on top) were welded in place. Next, the specimen was mounted and aligned in the hydraulic friction grips. A depth micrometer was used to center the specimen widthwise in the grips. The depth micrometer was used to prevent any misalignment which would introduce unwanted bending stresses into the test specimen after tension was applied. The specimen was located in the grips lengthwise using the two lines, located 12.7 cm apart, previously marked on the specimen's top surface (Figure 6). The lines were positioned directly above the middle two lamp filaments of the lower lamp assembly. After the test specimen was aligned it was held in position by pressurizing the hydraulic friction grips to 58.6 MPa. Then the zone 1-3 thermocouples were welded in place on the specimen's top surface located as shown in Figure 6. The welder was set in the low range in order to prevent pitting of the specimen's surface.

Next, the bottom lamp assembly was raised into position 7 mm directly below the test specimen and bolted in place. The middle two lamp filaments were kept directly below the two 12.7 cm apart marks previously marked on the specimen's top surface. An air jet tube was positioned approximately 13 cm from the specimen's edge, in order to provide the cooling air previously mentioned, and the thermocouple wires were tied to the tube to keep them out of the way.

Using an MTS extensometer (Figure 4) with quartz rods, strain was measured and fed back to the computer system through an analog-to-digital converter. The measured voltages were converted to strain by a PC microprocessor and were recorded every 5 - 7 cycles.

The extensometer was mounted after the test specimen was aligned and the lower lamp assembly bolted in place. Before mounting, the extensometer was calibrated if its quartz rods had been replaced. The rods were replaced if they were broken or if their pointed tips became rounded and dull. Extensometer rods with dull tips had to be replaced because they could slip on the specimen's edge and incorrectly measure strain. The quartz rods needed to be replaced and the extensometer recalibrated approximately every three tests.

The extensometer was calibrated using an MTS extensometer calibrator. The extensometer was mounted in the calibrator and the rod displacement zeroed. The rod tips were zeroed by placing them in the calibrator 12.7 cm apart. Then the rod tips were displaced at 20 different intervals. The displacement at each interval was measured using the calibrator and entered manually into a computer. The computer automatically measured the corresponding voltage measured by the extensometer for each displacement. A computer program was used to determine the straight line relationship between displacement and voltage for the

extensometer using linear regression. This relationship was stored in the computer and used when measuring strain with the extensometer.

After the extensometer was calibrated, as needed, it was mounted in place and zeroed. The extensometer mounted in a holder that bolted in place on the Schenck. The extensometer rods were placed pressing against the edge of the specimen and lateral pressure was applied by the spring-loaded holder to prevent the rods from slipping. The rods were tapped into position until the extensometer output read zero on a PC's monitor.

After the extensometer was in place the upper lamp assembly was positioned 14 mm directly above the lower lamp assembly and bolted in place. Then the extensometer was rechecked for a zero setting. This was to make sure that the extensometer was not bumped when positioning the upper lamp assembly.

Both the hydraulic friction grips and the quartz induction lamps required cooling to prevent them from being damaged. Protection was provided by a water cooling system. This system consisted of a pump, radiator, blower, and flexible tubing which circulated cooling water continuously through both the grips and the induction lamps.

A computer system was used to input, monitor, and control the thermo-mechanical loads and record data. It

consisted of a modular rack of equipment, Wavetek arbitrary waveform generator, and a PC microprocessor.

The modular equipment rack contained a load controller for the pneumatic load application system, analog-to-digital converter, type K thermocouple thermometer, and a Micricon 823 microprocessor. Mechanical loads were applied to the test specimen by the PC microprocessor using an arbitrary wave generator and the load controller. The PC simultaneously applied the thermal load using the quartz induction lamps. The induction lamps were controlled by the PC using an arbitrary waveform generator and the Micricon 823. During a data acquisition cycle, force, strain, and temperature measurements are taken at the test specimen and recorded by a PC microprocessor. These measurements were used by the microprocessor to update the amplitude and phase of the thermo-mechanical load profiles. Because the measurements were taken analog, they had to be converted to digital for use by the microprocessors. This was done by the analog-to-digital converter. Digital readouts located on the modular equipment rack, were also used to monitor, force, displacement, and temperature.

A computer program stored in a PC microprocessor was used to set up the test and record data. In order to run the test, various test specimen parameters, material properties, environmental properties, waveform parameters, and data acquisition parameters were entered interactively

into the program. The specimen parameters were: specimen identification number, geometry, thickness, and width. Typical material properties were: material type, yield strength, and Poisson's ratio. The test environment was lab air.

The PC was used to set up the desired mechanical and thermal waveforms in the Wavetek arbitrary waveform generator. The mechanical load was controlled by the PC using the Wavetek and the load controller. The thermal load was controlled by the PC using the waveform generator and the Micricon 823 microprocessor. The loads were created by drawing a trace of the desired waveform on the PC's monitor screen and entering the necessary waveform parameters into a computer program. These parameters included: maximum temperature, minimum temperature, load ratio, seconds per cycle, and maximum stress. The PC was programmed for triangular waveforms and constant loads.

In order to record data the following data acquisition parameters were entered interactively: initial sample number, initial cycle count, loop storage filename prefix, restart file save interval, restart file name, and active log filename. Data was recorded every 5 - 7 cycles during these tests. The PC updated the waveform's amplitude and phase after each data acquisition cycle. Seven cycles (42 minutes) was the longest period over which the smallest phase error (less than 10 degrees) could be maintained.

The program recorded the following: date, time, specimen identification number, sample number, cycle count, maximum stress, minimum stress, maximum temperature, minimum temperature, maximum strain, minimum strain, total samples acquired, load ratio, phase error, and a temperature zone summary. Various plots were available, such as: load/temperature versus time, load versus temperature, load/temperature profiles, zone temperature versus time, stress versus total strain, maximum/minimum strain versus cycles, maximum stress versus number of cycles to failure, and strain versus temperature.

III. Results and Discussion

An important objective of fatigue research is to predict the performance of materials in order to design damage tolerant structures. In order to accomplish this goal it is necessary to understand the inception and growth of the various damage mechanisms involved. Additionally, it is necessary to relate these damage mechanisms and their growth to the stresses causing them in the composite's fiber and matrix. In order to evaluate the effects of thermo-mechanical cycling seven rectangular test specimens were subjected to thermo-mechanical fatigue testing. Three of the test specimens were tested with the thermo-mechanical cycling in-phase and four were tested with the thermo-mechanical cycling 180 degrees out-of-phase.

The purpose of this chapter is to discuss the results of the thermo-mechanical testing. These results include 1) fatigue life curves, 2) scanning electron microscope fractography, 3) optical micrography, 4) specimen surface damage, 5) stress-strain response, 5) stress analysis, 6) comparison to existing theory, and 7) comparison to various other types of thermo-mechanical fatigue test results.

Fatigue Life Curves

The thermo-mechanical fatigue results from the in-phase and out-of-phase tests are plotted as life curves on a stress basis in Figure 7 and summarized in Table IV. The

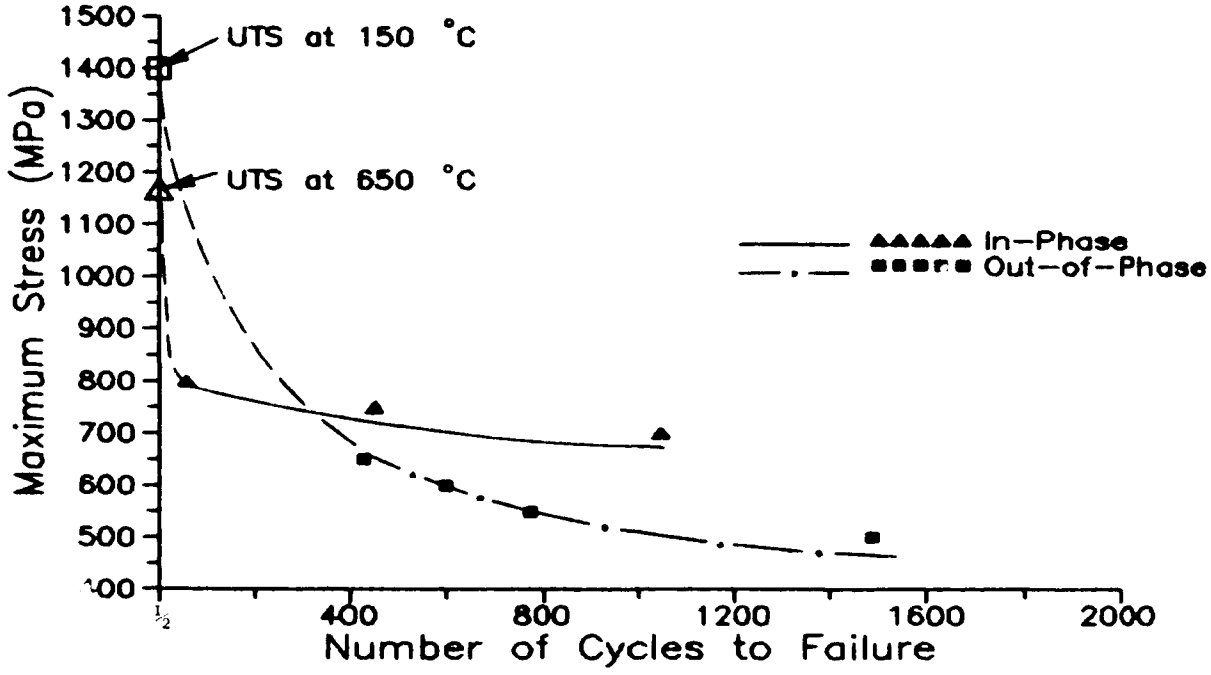

Figure 7A In-Phase and Out-of-Phase Thermo-mechanical Fatigue Life Results

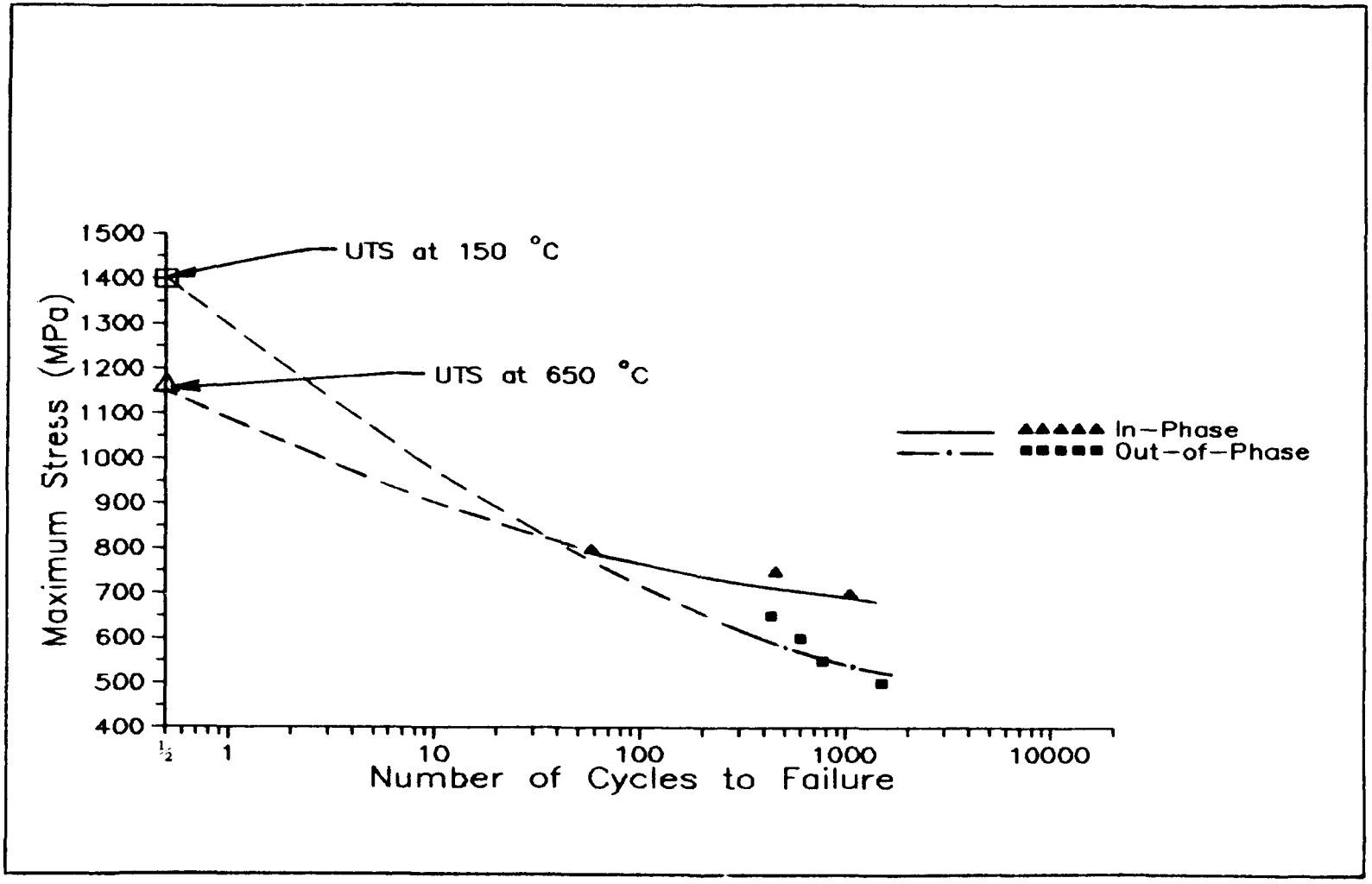

Figure 7B In-Phase and Out-of-Phase Thermo-mechanical Fatigue Life Results

Table IV. Thermo-Mechanical Fatigue Life Results

Thermo-Mechanical Fatigue Life Results			
Specimen Number	Maximum Applied Stress (MPa)	Cycles To Failure	Phase
90-052	800	58	I
90-054	750	451	I
90-053	700	1046	I
90-058	650	428	O
90-055	600	598	O
90-056	550	771	O
90-057	500	1487	O

plot of the out-of-phase test results has a steeper slope than the in-phase plot. This indicates that for a given stress level an out-of-phase test specimen fails sooner than its respective in-phase counterpart. These results agree with those previously found by Gambone at Allison Gas Turbine Division of General Motors Corporation (5:58).

Gambone tested three temperature ranges: 315 °C to 650 °C, 93 °C to 650 °C, and 315 °C to 760 °C. The last temperature cycle was only out-of-phase. All tests were strain controlled with a mechanical strain ratio of 0.1. The 93 °C - 650 °C temperature cycle was also tested using a mechanical strain ratio of 0.5. Both the thermal and mechanical loads were 90 seconds long with a triangular profile. Fatigue lives were in the 100 - 10000 cycles range.

Scanning Electron Microscope Fractography

As previously mentioned, in order to understand why an out-of-phase test fails sooner than its respective in-phase counterpart, it is necessary to understand any differences in the damage mechanisms involved. It is also necessary to analyze the stresses that occurred throughout the test cycle and to relate these stresses to the damage observed in the test specimen. The damage mechanisms were investigated by examining and comparing the fracture surfaces from both in-

phase and out-of-phase test specimens using the scanning electron microscope.

A typical scanning electron microscope fractograph of the fracture surface taken from an in-phase test specimen is shown in Figure 8. Investigation of the fracture surface reveals that test specimens subjected to in-phase testing were unable to support crack growth in the matrix and failed immediately after the initiation of fatigue damage in the fibers. The features illustrated here resemble those found on fracture surfaces from static tensile failures. The surface of the matrix is rough across the entire fracture area. This is in sharp contrast to a fatigue failure where flat smooth regions of fatigue cracking in the matrix are normally accompanied by areas of rough tensile matrix failure. In addition, the figure shows that the matrix is debonded (pulled away) from around each of the fibers and areas where fibers are pulled out. Both of these conditions are typical of tensile failures.

This is consistent with the high longitudinal stress in the fiber and the low longitudinal stress in the matrix that occurred during in-phase test conditions. The high stress in the fiber was more dominant. After the fibers started to break due to fatigue damage, the part of the load that they had carried was transferred to the matrix which could not handle it. The specimen then failed suddenly due to the broken fibers, which is the case for static tensile

Figure 8 Typical In-phase Fracture Surface
(Specimen 90-052, σ_{max} = 800 MPa, Magnification 200X)

failures, without any fatigue cracking occurring in the matrix.

A typical fractograph of the fracture surface taken from an out-of-phase test specimen is shown in Figure 9. The fracture surface reveals a fair amount of fatigue cracking in the matrix. The cracking appears as flat smooth regions compared to the rough surface area of the static tensile failure region. Crack initiation sites in the matrix typically occurred in two places. One was from the composite's surface, randomly located along the fracture surface's perimeter. The other sites were matrix cracking originating from the interface reaction zone which progressed around the fibers in circular rings. Changes observed in the secant modulus probably occurred prior to damage appearing on the surface. This indicated that the cracks originating from the interface reaction zone probably occurred prior to any surface damage. The cracks in the interface reaction zone occurred only in the outer laminas of the composite from the shortest out-of-phase test (428 cycles), indicating that the longitudinal stress was higher in these laminas. For longer tests this cracking around individual fibers progressed into a larger crack region. This larger region of flat smooth fatigue cracking in the matrix surrounded an internal rough region of static tensile failure located in the center of the fracture surfaces's crossection. This suggests that the composite's surface and

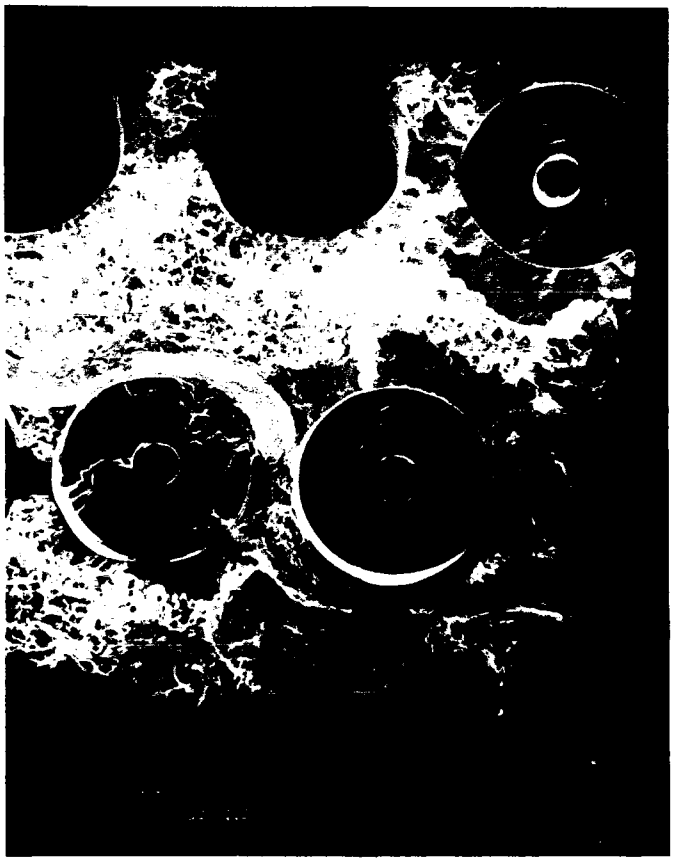

Figure 9 Typical Out-of-phase Fracture Surface
(Specimen 90-058, σ_{max} = 650 MPa, Magnification 200X)

the interface reaction zone in the outer lamina played a key role in damage initiation and progression for out-of-phase test conditions.

Fatigue cracking in the matrix is consistent with the high longitudinal stress in the matrix and the low longitudinal stress in the fiber that occurred during out-of-phase test conditions. The high stress in the matrix was more dominant than the low stress in the fiber. As fatigue cracking progressed, the load previously carried by the crack regions was transferred to the remaining undamaged regions until the undamaged areas could no longer support the load. The undamaged regions then failed suddenly due to static tensile failure.

The crack initiation sites in the interphase reaction zone and on the composite's surface occur in the two weakest locations found in the matrix. The mechanical properties at the interphase were degraded by the manufacturing process and the surface was damaged by oxidation caused by the thermal test cycle. That damage initiated at the weakest points is to be expected.

Optical Micrography

In addition, the test specimens were sectioned and the damage was investigated in regions away from the fracture surface. Typical micrographs of longitudinal and transverse sections viewed under a high power optical microscope are

shown in Figures 10 and 11, respectively. The micrographs showed no essential difference between the in-phase and out-of-phase damage mechanisms except for surface damage. This is in sharp contrast to the fractographs of the fracture surfaces which suggest that the failures are fundamentally different. This is reasonable, since, the micrographs show damage initiation and the fractographs of the fracture surface show the final failure. Basically, the damage initiation is the same for both in-phase and out-of-phase test conditions but the progression to final failure is different.

The micrographs of the sections revealed that all test specimens had both transverse and longitudinal cracking in the matrix originating the interface reaction zone. All cracks were through the grains rather than following the grain boundaries in the matrix. The transverse cracks shown in Figure 11 occurred equally as often in specimens from both the in-phase and the out-of-phase tests. However, the longitudinal cracks shown in Figure 10 were larger and occurred more often in specimens subjected to out-of-phase testing. All test specimens had broken fibers as shown in Figure 12. Cracking at the surface in the matrix as shown in Figure 13 was found only in the out-of-phase test specimens.

All of the test specimens had both broken fibers and cracks in the matrix. In order to understand how the damage

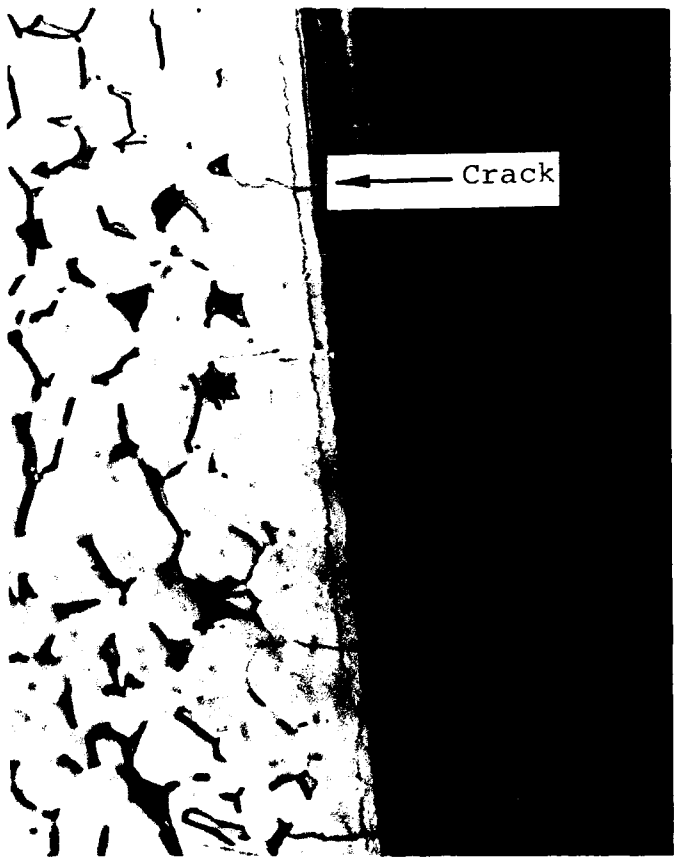

Figure 10 Typical Longitudinal Cracking
(Specimen 90-057, σ_{max} = 500 MPa, Magnification 1000X)

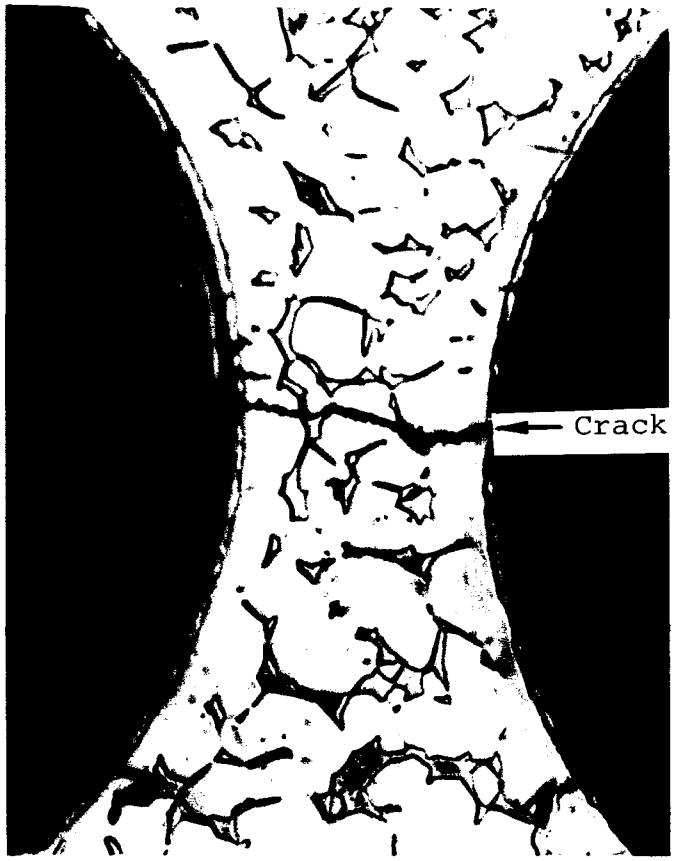

Figure 11 Typical Transverse Cracking
(Specimen 90-057, σ_{max} = 500 MPa, Magnification 1000X)

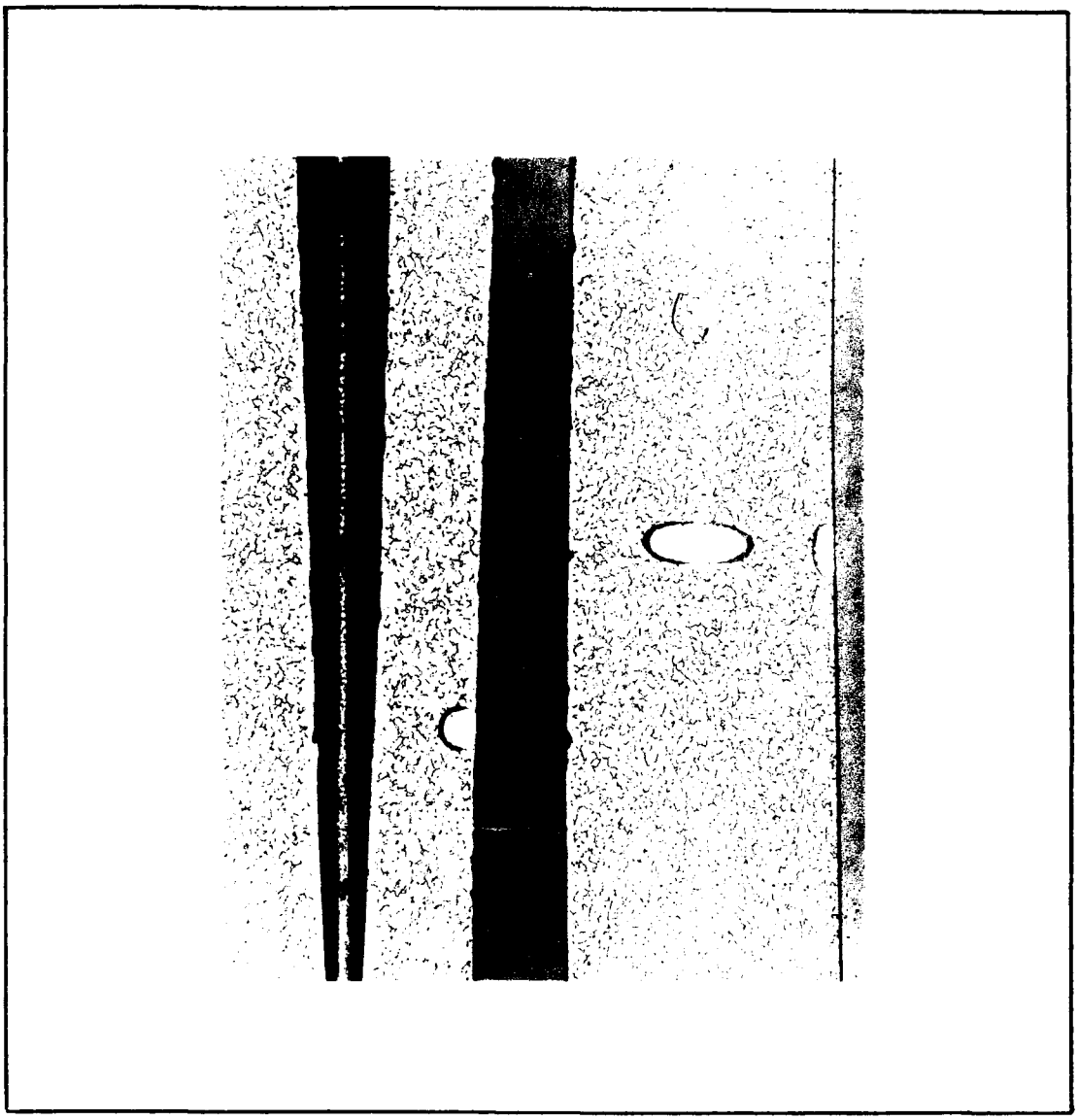

Figure 12 Typical Broken Fibers
(Specimen 90-052, σ_{max} = 800 MPa, Magnification 100X)

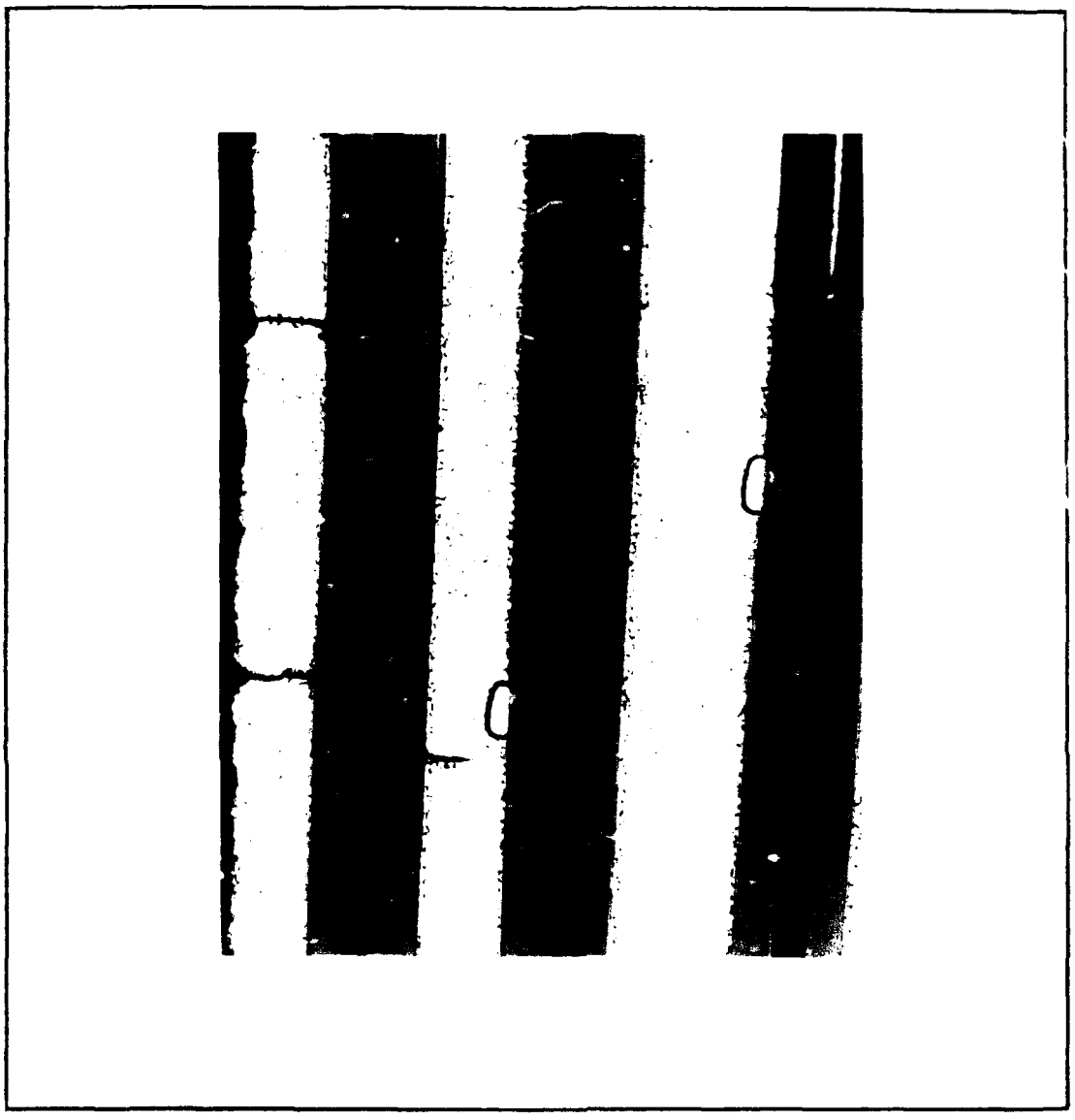

Figure 13 Typical Out-of-phase Surface Damage
(Specimen 90-057, σ_{max} = 500 MPa, Magnification 100X)

initiated it is necessary to understand which occurred first. At the present time no evidence of fiber fatigue exists. Studies show that fibers fail instantaneously due to tensile overload. Therefore, the cracking in the matrix occurred first. The damage initiation site for both the in-phase and out-of-phase test specimens is the cracking in the interface reaction zone.

Even though the damage initiation is the same for both cases, the progression is not. In the in-phase case the cracking starts in the interface. Because of the crack some of the load previously carried by the matrix is transferred to the fibers. During the in-phase test the stress in the fibers was already high and the additional increase in stress was enough to start breaking the weakest fibers. The fibers broke anywhere along their length at the weakest point, not necessarily next to a crack in the matrix. The final fracture surface does not need to correspond to regions of cracking in the matrix. The load previously carried by the broken fibers was transferred to the matrix which could not take it and the composite failed suddenly due to the tensile load.

For out-of-phase test conditions the damage initiation site is also the interphase reaction zone. However, the stress in the fiber was low and fatigue cracking progressed until enough of the load was transferred from the crack

areas to the undamaged region for failure to occur from the static tensile load.

Surface Damage

All test specimens were inspected for surface damage before and after testing. Prior to testing the specimens were polished to remove any damage from machining from which unwanted cracks might originate during testing. This was also done in order to provide a smooth surface on which surface cracking might be replicated using replication tape. After polishing the specimen's edges were viewed under a high power optical microscope. Typical damage was fiber breakage and pullout due to machining that occurred when the specimens were cut to width in the shop as shown in Figure 14. After testing all specimens had additional broken fibers along the exposed edges as shown in Figure 15. These fibers probably broke right away because they were already damaged and weakened by exposure to machining and polishing. All test specimens were heavily oxidized after testing due to the thermal cycling. The in-phase test specimens showed no additional surface damage (Figure 16). However, the out-of-phase test specimens had surface cracks across the face as shown in Figure 17. None of the surface cracks appeared until the final test cycles. Therefore it was not possible to use the replication tape to record their progression. Additionally, the quality of the replication would have been

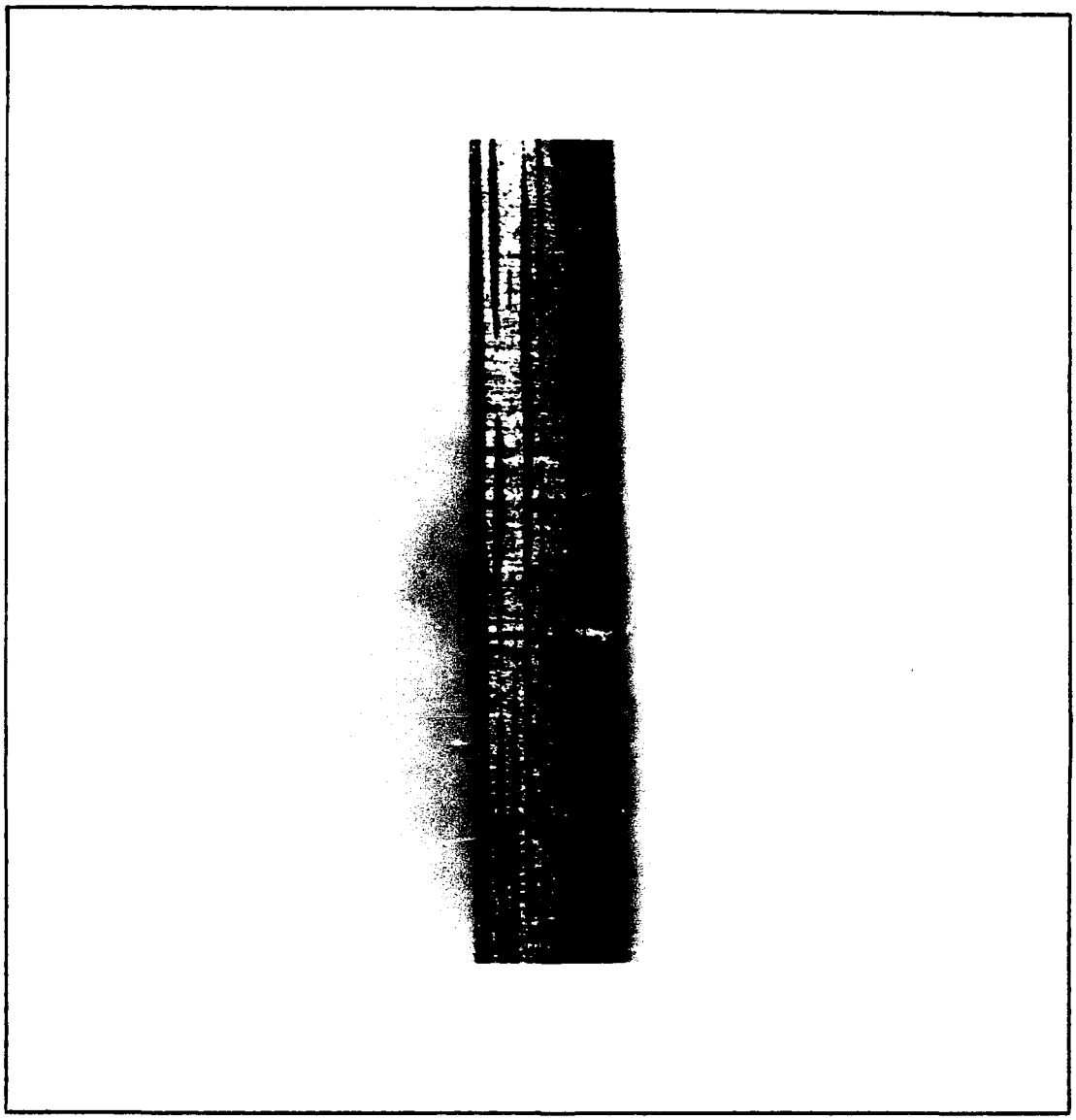

Figure 14 Typical Fiber Breakage and Pullout Along Exposed Edges (Specimen 90-052, Magnification 20X, Side View)

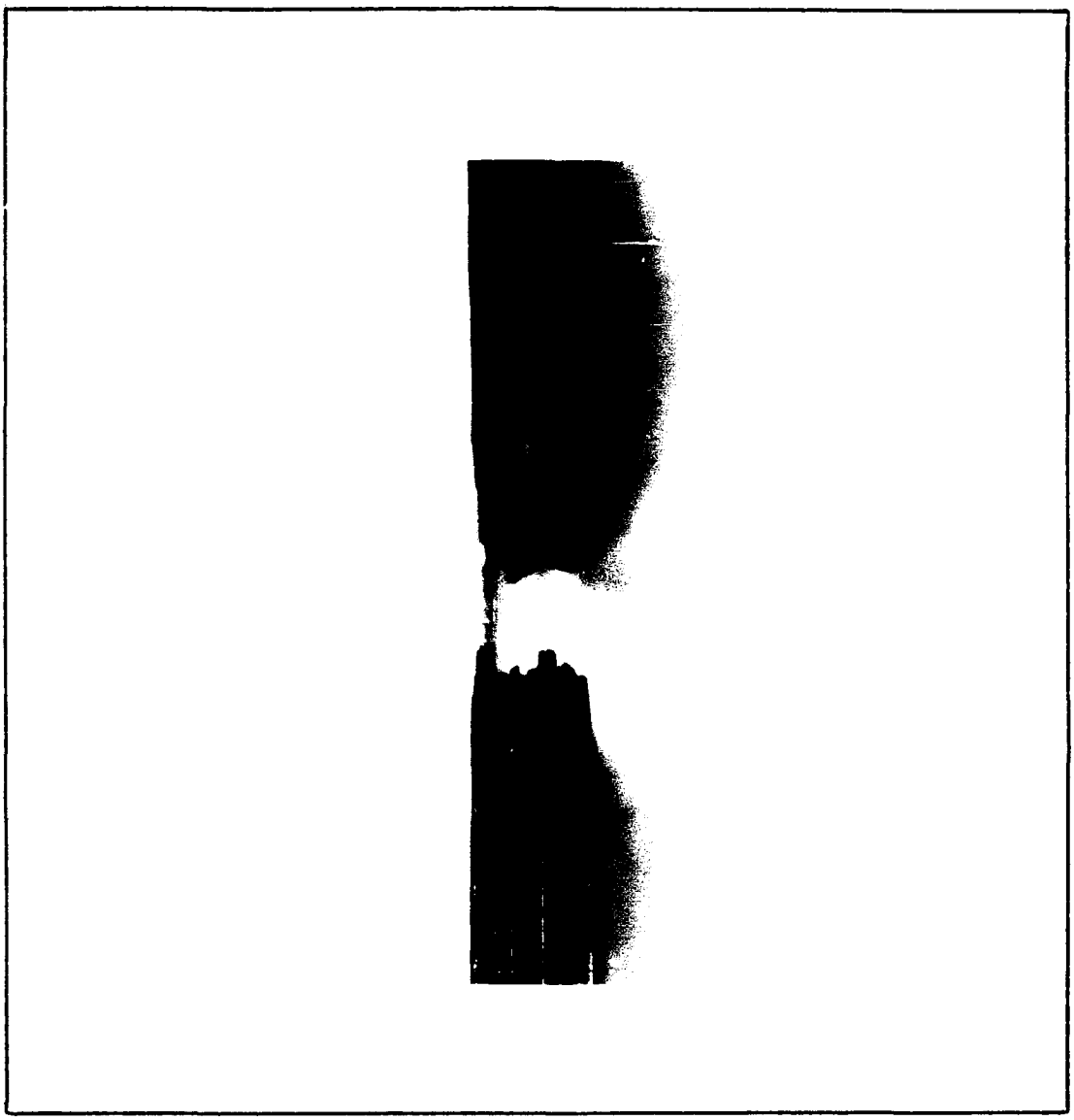

Figure 15 Typical Broken Fibers Along Exposed Edges
(Specimen 90-054, σ_{max} = 750 MPa, Magnification 20X, Side View)

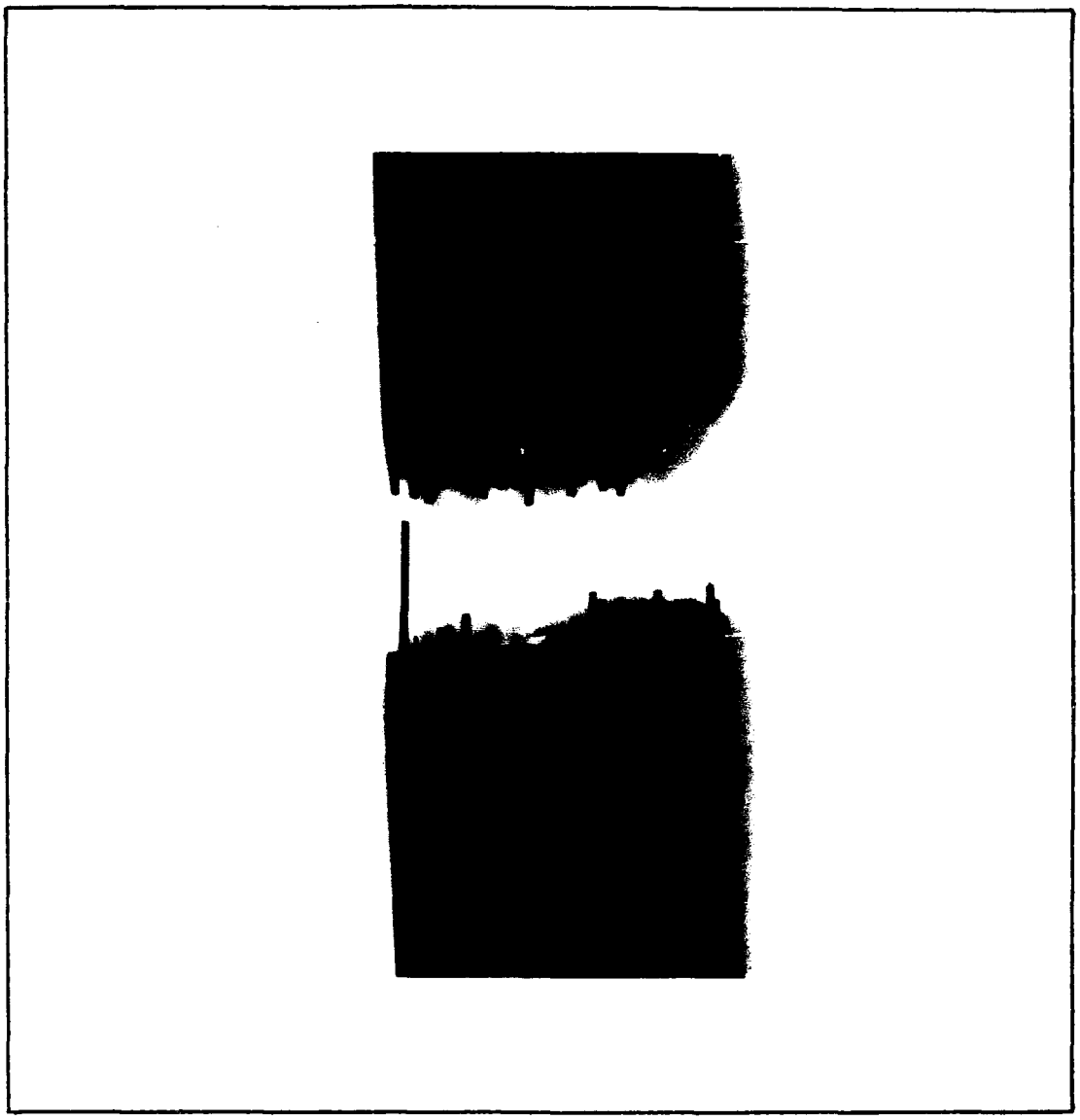

Figure 16 Typical Surface After In-phase Testing
(Specimen 90-054, σ_{max} = 750 MPa, Magnification 20X, Front View)

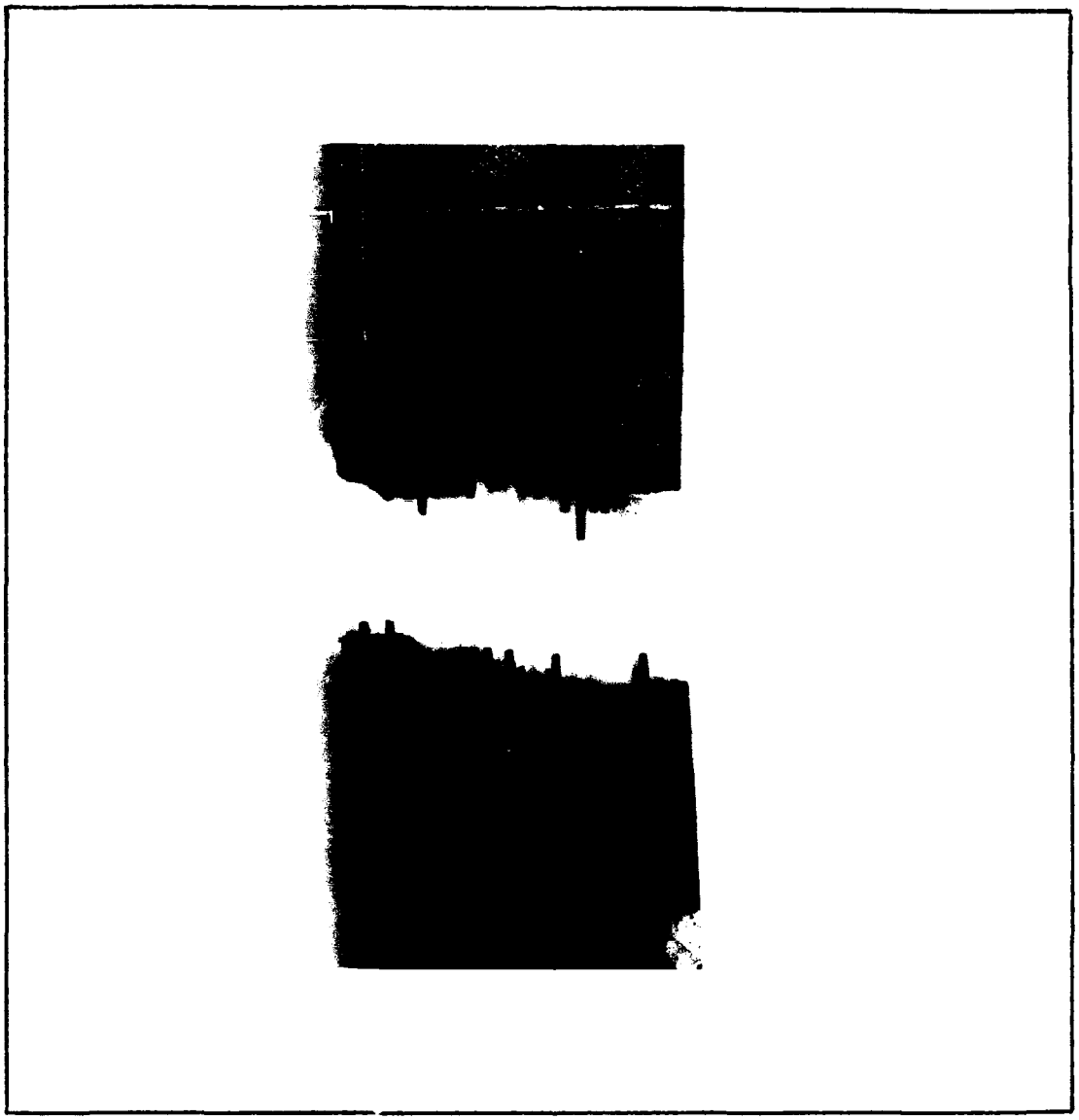

Figure 17 Typical Out-of-phase Test Specimen Surface Cracking (Specimen 90-057, σ_{max} = 500 MPa, Magnification 200X, Front View)

poor because of the oxidation on the test specimen's external surfaces.

Gambone's study reported (5:58) no essential difference in the damage mechanisms from the in-phase and out-of-phase tests. Their report indicates that damage initiated at the test specimen's corners and across the face, similar to the cracking previously shown in Figure 17 from the out-of-phase tests. Their report indicates that this cracking occurred at multiple initiation sites across the entire test specimen gage length. This investigation could not duplicate Gambone's results.

Stress - Strain Response

In addition to inspecting the surface for damage, the stress-strain response of the test specimens were monitored throughout testing in order to determine when damage first initiated. Any increase in the secant modulus would indicate that crack initiation and growth was occurring in the composite. This method has an advantage over surface inspections because it can detect internal damage that may occur prior to surface damage. Additionally, there may be no surface damage which was generally the case for the in-phase tests.

The typical stress-strain response for a specimen subjected to in-phase test conditions (σ_{max} = 800 MPa) is shown in Figure 18. The first cycle and the last two

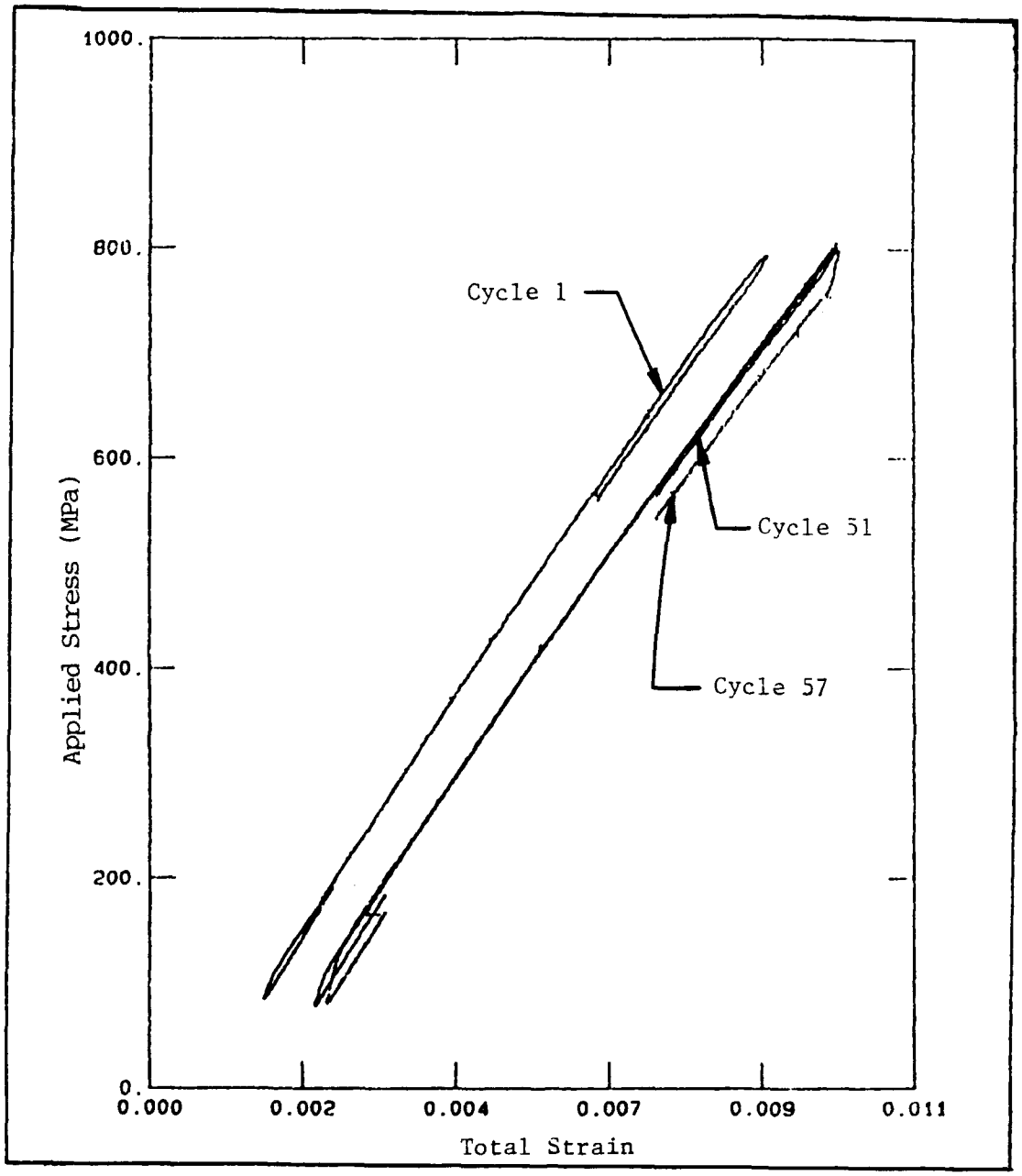

Figure 18 Typical Stress-Strain Response

recorded cycles before failure are plotted. The mechanical strain offset shown is that which naturally accumulated throughout the test. The figure shows that there was no change in the overall slope of the hysteresis loops. This indicates that there was no change in the secant modulus which would have indicated that failure was approaching. In general, these hysteresis loops are open and show no irregularities. Open loops can be an indication of inelastic deformation. Inelastic deformation did occur during the first test cycle during which the yield strength of the test material was exceeded. Above the yield strength the behavior of the test material was elastic-plastic. However, most of the inelastic deformation would have occurred during the first cycle. The small phase angle errors (1-10 degrees) that occurred in the thermo-mechanical load control during testing also produced open loops. Cycles with zero phase angle error showed closed hysteresis loops while cycles with nonzero phase angles showed open hysteresis loops. The phase angle error was probably responsible for most of the open loops observed, except for the first cycle.

A typical plot of the total strain versus the number of test cycles for an in-phase test is shown in Figure 19. As shown in the figure, the cyclic mean strain increased rapidly during the first few test cycles and then very slightly throughout the remaining test cycles. The increase

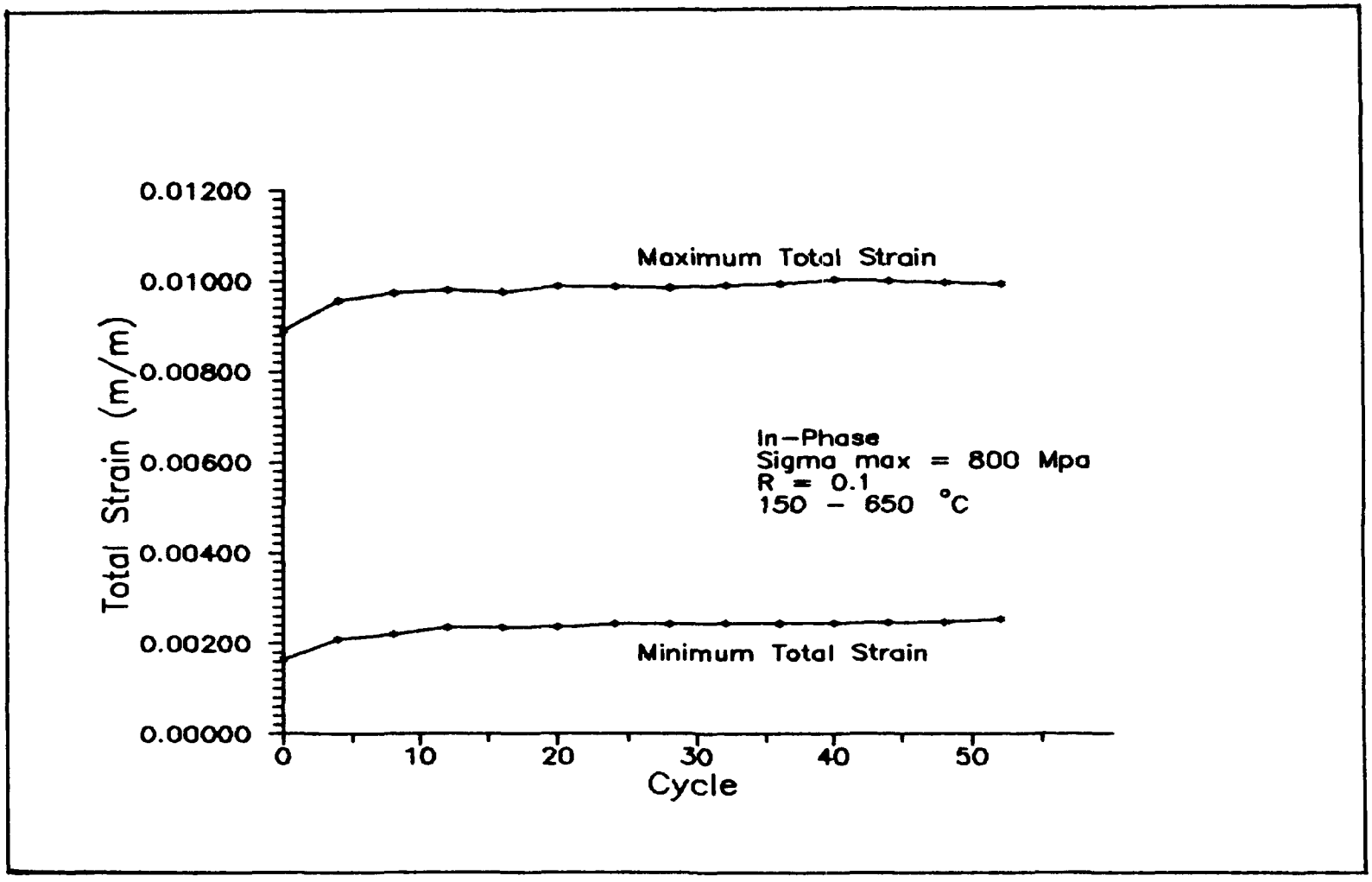

Figure 19 Typical Change in Maximum and Minimum Strain During In-Phase Thermo-mechanical Fatigue Testing

in mean strain observed during in-phase testing was probably due to creep. At 650 °C a titanium based matrix tends to creep readily and the in-phase test conditions are highly conducive to creep (1:5). This is because during an in-phase test the maximum stress occurs at the high temperature where the matrix is subject to creep and the slow 6 minute cycle would allow enough time for creep to occur. At the high temperature and maximum load the matrix relaxes. Part of the stress formally carried by the matrix is transferred to the fiber.

Hysteresis loops did not exist for the out-of-phase test conditions. During out-of-phase testing, the net difference between the maximum and minimum total strains that occurred during the cycle was approximately 0.00010 m/m. This region was too small to divide up into the sub-intervals required to gather data and plot the hysteresis loops. In the future, it would be better to change the computer programming to calculate the mechanical strain and plot the hysteresis loops using mechanical strain rather than total strain for out-of-phase testing.

The secant modulus was calculated and the first three of the four out-of-phase tests showed no change. For these test specimens the mean total strain decreased early in life and then stabilized, as shown in Figure 20. Thus, for the first three out-of-phase tests there was no discernable phenomenological change indicating failure was approaching.

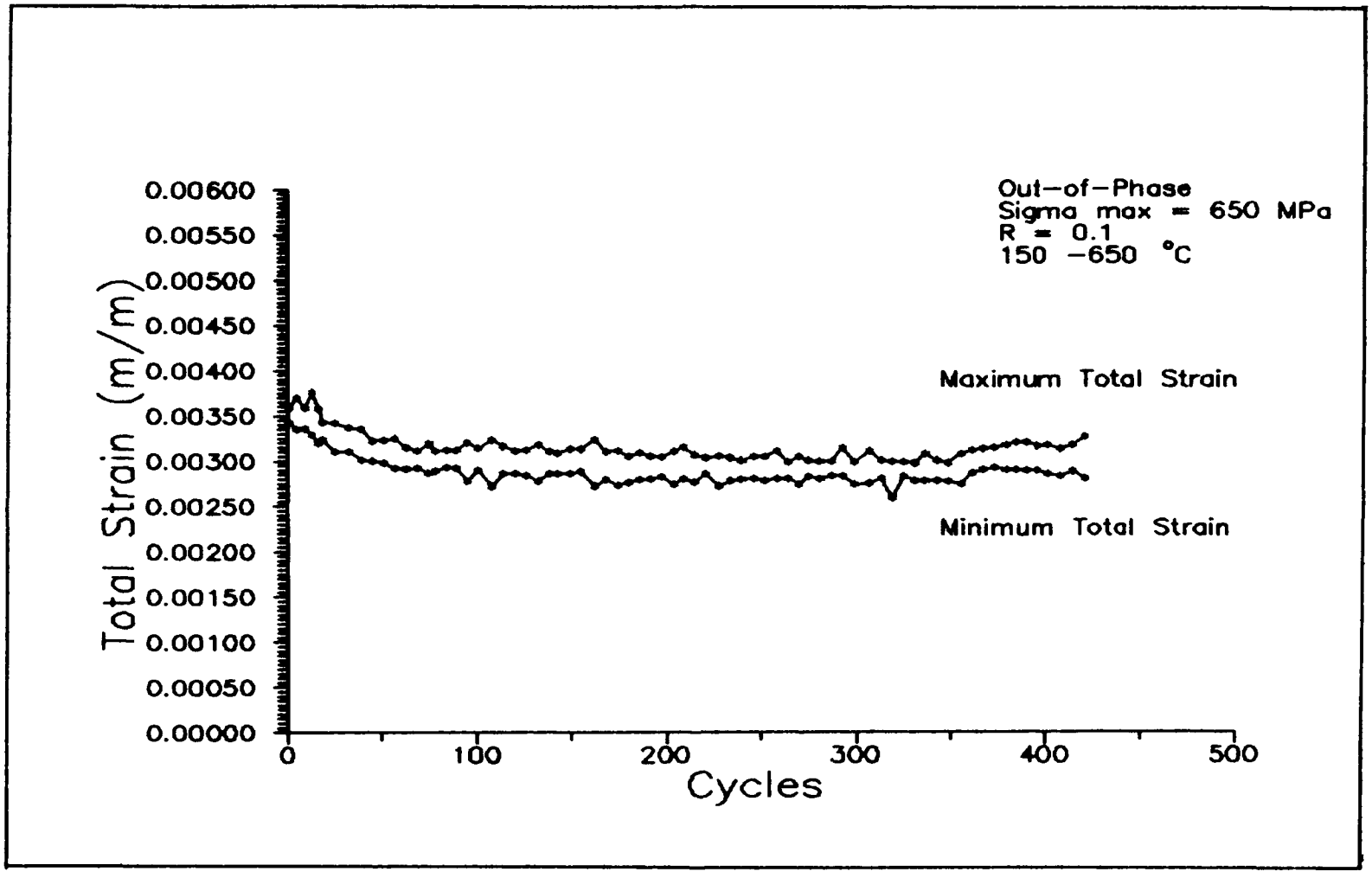

Figure 20 Typical Change in Maximum and Minimum Strain During Out-of-Phase Thermo-Mechanical Fatigue Testing

The fourth and longest test (1487 cycles) showed a large increase in modulus, followed by a large decrease, accompanied by a rapid increase in the average total strain. This change indicating failure was approaching occurred approximately 100 cycles before failure (Figure 21). The abrupt failure seemed to be internal because the modulus changed before surface cracking was discernable to the naked eye. All surface cracking appeared on surfaces that would have been visible during the test. None occurred on the bottom surface which was not visible. However, it was not physically possible to observe any of the surfaces of the test specimen under a microscope during test. The damage probably initiated at the weakest point in the matrix which was the interface reaction zone. Unlike the first three tests, the mean total strain increased throughout the test specimen's life. This was probably due to the initiation and slow growth of cracks in the interface reaction zone.

Unlike in-phase test conditions, out-of-phase tests are not conducive to creep. This is because the high stress level occurs at the minimum temperature where the matrix is not subject to creep. The decrease in mean strain seen in the first three out-of-phase tests might be the result of work hardening of the matrix (1:5). However, this does not explain why the mean strain increased throughout the fourth test. The increase in mean strain probably means that the matrix cracking occurred and progressed slowly, rather than

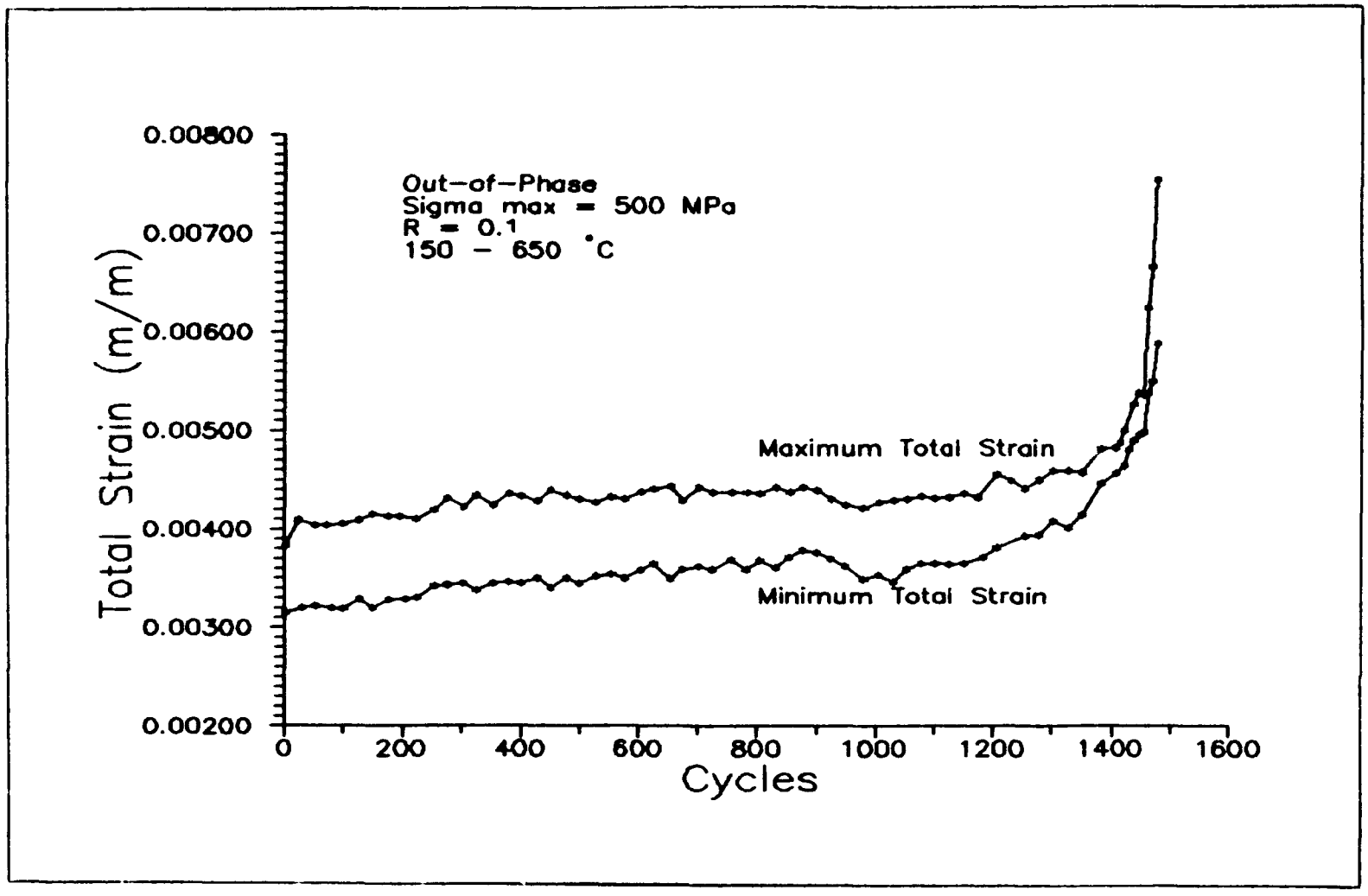

Figure 21 Out-of-Phase Test Showing Change in Secant Modulus

abruptly. Additionally, the fourth test gave indication that failure was approaching, whereas, the first three tests gave none. It may have been that the fourth test specimen was better able to support crack growth at the lower mechanical stress level applied during the longest out-of-phase test.

In Table V the maximum applied mechanical stress and the maximum measured total strain that occurred during each of the in-phase and out-of-phase test cycles are given. The amount of mechanical strain that was present in the total measured strain is also given. The maximum measured total strains from the in-phase test conditions either meet or exceed the total strains at static failure (approximately 0.85 at 650 °C) observed by Gambone, previously shown in Table III. However, the maximum applied mechanical stresses used during in-phase test conditions of 800, 750, and 700 MPa are considerably below the Ultimate Tensile Strength observed by Gambone of approximately 1 57 MPa at 650 °C. Additionally, the resulting fatigue lives were in the 58 - 1046 cycles range which rules out the possibility of a pure tensile failure. The larger total strains observed during this study are probably due to the variability in Young's modulus and the coefficient of thermal expansion between the test specimens Gambone used and those used in this study.

Table V. Maximum Total Strain Response During Testing

In-Phase Test Conditions

Applied Mechanical Stress (MPa)	Max Total Strain (Percent)	Mechanical Strain (Percent)
800	0.991	0.451
750	0.811	0.423
700	0.813	0.395

Out-of-Phase Test Conditions

Applied Mechanical Stress (MPa)	Max Total Strain (Percent)	Mechanical Strain (Percent)
650	0.419	0.037
600	0.402	0.034
550	0.410	0.031
500	0.413	0.028

Damage Summary

In summary, scanning electron microscope fractographs revealed that the test specimens subjected to in-phase test conditions were unable to support a crack. This was in sharp contrast to out-of-phase test conditions. During out-of-phase test conditions, cracking in the matrix initiated at the surface and in the interface reaction zone. The cracks in the interface progressed in circular rings around the fibers. The surface cracks were randomly located along the fracture surfaces' perimeter and the interface reaction zone cracks were located in the outer three laminas of the composite. The cracking in the matrix surrounding the individual fibers then coalesced forming an outer region of smooth flat fatigue cracking. This outer ring surrounded an inner rough region of static tensile matrix failure located in the center of the fracture surfaces' crossection. All test specimens were heavily oxidized caused by the thermal cycling. In-phase test specimens showed no additional surface damage. Whereas, out-of-phase test specimens had surface cracking. Changes in the secant modulus indicated that damage began internally prior to surface cracking in the out-of-phase tests. Transverse and longitudinal sections were taken in areas away from the fracture surface and viewed under the optical microscope. These sections revealed that all test specimens had both longitudinal and

transverse cracking in the matrix in addition to broken fibers.

Stress Analysis

The damage mechanisms previously discussed are due to the individual stresses in the fiber and matrix that occurred during the test cycle. Ultimately, these stresses control the differences in fatigue life observed between the in-phase and out-of-phase test conditions. Therefore, it is important to relate the damage mechanisms previously discussed to the individual stresses found in the composite constituents.

In order to accomplish this goal the computer code METCAN2 (METal Matrix Composite ANalyzer) developed by NASA Lewis was used to calculate the stresses that occurred in the fiber and matrix throughout the test cycles. The multi-cell model used in METCAN2 was designed to calculate laminate properties and stress strain behavior in an average sense. The model used the coordinate system and square unit cell divided into the subregions shown in Figure 22. The subregions were used to model the variation in constituent properties and stress throughout an individual lamina (2:23-27). The micromechanics equations used and the computer program are discussed in more detail in Appendix A.

Residual Stresses

The first step was to analyze the stresses in the fiber and matrix that occurred from the processing temperature of 900 °C through cooldown to room temperature at 23 °C. These stresses are plotted in Figure 23. At the processing temperature all stresses were zero. The process of cooling down created longitudinal tensile stresses (σ_{11}) in the matrix and longitudinal compressive stresses in the fiber. This was due to a mismatch in the thermal coefficients of expansion between the matrix and fiber. The coefficient was larger for the matrix. Therefore, the matrix tried to contract more than the fiber. This put the fiber into compression and the matrix into tension.

In addition, compressive transverse stresses were created in the fiber during cooldown. These stresses were equal across the fiber in both the σ_{22} and σ_{33} directions. This was also due to the mismatch in coefficients of thermal expansion between the fiber and matrix. As the composite cooled down, the matrix squeezed the fiber more tightly.

METCAN2 showed interlamina variation in the transverse stresses across the matrix. The matrix was divided into the regions A and C, as previously shown in Figure 22. Region A was in tension and the stresses σ_{22} and σ_{33} were equal within the region. Region C was in compression and the transverse stresses again were equal.

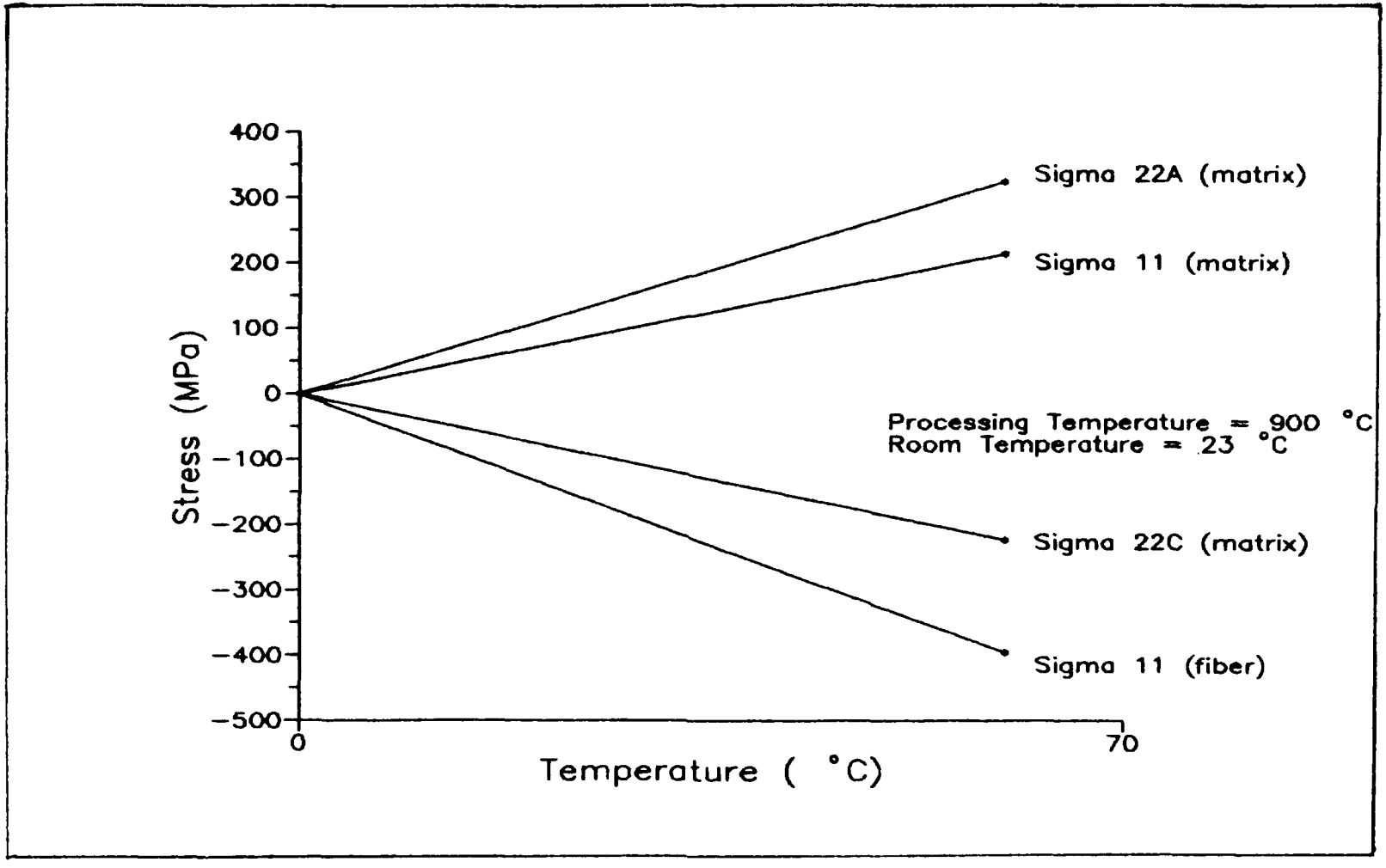

Figure 23 Residual Stresses Due to Cool–Down from Processing Temperature

Thermo-mechanical Stresses

In thermo-mechanical cycling both thermal and mechanical loads create stresses in the fiber and matrix. These are in addition to the residual stresses discussed above. In addition, the applied thermal and mechanical loads may be either in-phase or out-of-phase. All this created a complicated stress state within the composite at any given point during testing.

The stresses that occurred in the fiber and the matrix throughout each test cycle were calculated using an elastic analysis for both the in-phase and the out-of-phase test conditions. These stresses are plotted from a typical in-phase test in Figure 24 and from a typical out-of-phase test in Figure 25. The plotted test cycles had a maximum applied mechanical stress of 500 MPa, a ratio of the minimum to maximum mechanical stress of 0.1, and a temperature range of 150 - 650 °C.

The METCAN2 analysis revealed that the average stress in the fiber and the matrix was equal in both the in-phase and the out-of-phase testing for the same applied thermo-mechanical loads. Additionally, the transverse stresses in the fiber and matrix are independent of both the mechanical loading and the phase. Therefore, the transverse stresses are due to the thermal cycling only.

During out-of-phase conditions the maximum mechanical load was applied at the minimum temperature. At this point,

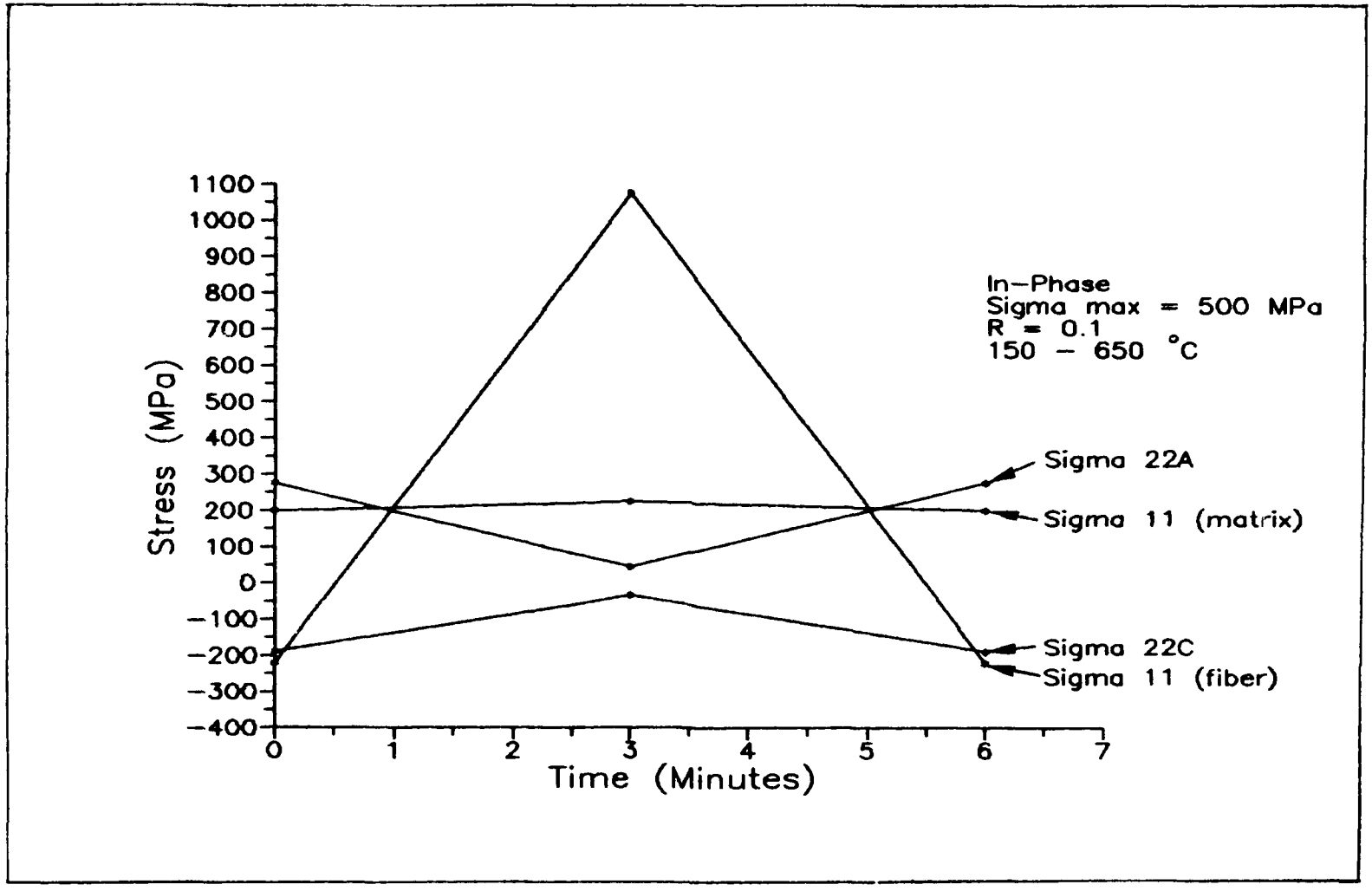

Figure 24 Stresses Throughout One In−Phase Cycle

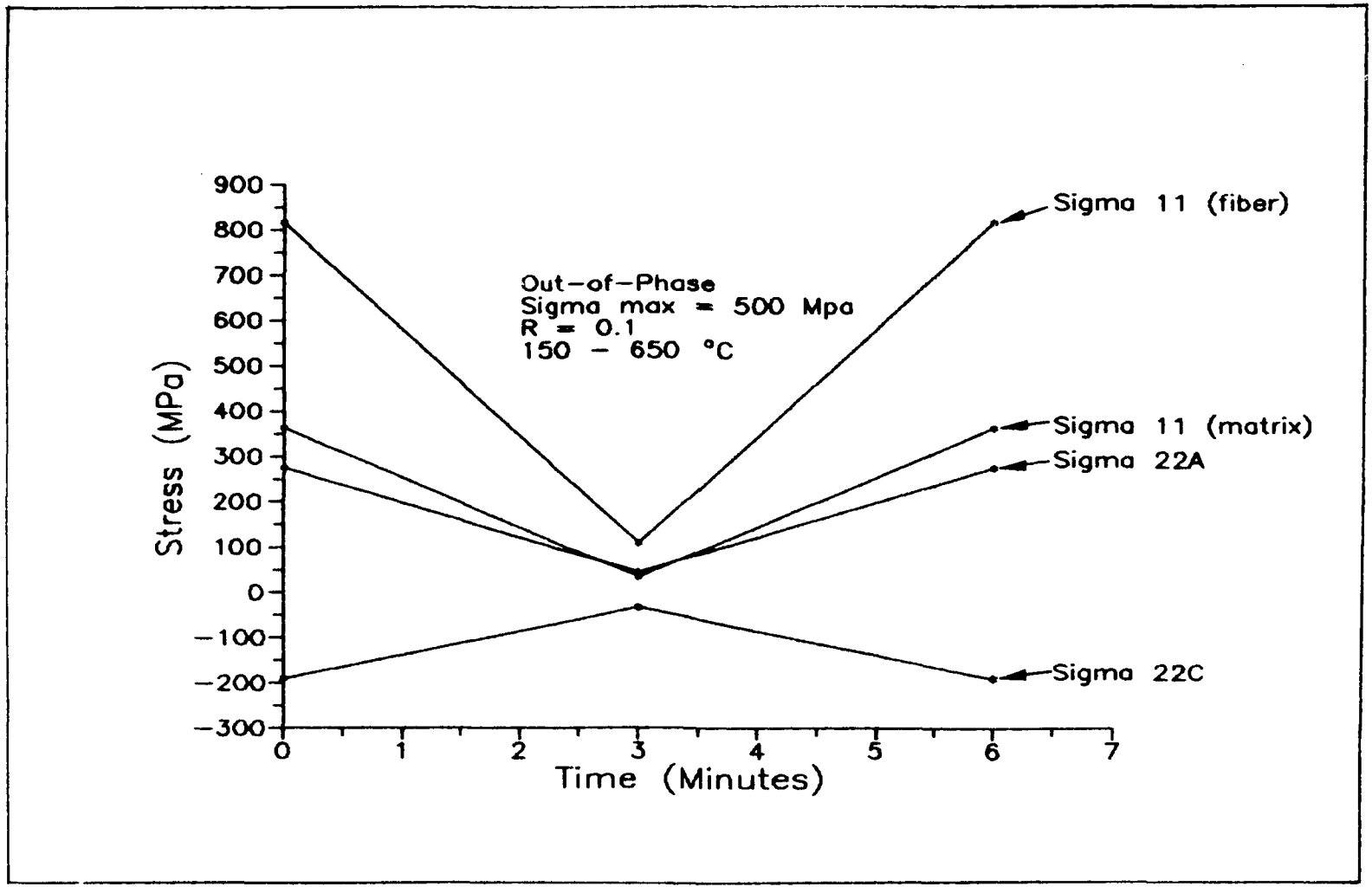

Figure 25 Stresses Throughout One Out-of-Phase Cycle

produced by thermal expansion mismatch, the tensile stresses in the matrix and the compressive stresses in the fiber were at a maximum. This condition resulted in maximum longitudinal stresses in the matrix. This was because the matrix stresses produced by the mechanical loading added to the stresses produced by the thermal expansion mismatch. In addition, the longitudinal stresses in the fiber were minimized. The compressive stresses in the fiber due to the thermal expansion mismatch were subtracted from those produced by the mechanical load.

During in-phase conditions the opposite was true. Since the maximum mechanical load was applied at the maximum temperature, the in-phase conditions maximized the longitudinal stresses in the fiber while minimizing these same stresses in the matrix. The matrix stresses produced by the mechanical loading still added to those produced by the thermal expansion mismatch. However, the thermal stresses were at a minimum instead of a maximum. This resulted in minimum longitudinal stresses in the matrix. The total stresses in the fiber were still found by subtracting the compressive stresses due to the thermal expansion mismatch from the tensile stresses produced by the mechanical load, but the compressive stresses are at a minimum. This resulted in maximum longitudinal stresses in the fiber.

Basically, during in-phase test conditions the fiber experiences high stress levels and during out-of-phase conditions the matrix experiences the high stress levels instead. The longitudinal stresses in the matrix are compared from both conditions in Figures 26 and the longitudinal stresses in the fiber in Figure 27. The stresses shown in the figures are for a 500 MPa mechanical load cycle. However, the results can be generalized to any of the test cycles utilized for this study.

Thermo-mechanical Stresses Related to Fatigue Life

As previously discussed, for a given stress level an out-of-phase test specimen fails sooner than its respective in-phase counterpart. METCAN2 analysis of the constituent stresses revealed that the longitudinal stress increased in the matrix and decreased in the fiber for out-of-phase test conditions when compared to in-phase conditions. The transverse stresses were equal for both conditions. Accordingly, it has been suggested that the increase in the longitudinal stress in the matrix caused the decrease in fatigue life observed.

In order to check this assumption, two types of fatigue life curves were plotted for the longitudinal stress in the matrix calculated by METCAN2 (Figures 28 and 29). The first type plotted the maximum value of the respective stress versus the number of cycles to failure for each test. The

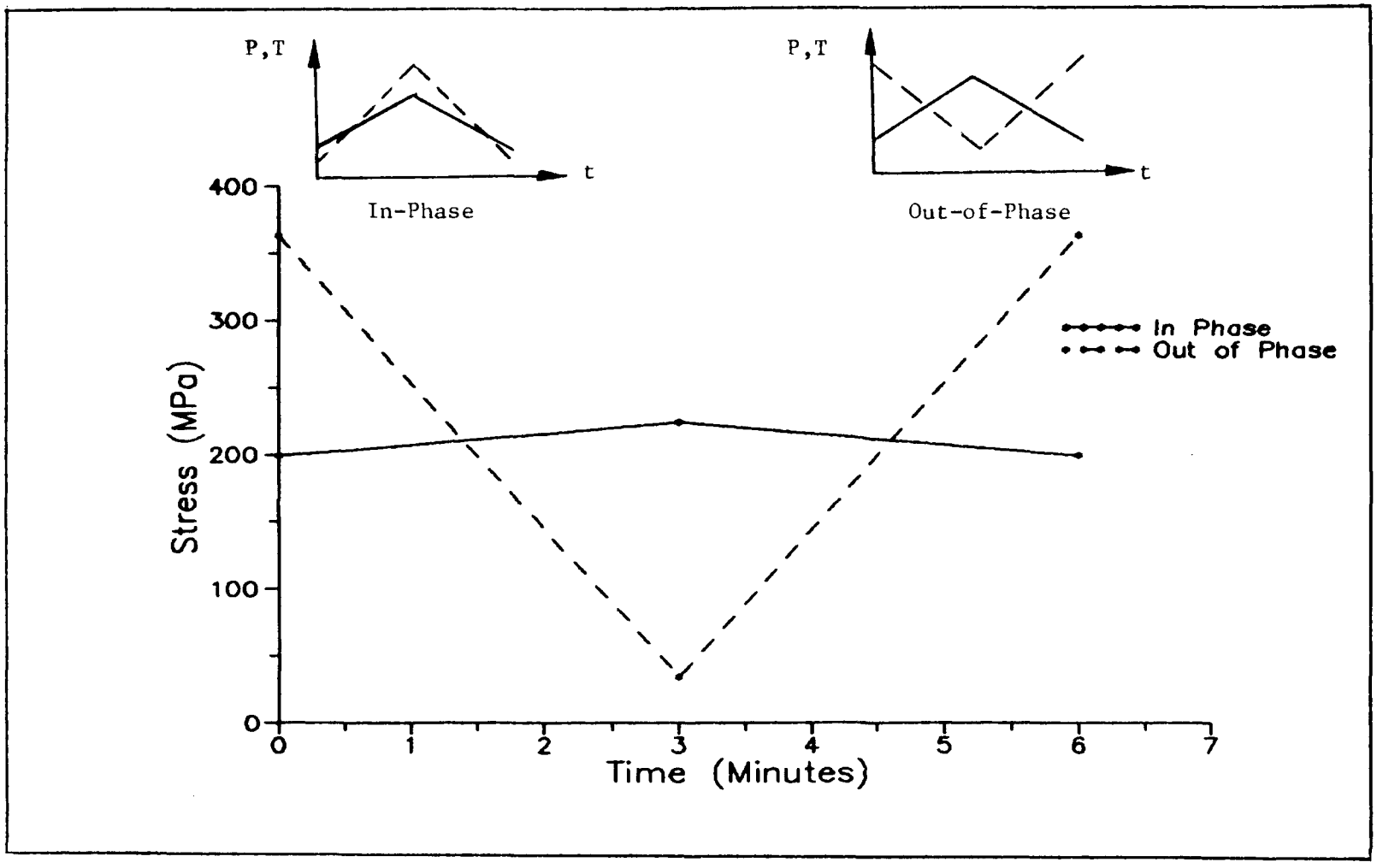

Figure 26 Comparison of Sigma 11 (in matrix) Between In-Phase and Out-of-Phase Cycles (Sigma max = 500 MPa, R = 0.1, 150-650 °C)

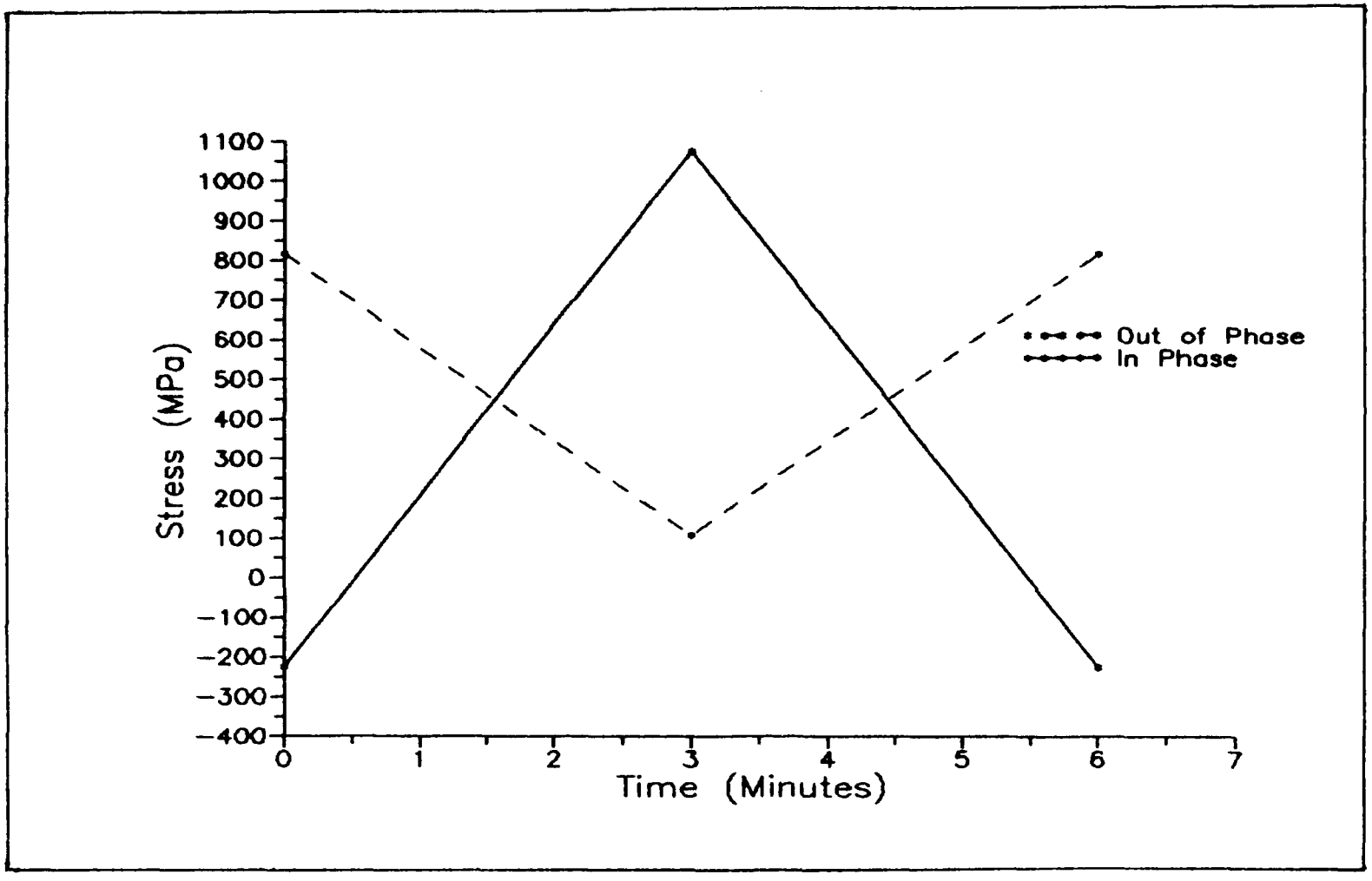

Figure 27 Comparison of Sigma 11 (in fiber) Between In-Phase and Out-of-Phase Cycles (Sigma max = 500 MPa, R = 0.1, 150-650 °C)

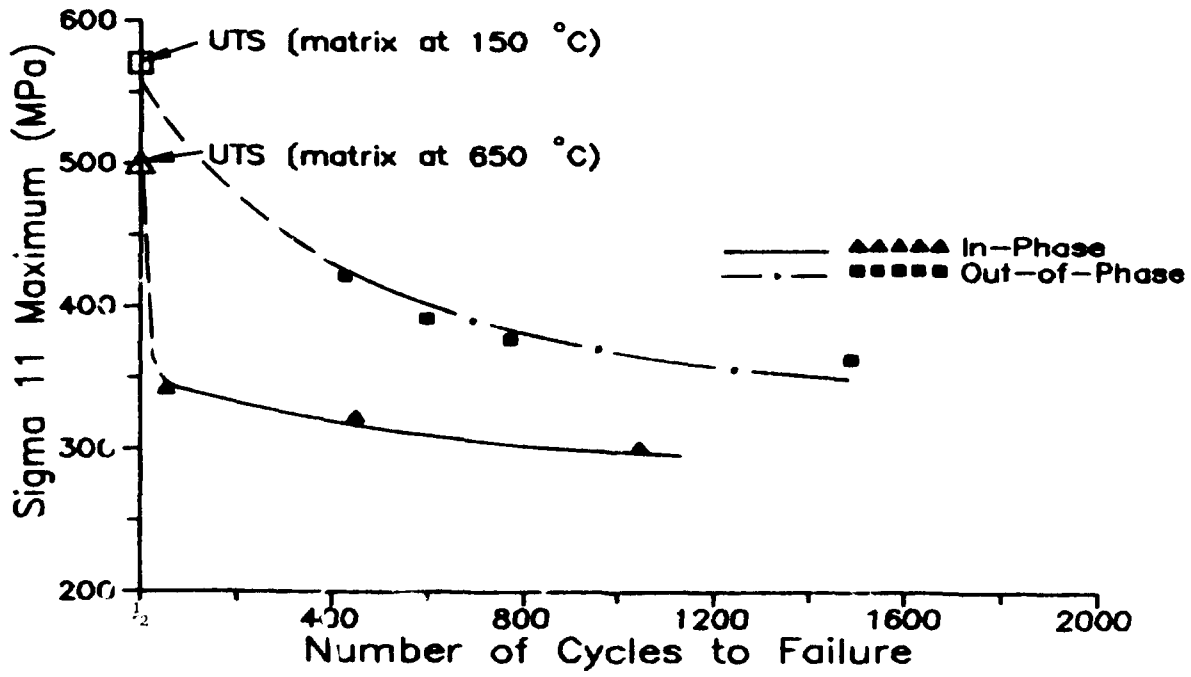

Figure 28A Sigma 11A Maximum (in matrix) Versus Number of Cycles to Failure from In-Phase and Out-of-Phase Test Conditions

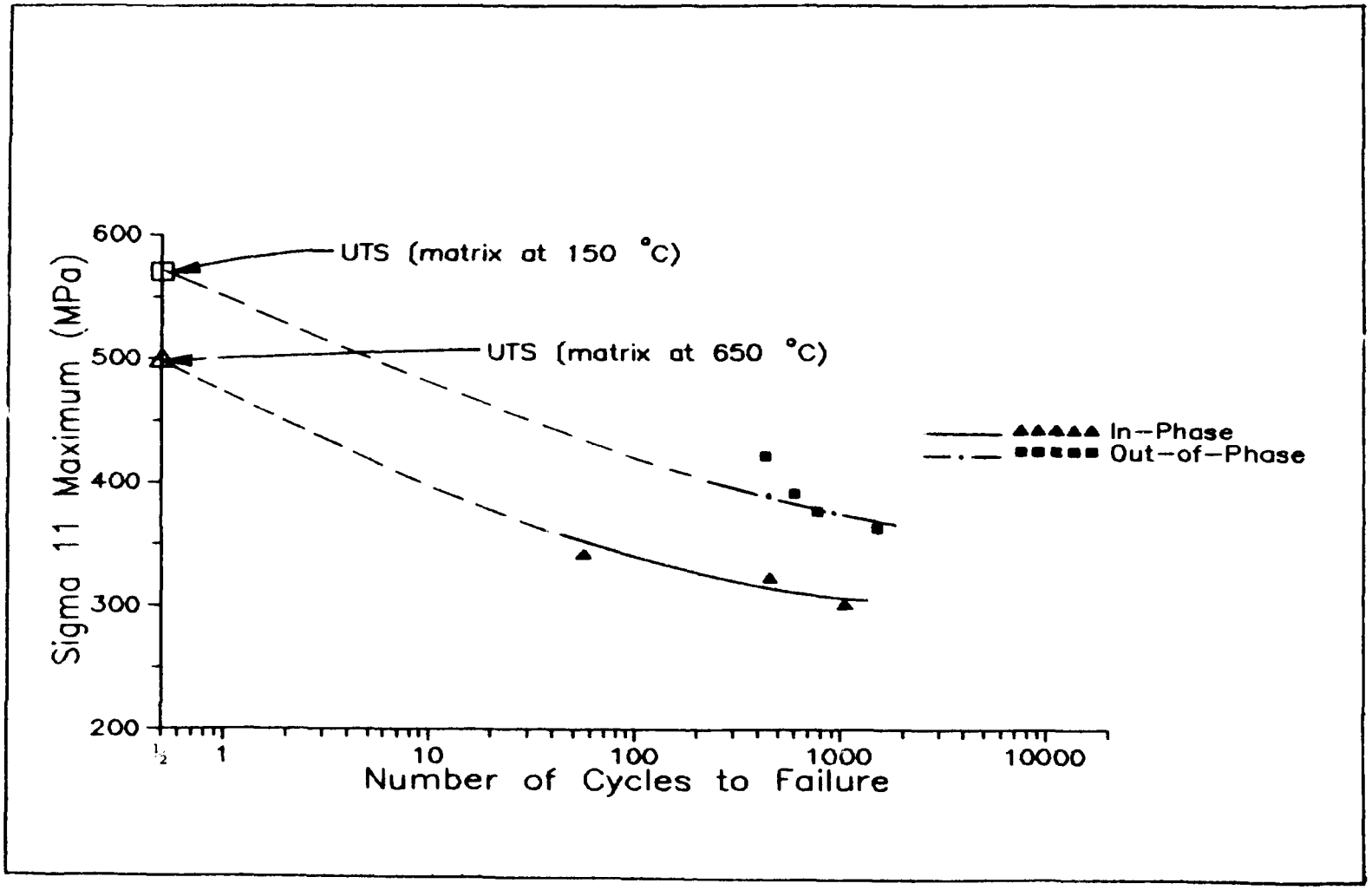

Figure 28B Sigma 11 Maximum (in matrix) Versus Number of Cycles to Failure from In-Phase and Out-of-Phase Test Conditions

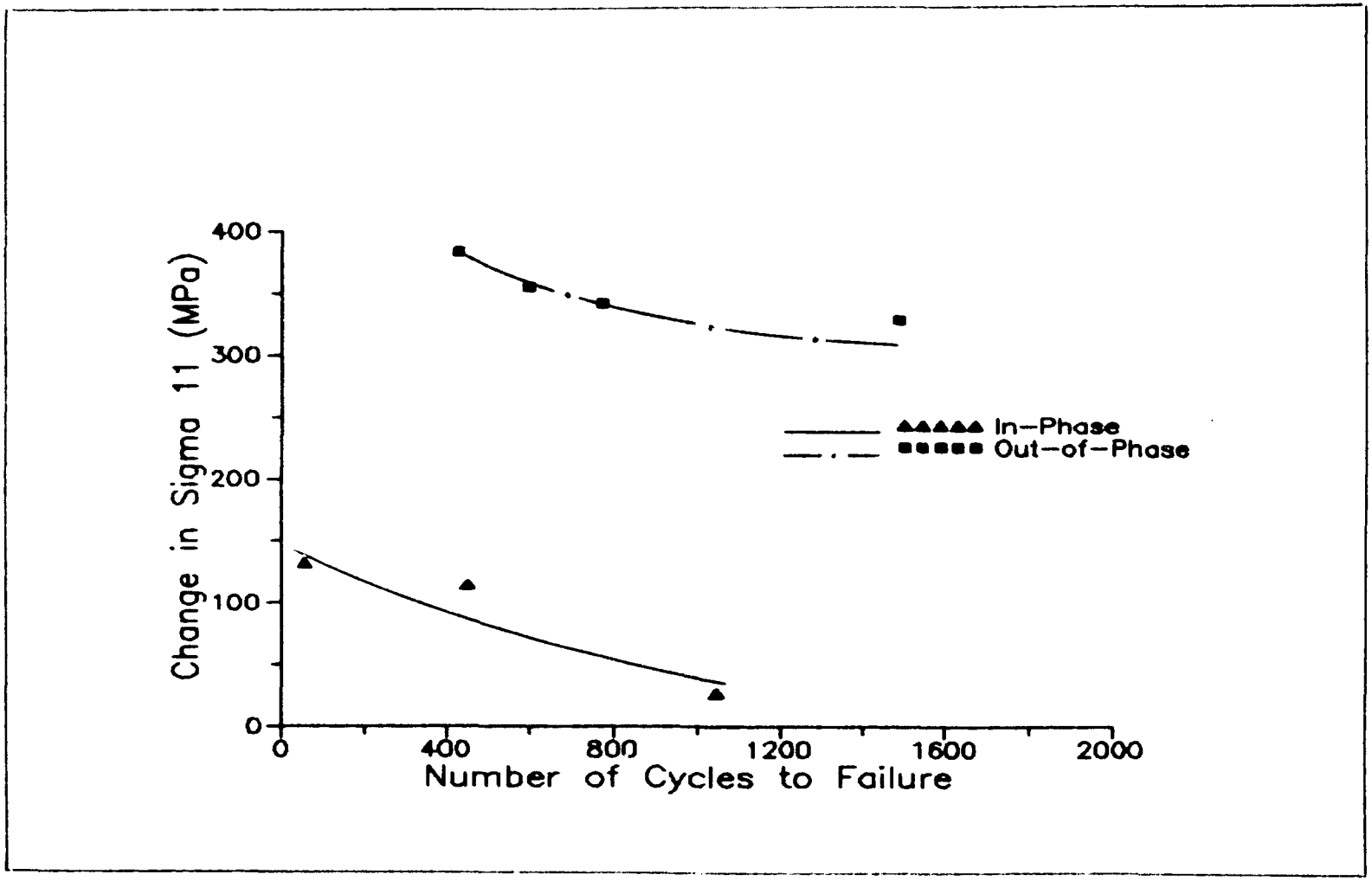

Figure 29A Change in Sigma 11 (in matrix) Versus Number of Cycles to Failure from In-Phase and Out-of-Phase Test Conditions

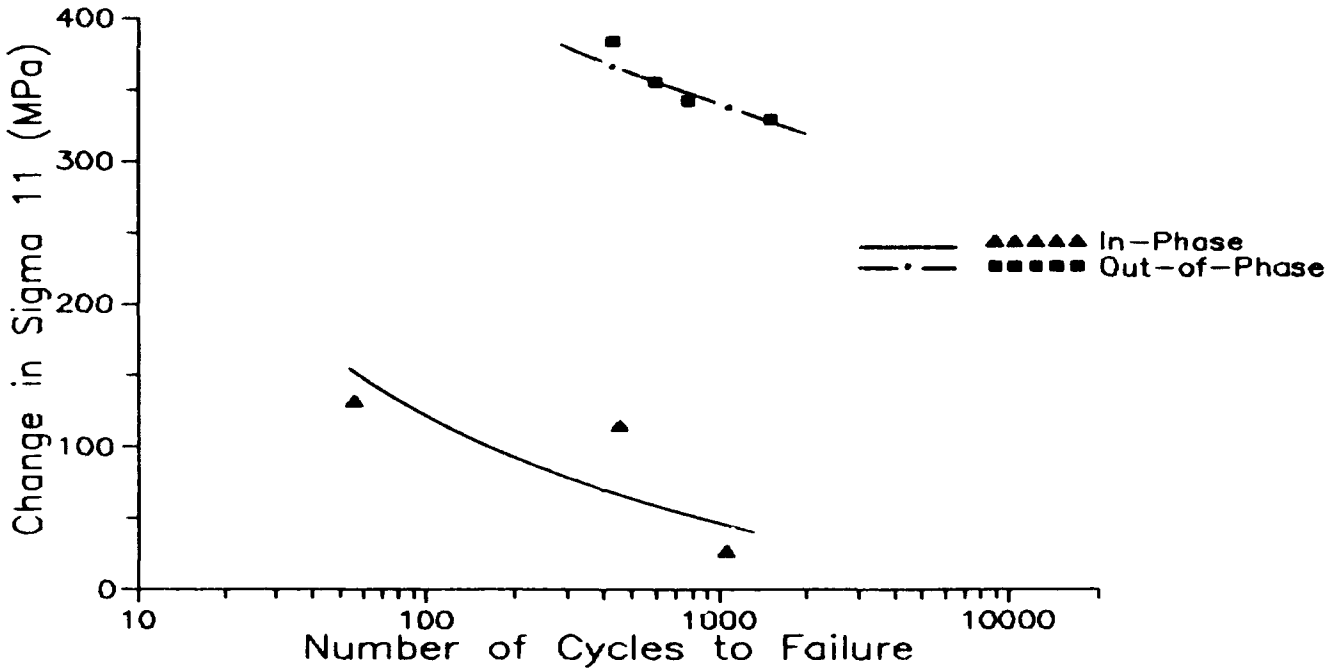

Figure 29B Change in Sigma 11 (in matrix) Versus Number of Cycles to Failure from In-Phase and Out-of-Phase Test Conditions

second type plotted the maximum change in the same stress versus the number of cycles to failure for each test. If either σ_{11} maximum or σ_{11} controlled the changes in fatigue life their respective plots from both the in-phase and out-of-phase tests should show a trend and reduce to a single line. As can be seen in the figures, they do not. This indicates that σ_{11} in the matrix is not controlling the changes observed in fatigue life.

In addition, the longitudinal stresses in the fiber were plotted versus the number of cycles to failure following the same procedures, as outlined above, for the matrix. The plots are shown in Figures 30 and 31. Again the plots show no trends indicating that σ_{11} in the fiber is controlling the changes in fatigue life.

Since, neither σ_{11} in the matrix or fiber controls the changes in fatigue life observed, the fatigue life must be governed by some combination of both.

Comparison to Existing Theory

In the following discussion the results of the thermo-mechanical testing are compared to existing failure theory. At the present time established failure theory exists only for polymer composites subjected to tensile fatigue testing. The is because metal matrix composites are new and failure theory concerning the thermo-mechanical fatigue of them has not yet developed.

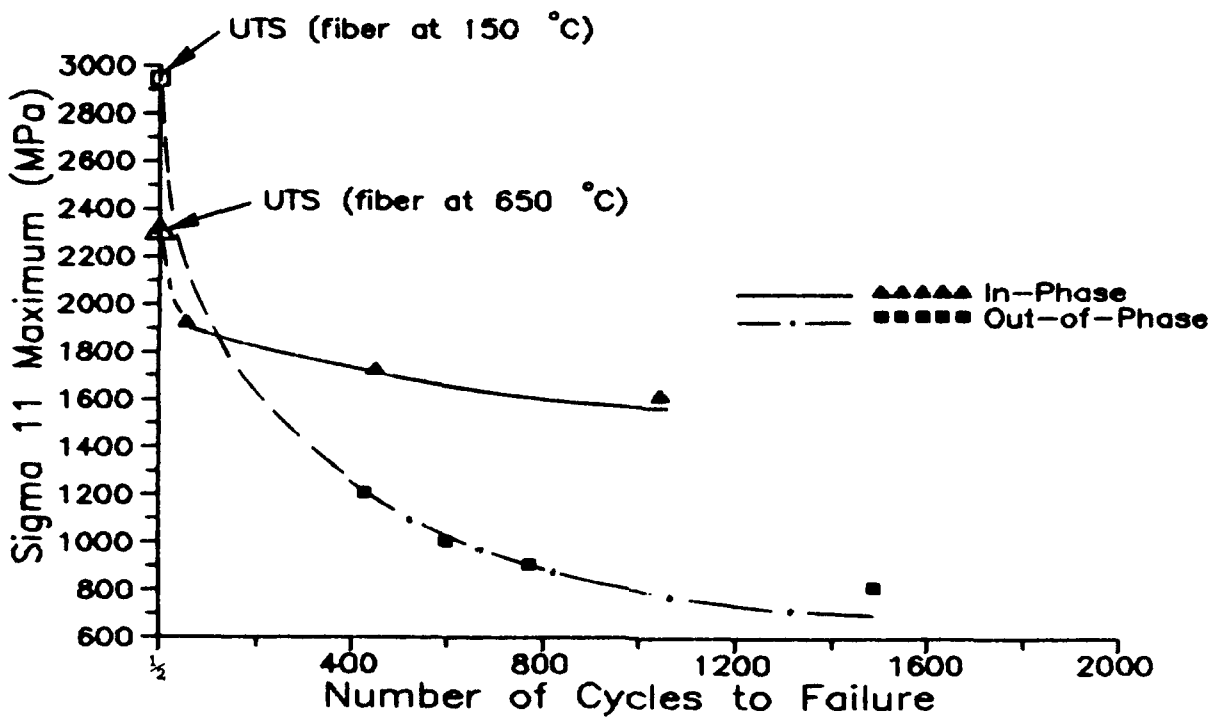

Figure 30A Sigma 11 Maximum (in fiber) Versus Number of Cycles to Failure from In-Phase and Out-of-Phase Test Conditions

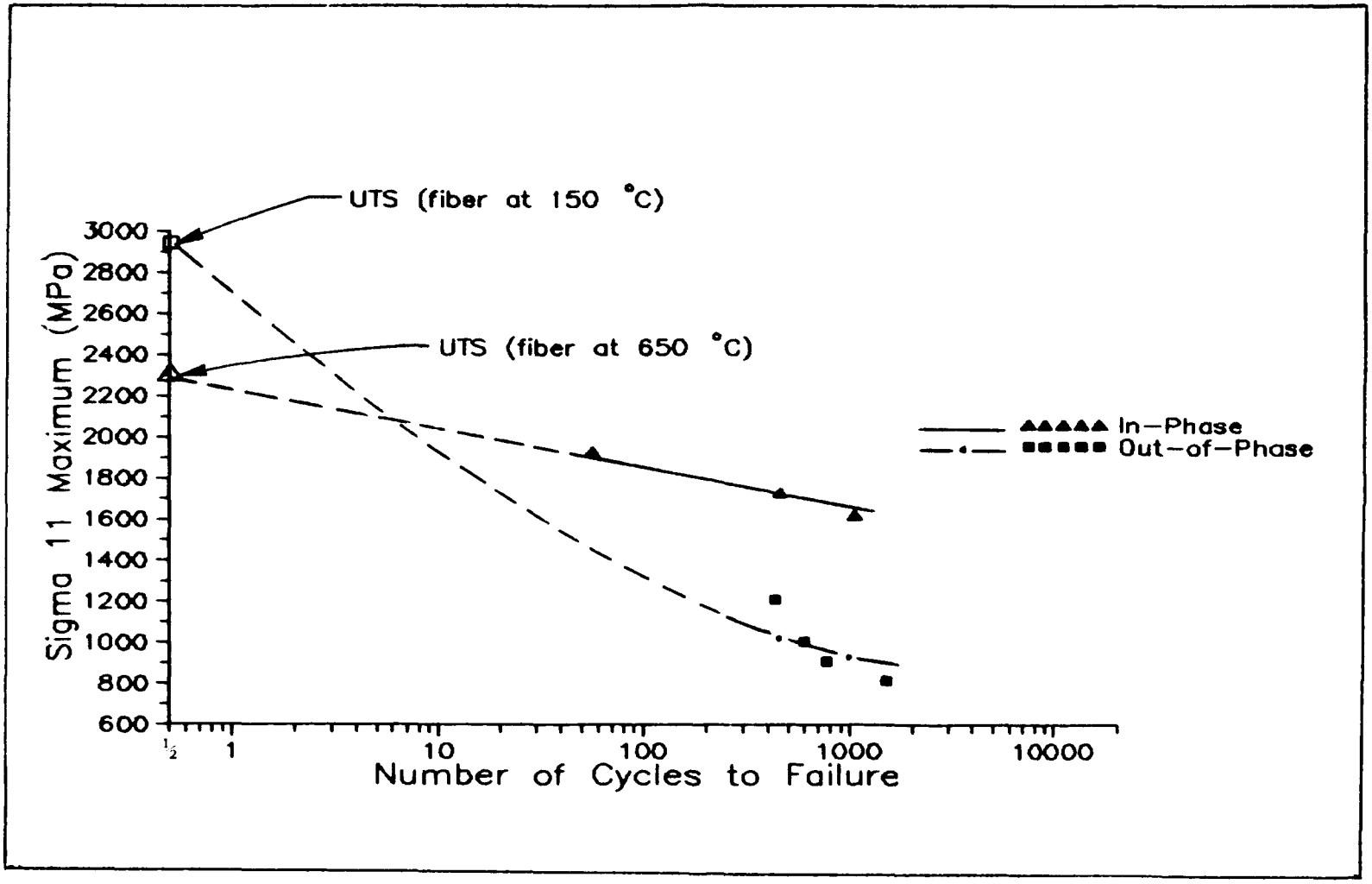

Figure 30B Sigma 11 Maximum (in fiber) Versus Number of Cycles to Failure from In-Phase and Out-of-Phase Test Conditions

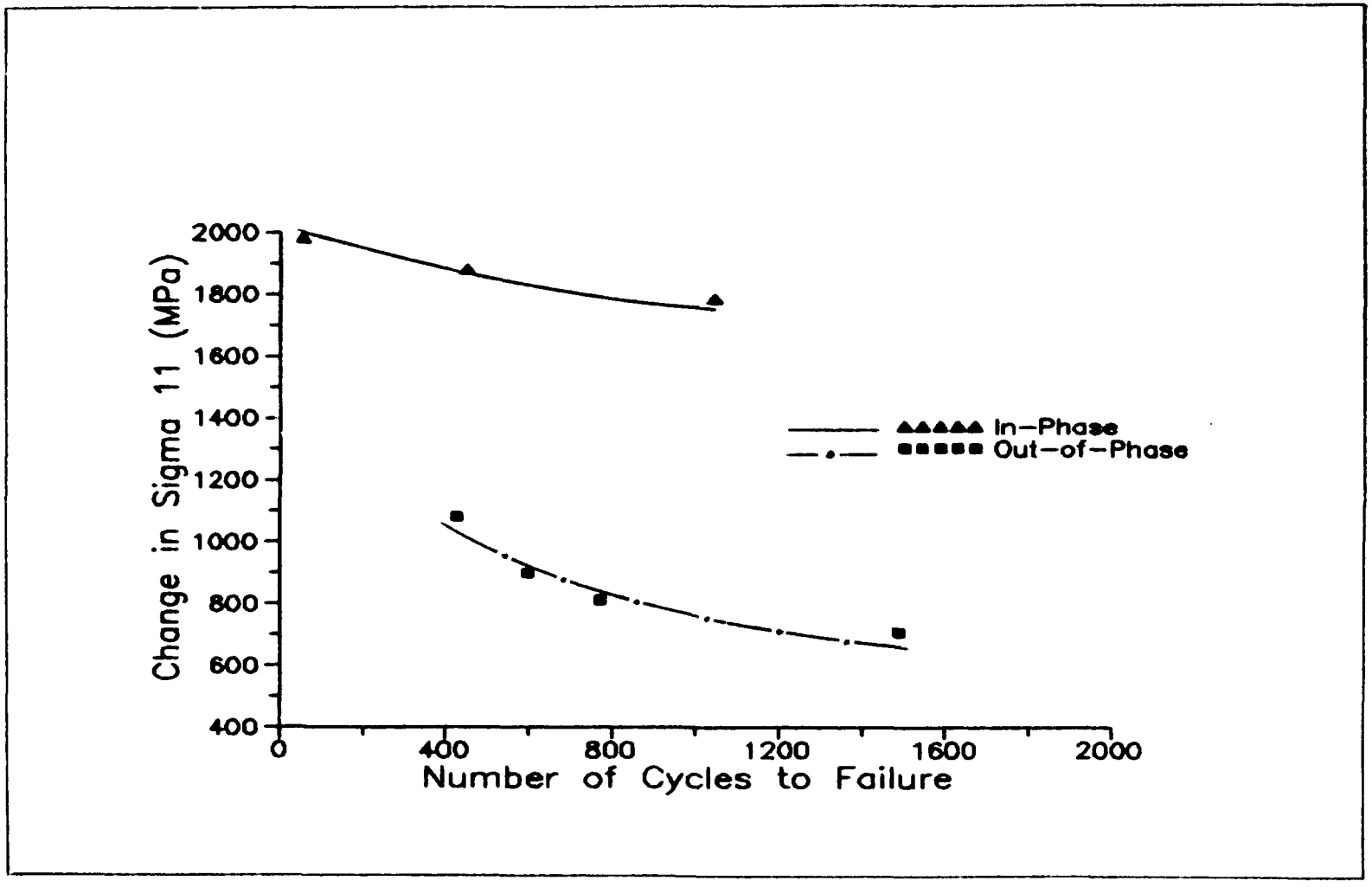

Figure 31A Change in Sigma 11 (in fiber) Versus Number of Cycles to Failure from In-Phase and Out-of-Phase Test Conditions

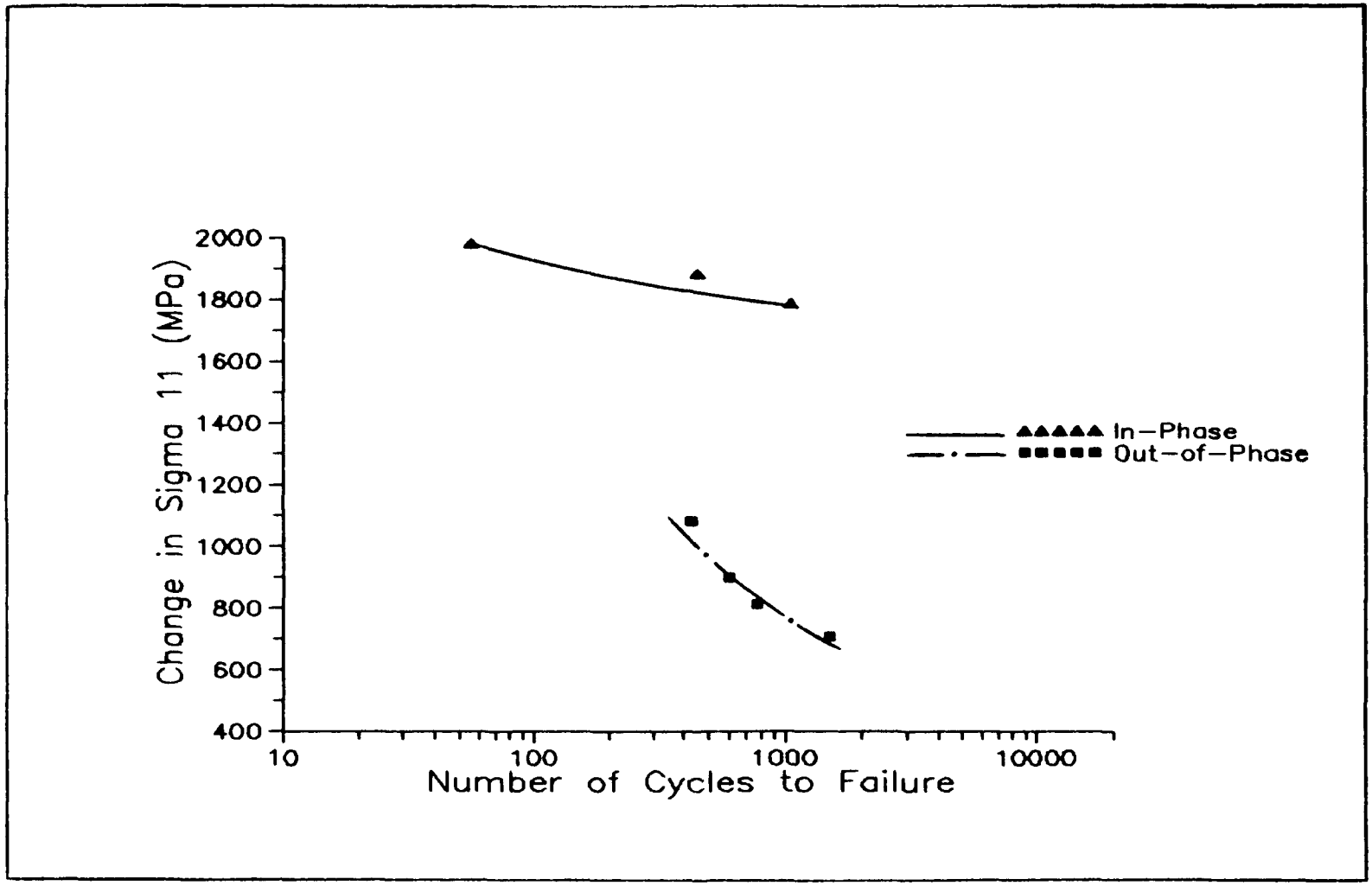

Figure 31B Change in Sigma 11 (in fiber) Versus Number of Cycles to Failure from In-Phase and Out-of-Phase Test Conditions

An empirical fatigue life diagram for tensile fatigue of unidirectional polymer composites is shown in Figure 32. In the figure strain is plotted versus the logarithm of the number of cycles to failure. The fatigue life curve has different regions, each corresponding to different underlying damage mechanisms.

The horizontal band at the top of the figure corresponds to a region dominated by fiber breakage. Fiber breakage occurs at stresses (strains) above the strength of the weakest fiber in the composite. On the first application of the maximum stress, fibers whose strengths are below the applied stress break. Repeated application results in additional broken fibers. This process continues for only a few cycles until final failure occurs.

The sloping band in the middle of the figure represents a region dominated by matrix cracking and interfacial shear failure. Cracking originates in the matrix when the applied cyclic stress (strain) exceeds the fatigue limit in the matrix. At low stresses a crack originating in the matrix will stop at the interface. While at higher stresses, the stress at the crack tip exceeds the fracture strength of the fibers and leads to fiber failure. After the fiber fails, the matrix crack now propagates under fatigue in the opening mode as a macrocrack until it hits an interface. The shear stresses at the interface then propagate the crack at the interface in the sliding mode, leading to progressive

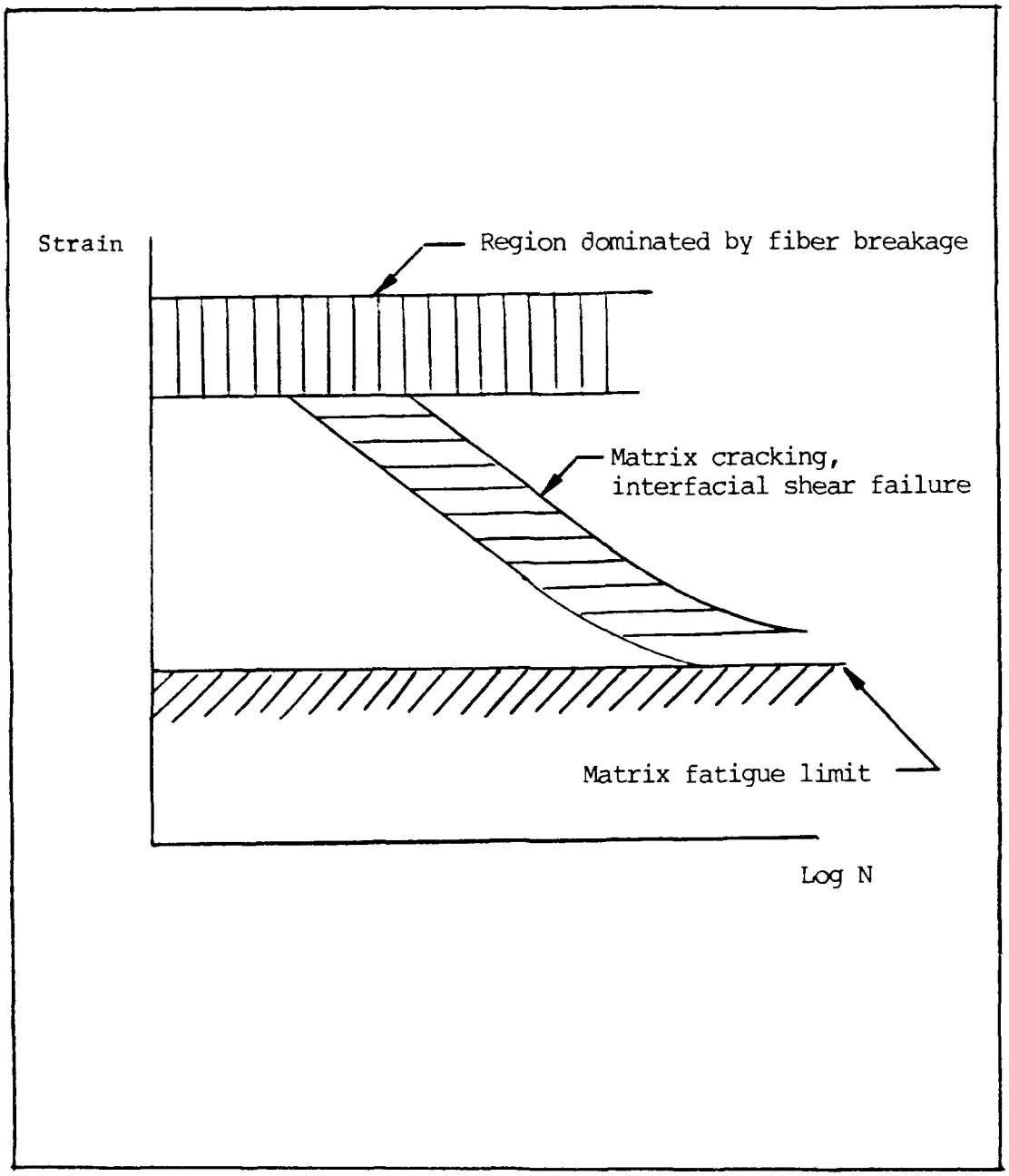

Figure 32 Empirical Fatigue Life Diagram

failure of the interface. Thus, the failure initiation and propagation is dependent upon the stresses in both the fiber and matrix, as well as, the shear stress at the interface.

The horizontal line at the bottom of the diagram represents the fatigue limit of the matrix. Because damage progression is matrix dependent, its initiation depends upon the endurance limit of the matrix. At stresses (strains) below the endurance limit of the matrix fatigue damage does not occur.

Fatigue life plots of the results from both the in-phase and the out-of-phase tests compare to the region previously discussed that corresponded to matrix cracking and interfacial shear failure. Figure 33 is a plot of the maximum longitudinal stress in the fiber versus the number of cycles to failure for both the in-phase and out-of-phase tests. The figure suggests that the plots from both the in-phase and out-of-phase tests converge at some higher stress where the failure becomes fiber dominated.

Figure 34 is a plot of the maximum longitudinal stress in the matrix versus the number of cycles to failure from both the in-phase and out-of-phase tests. The figure suggests that the plots from both tests may converge at the endurance limit of the matrix. Therefore, the results from the in-phase and out-of phase tests appear to be in the middle region dominated by matrix cracking and interfacial shear failure.

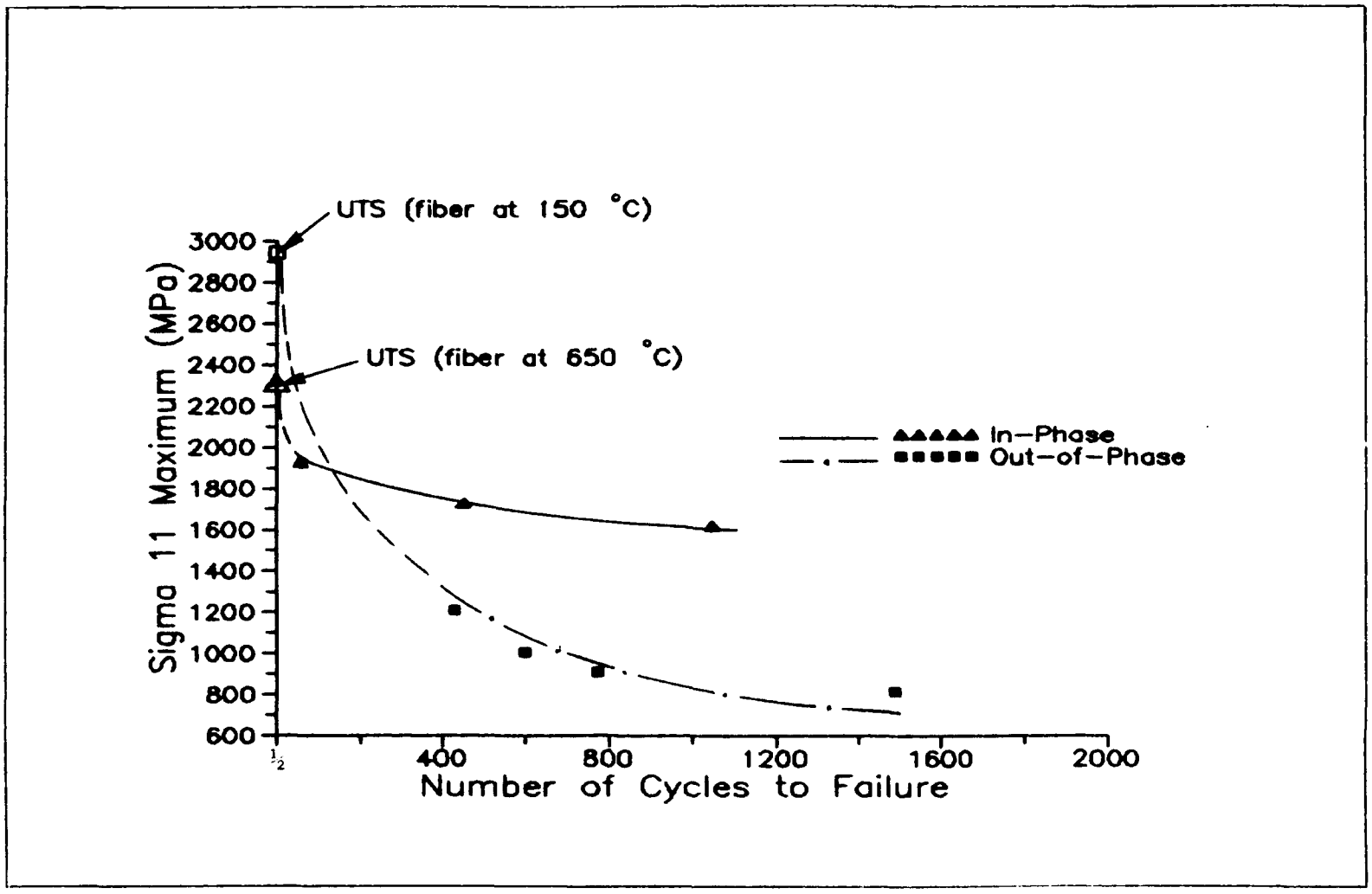

Figure 33A Possible Fiber Dominated Region for In-Phase and Out-of-Phase Test Conditions

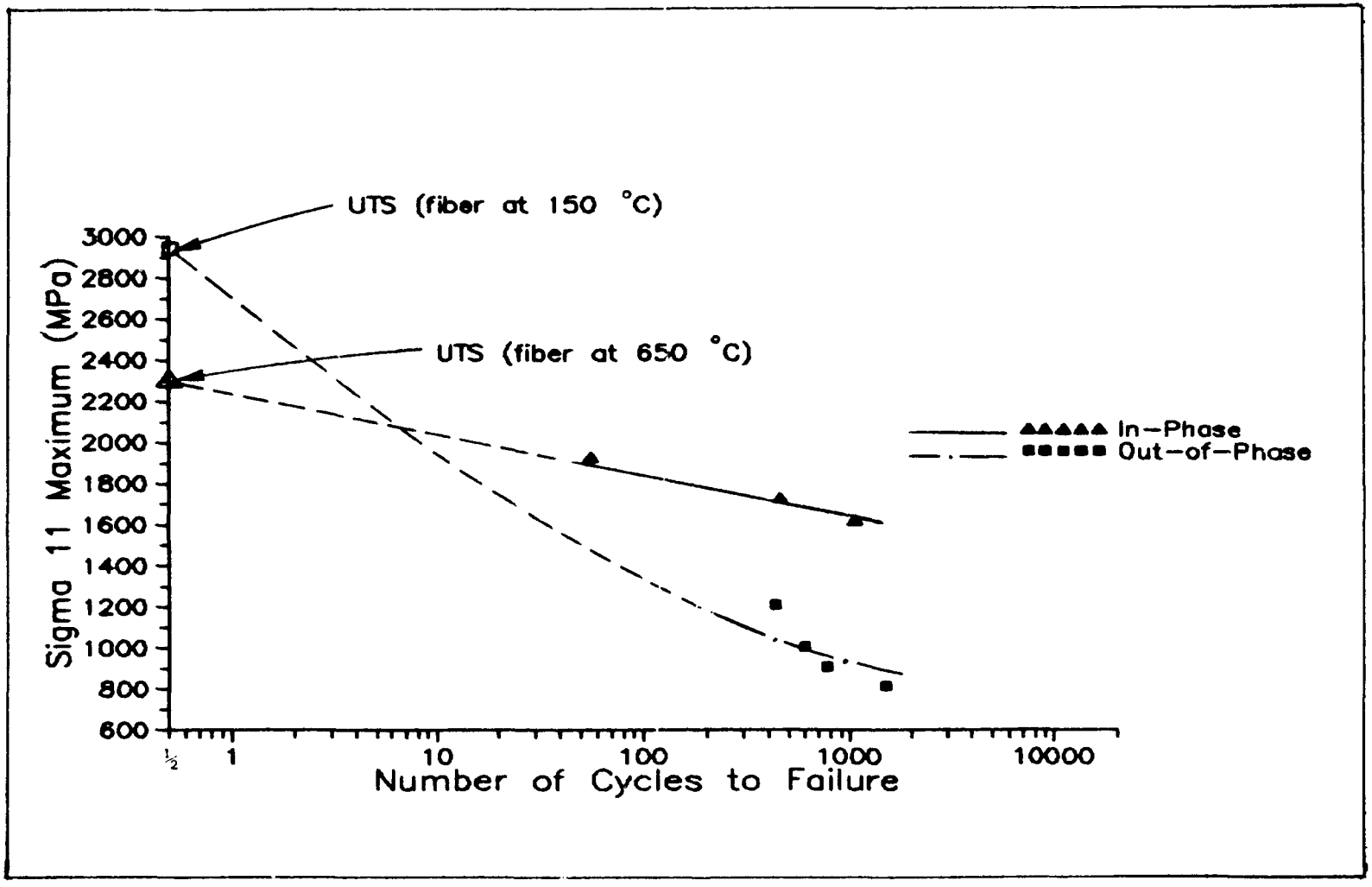

Figure 33B Possible Fiber Dominated Region for In-Phase and Out-of-Phase Test Conditions

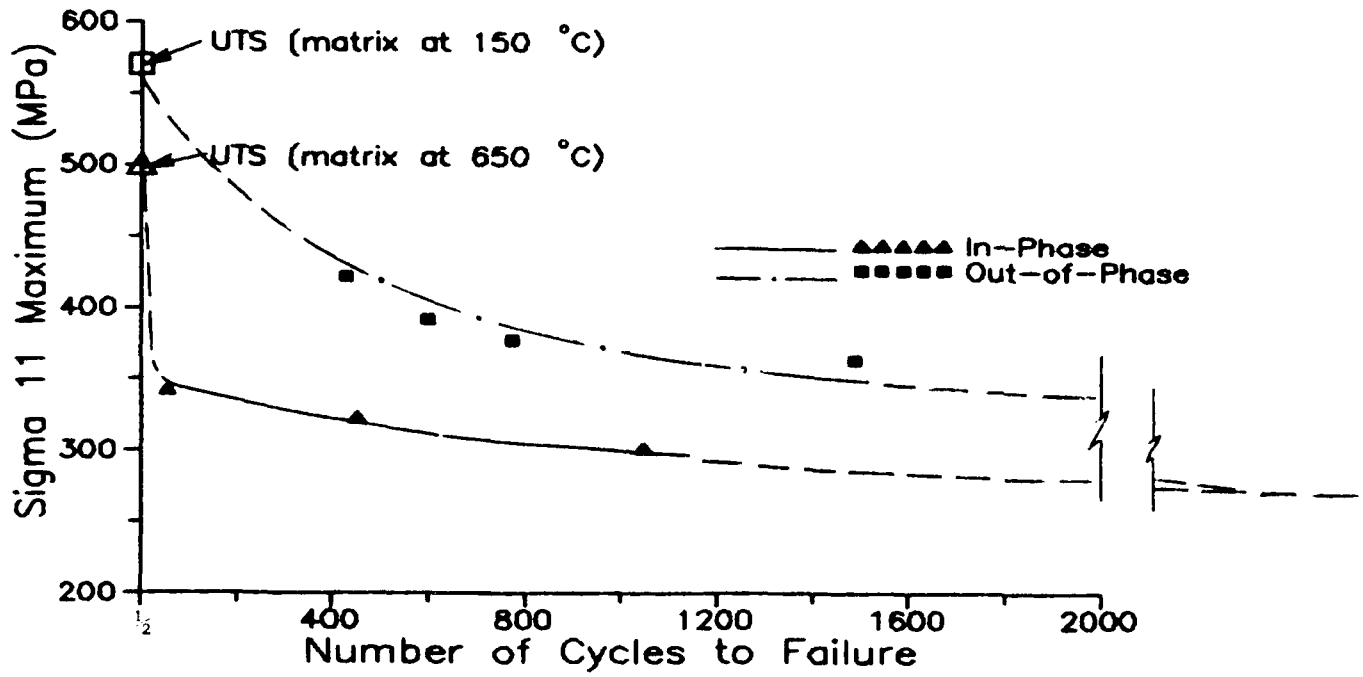

Figure 34A Possible Matrix Dominated Region for In-Phase and Out-of-Phase Test Conditions

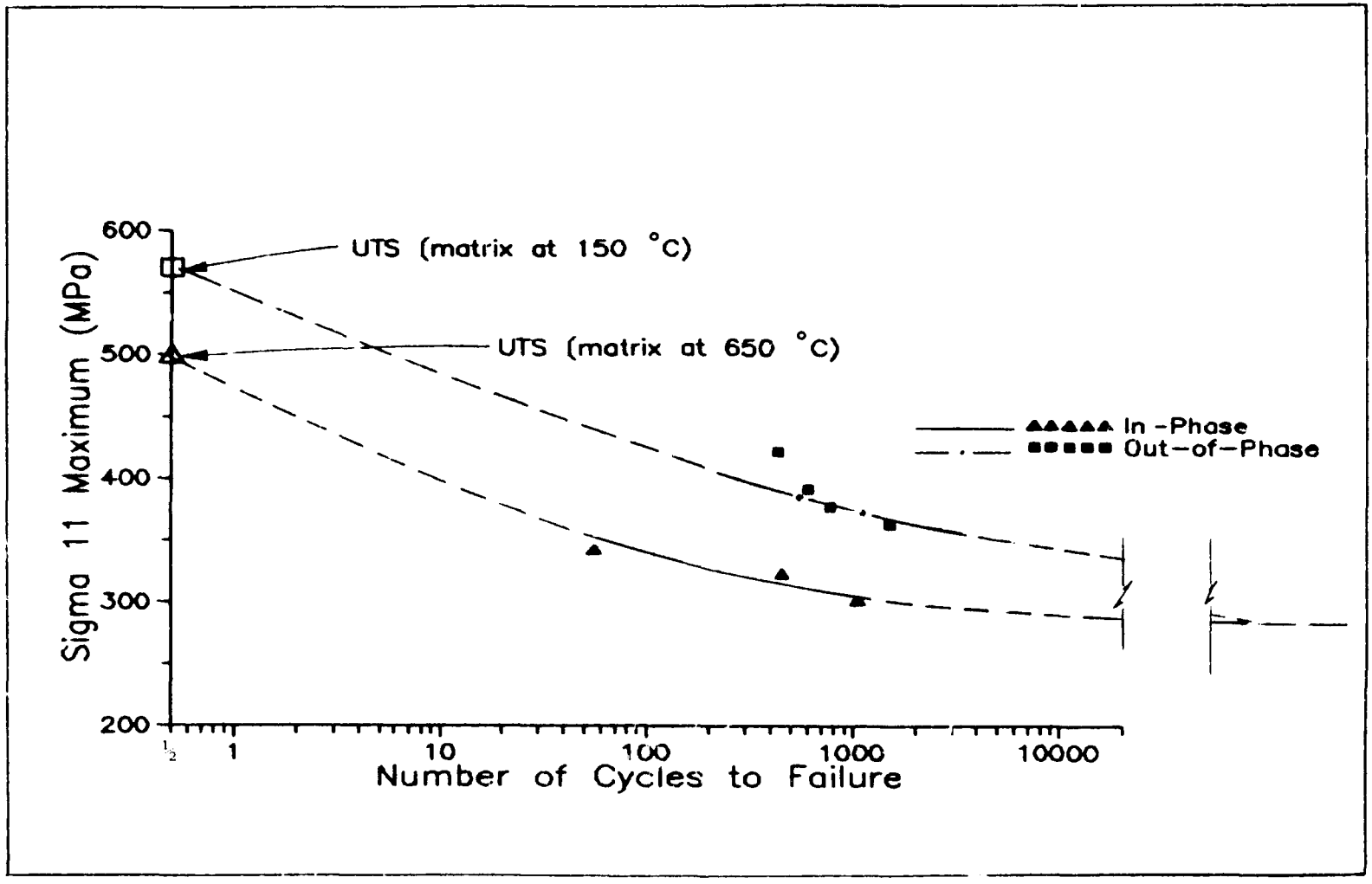

Figure 34B Possible Matrix Dominated Region for In-Phase and Out-of-Phase Test Conditions

Additional testing is needed in order to complete the plots and determine whether or not this is a valid conclusion. Also, crack initiation and progression in the matrix appears to be different for thermo-mechanical fatigue when compared to the tensile fatigue of polymer composites. In the out-of-phase thermo-mechanical case previously discussed, cracking originated at the interface and progressed into the matrix. This is exactly the opposite of what happens in tensile fatigue of polymer composites.

Comparison to Other Thermo-mechanical Fatigue Data

Additionally, the results from the in-phase and out-of-phase tests were compared to other data taken from constant load and isothermal testing. This data was obtained from the Air Force Wright Research and Development Center (9). A summary of the test conditions is shown in Figure 35. During constant load testing the mechanical load was held constant and the thermal load was varied between 150 - 650 °C using a triangular wave profile and a six minute cycle. During the isothermal tests the temperature was held constant at 650 °C and the mechanical load was varied using a triangular wave profile and a six minute cycle. The ratio of the minimum to the maximum mechanical stress was 0.1. The in-phase, out-of-phase, constant load, and isothermal tests are of interest because they are closely related.

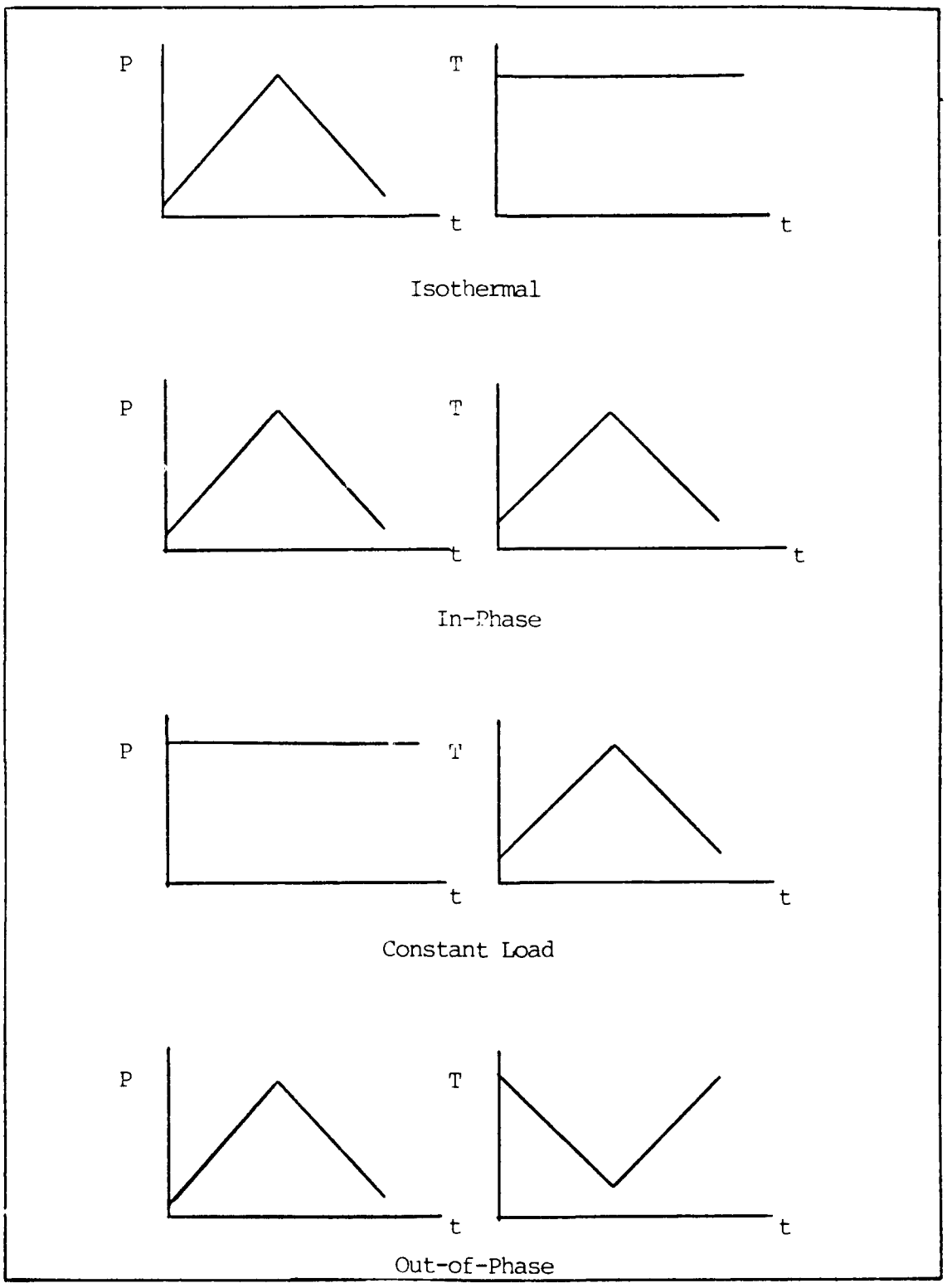

Figure 35 Summary of Various Test Conditions

A fatigue life curve for all four tests is shown in Figure 36. The results are summarized in Table VI. The figure reveals that for a given mechanical load the isothermal test had the longest fatigue life. This was followed by the in-phase test, then the constant load test, and finally the out-of-phase test which had the shortest fatigue life.

METCAN2 was again used to calculate the stresses that occurred throughout the various test cycles. As previously discussed for the in-phase and out-of-phase tests, fatigue life curves were constructed and used to compare the tests. Two types of plots were again constructed. The first type plotted σ_{11} maximum versus the number of cycles to failure and the second type replaced σ_{11} maximum with $\Delta\sigma_{11}$. All four tests were plotted on the same graph and trends where any of the four plots reduced to a single line were checked for. As before, a trend between plots would indicate that a single stress controlled the changes in fatigue life.

Figure 37 is a plot of σ_{11} maximum in the matrix versus the number of cycles to failure. The figure shows four distinct plots; one for each test condition. A possible exception are the plots from the in-phase and the isothermal tests. The absence of any trends indicates that none of the four test conditions were related by σ_{11} maximum in the matrix

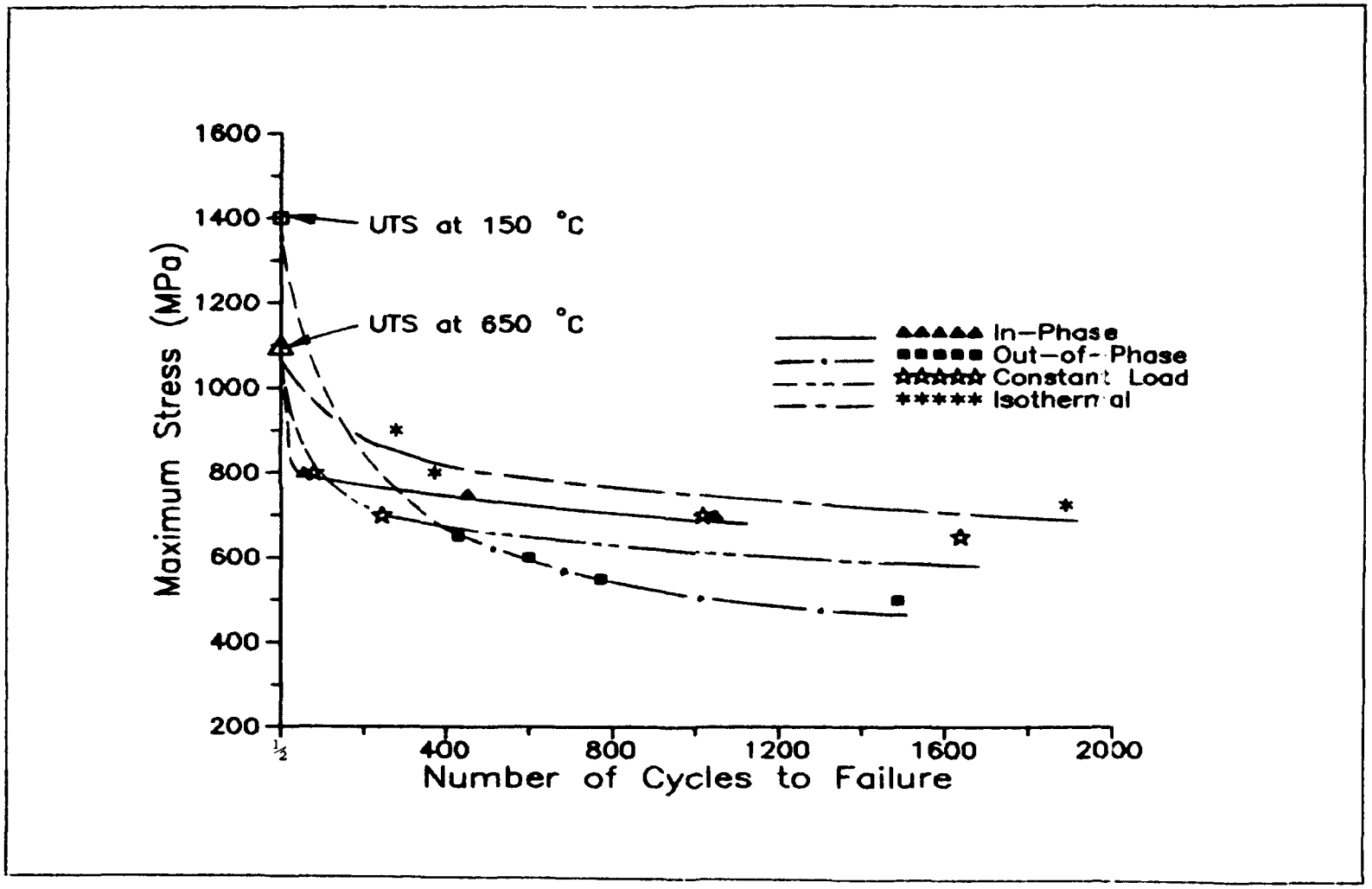

Figure 36A Thermo-mechanical Fatigue Life Results from Various Test Conditions

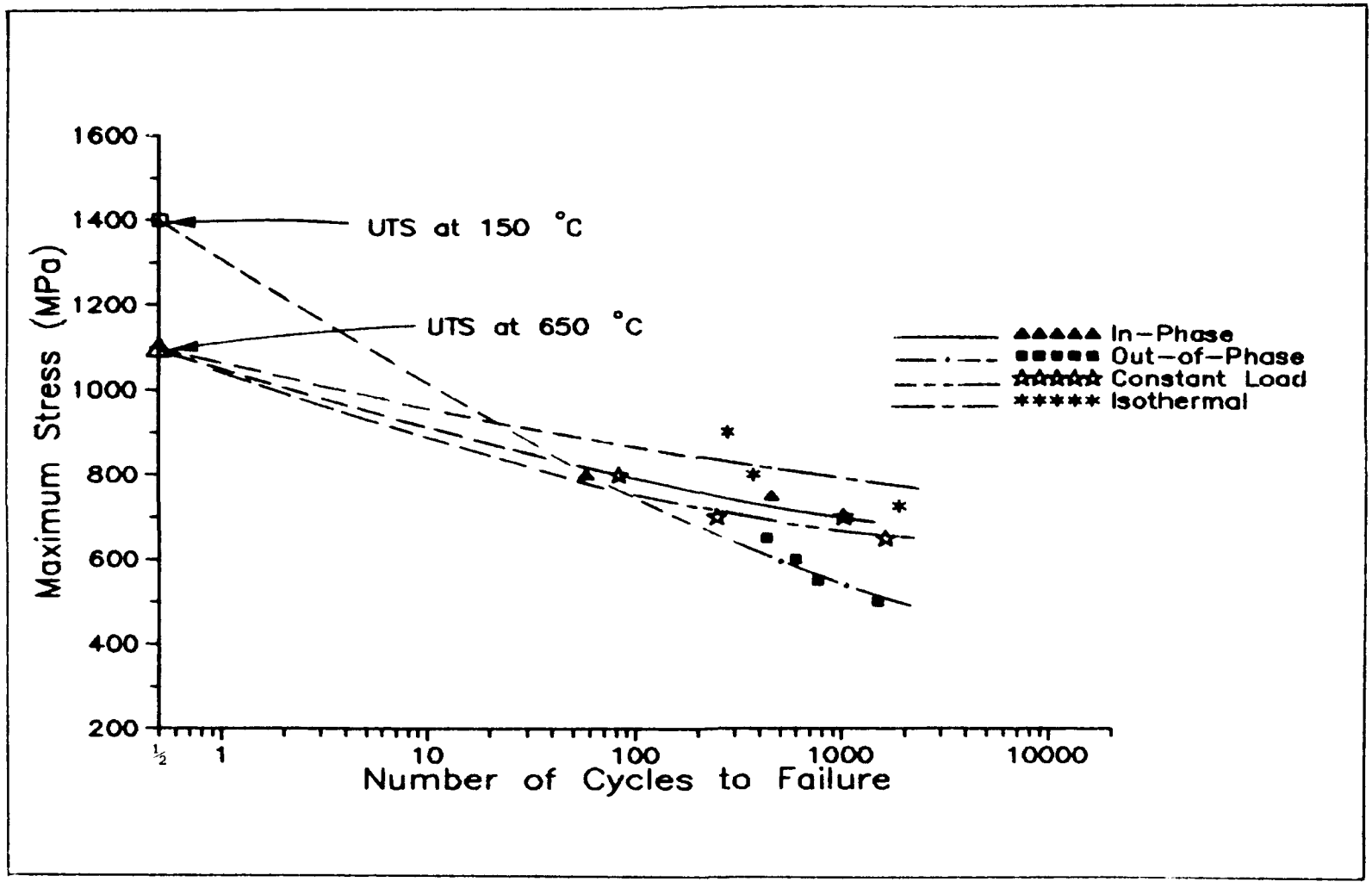

Figure 36B Thermo-mechanical Fatigue Life Results from Various Test Conditions

Table VI. Thermo-mechanical Fatigue Life Results from Various Test Conditions

Test Conditions	Applied Mechanical Stress (MPa)	Number of Cycles to Failure
In-Phase	800	58
	750	451
	700	1046
Out-of-Phase	650	428
	600	598
	550	771
	500	1487
Constant Load	800	83
	700	245
	700	1016
	650	1634
Isothermal	900	280
	800	375
	725	1890

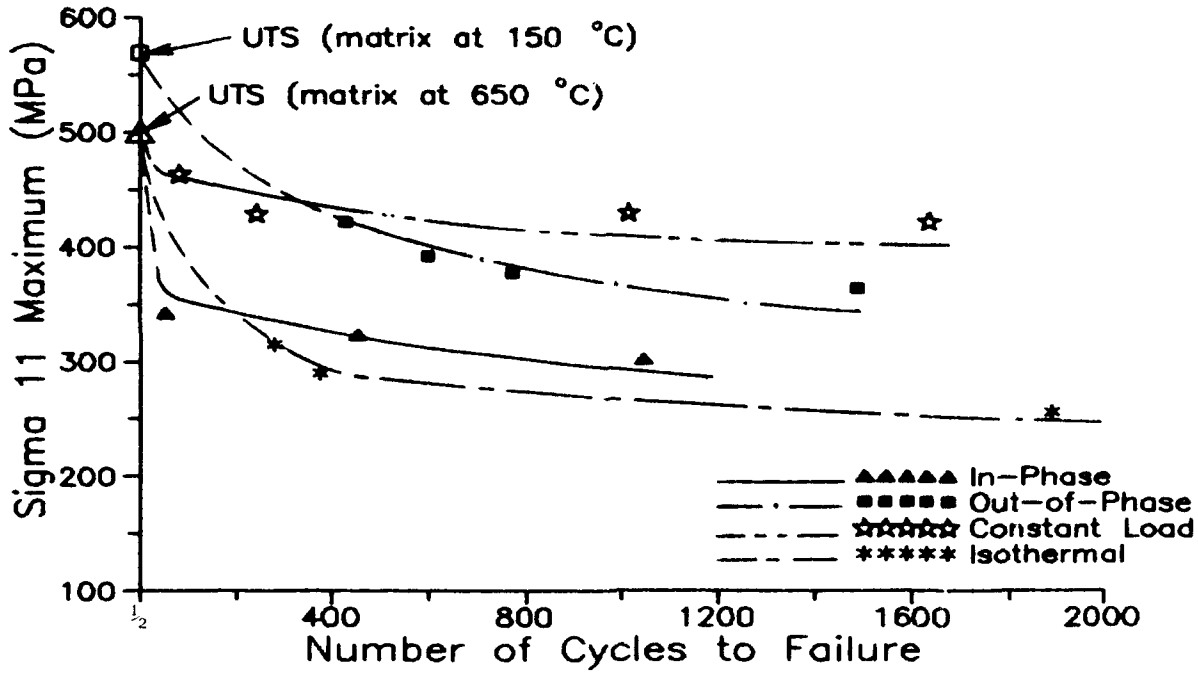

Figure 37A Sigma 11 Maximum (in matrix) Versus Number of Cycles to Failure from Various Test Conditions

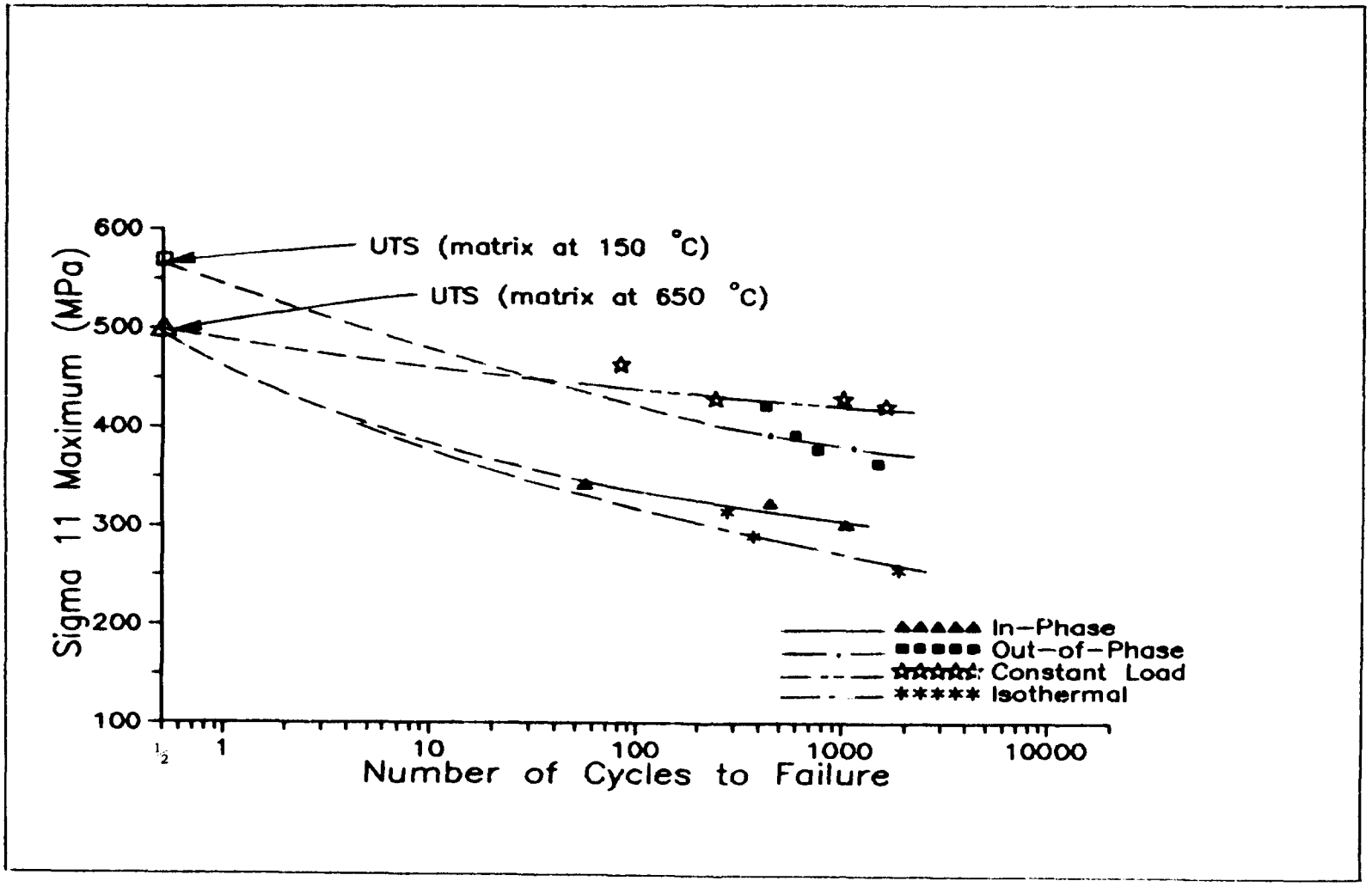

Figure 37B Sigma 11 Maximum (in matrix) Versus Number of Cycles to Failure from Various Test Conditions

Figure 38 is a plot of $\Delta\sigma_{11}$ in the matrix. Again there are no trends in the longitudinal stresses from any of the various test conditions. This is also true for σ_{11} maximum and $\Delta\sigma_{11}$ in the fiber as shown in Figures 39 and 40, respectively.

Figure 41 is a plot of the maximum longitudinal stress in the fiber versus the number of cycles to failure for the isothermal, in-phase, constant load, and out-of-phase tests. This figure suggests that the plots converge from all four tests at some higher stress level where the fatigue life is fiber controlled.

Figure 42 is a plot of the maximum longitudinal stress in the matrix versus the number of cycles to failure for all four tests. The figure suggests that the plots from the tests converge at the endurance limit of the matrix. Again the results appear to correspond to the middle region of Figure 32, as previously discussed. This region corresponds to matrix cracking and interfacial shear failure and the fatigue life is controlled by σ_{11} in both the fiber and matrix and the shear stress at the interface.

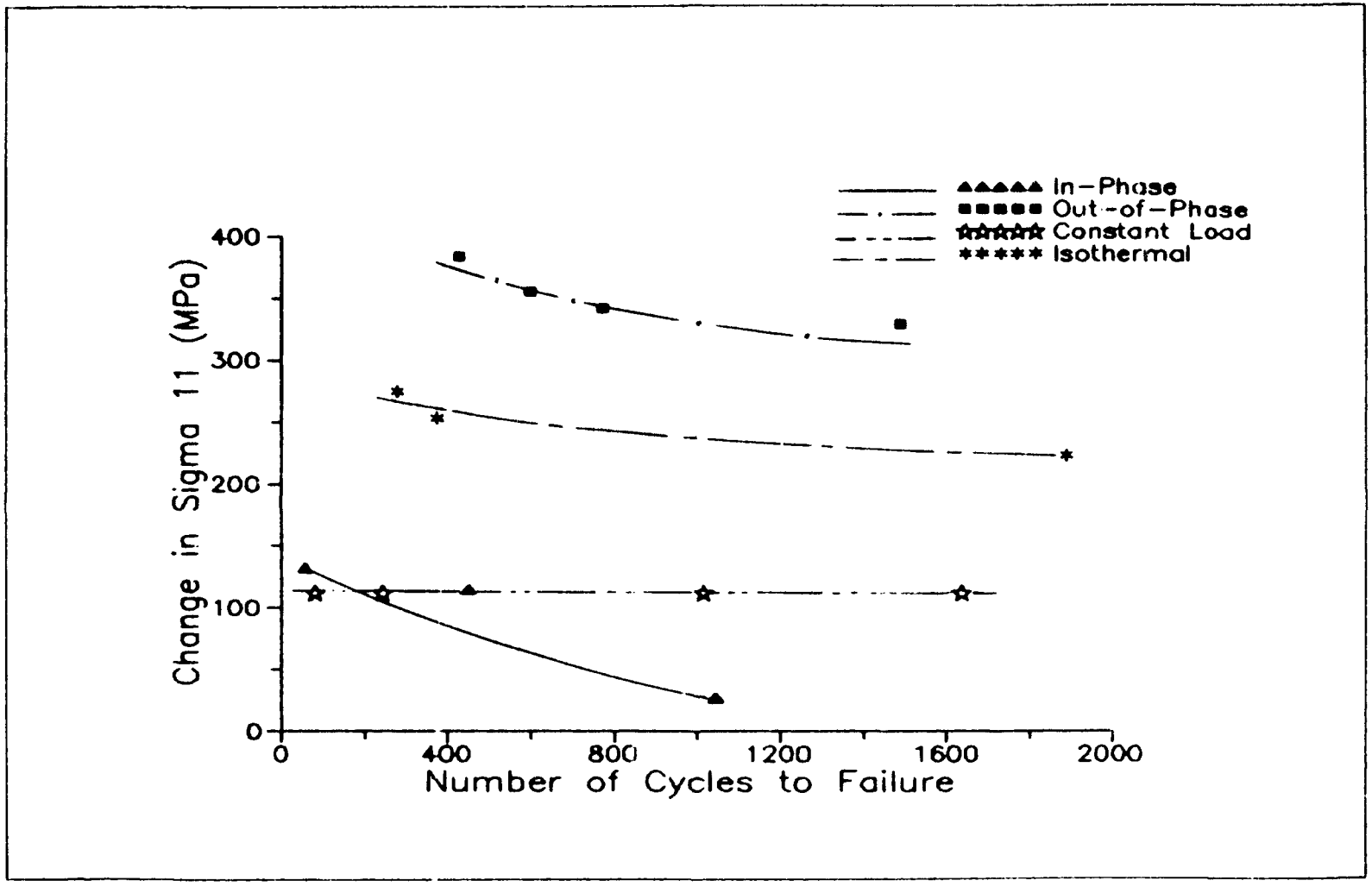

Figure 38A Change in Sigma 11 (in matrix) Versus Number of Cycles to Failure from Various Test Conditions

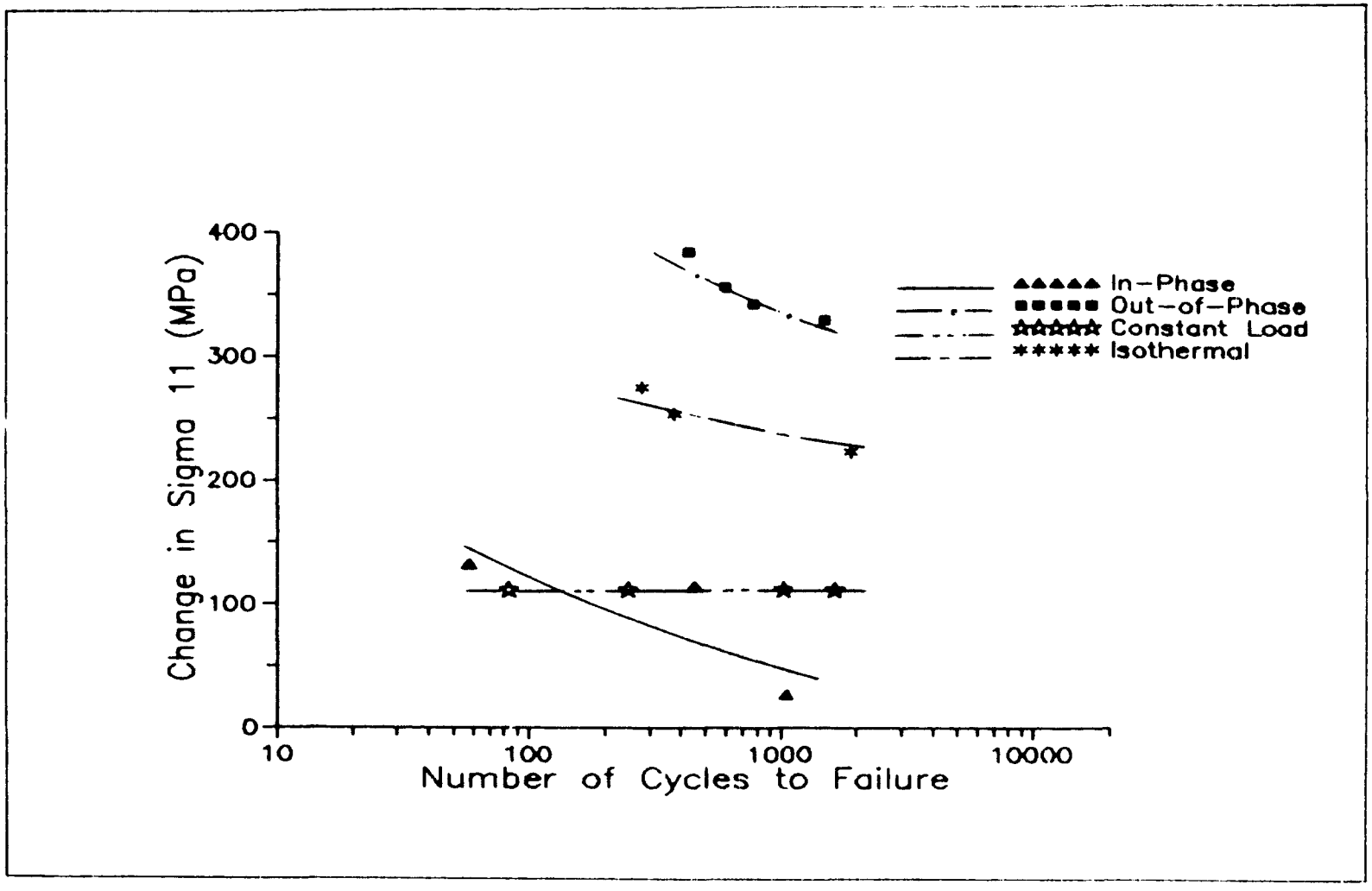

Figure 38B Change in Sigma 11 (in matrix) Versus Number of Cycles to Failure from Various Test Conditions

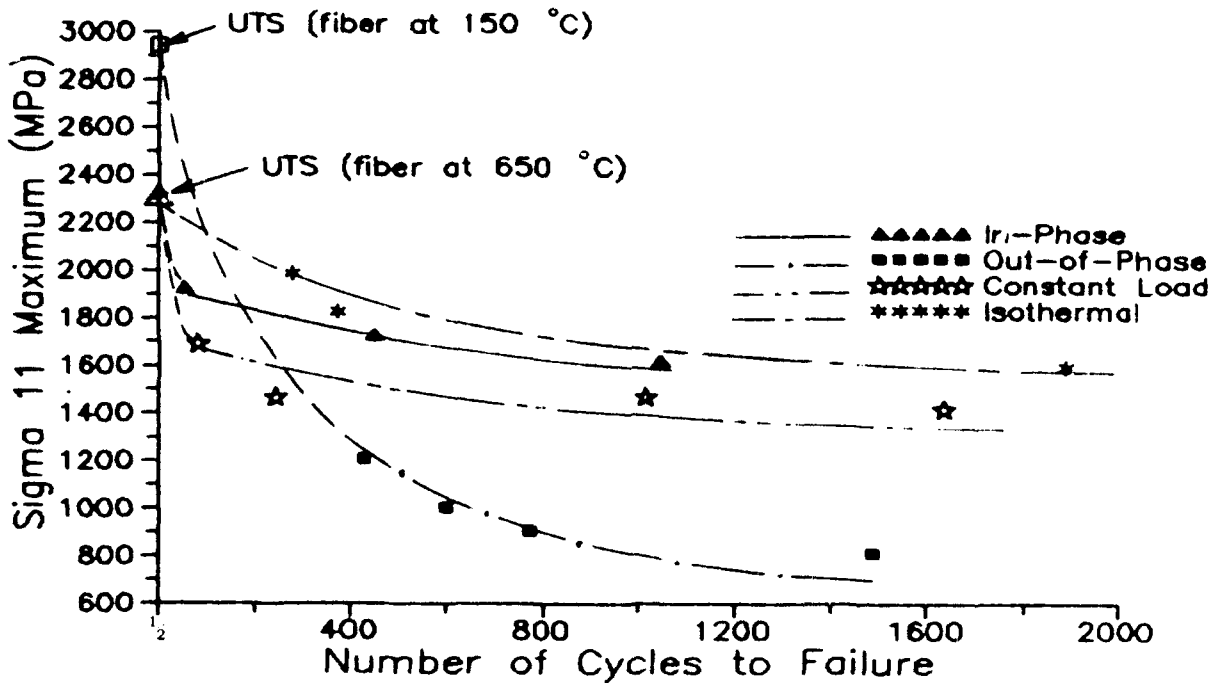

Figure 39A Sigma 11 Maximum (in fiber) Versus Number of Cycles to Failure from Various Test Conditions

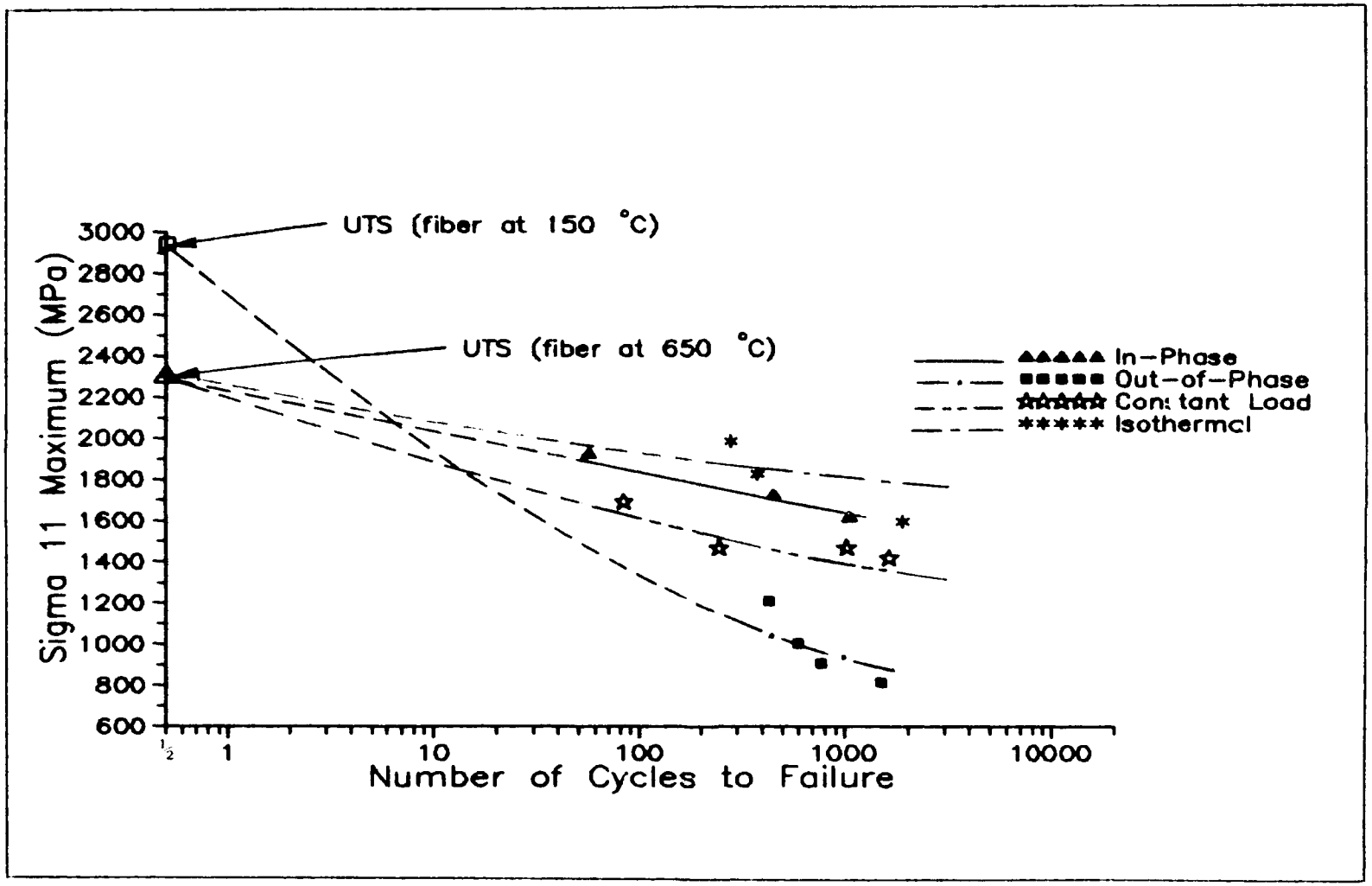

Figure 39B Sigma 11 Maximum (in fiber) Versus Number of Cycles to Failure from Various Test Conditions

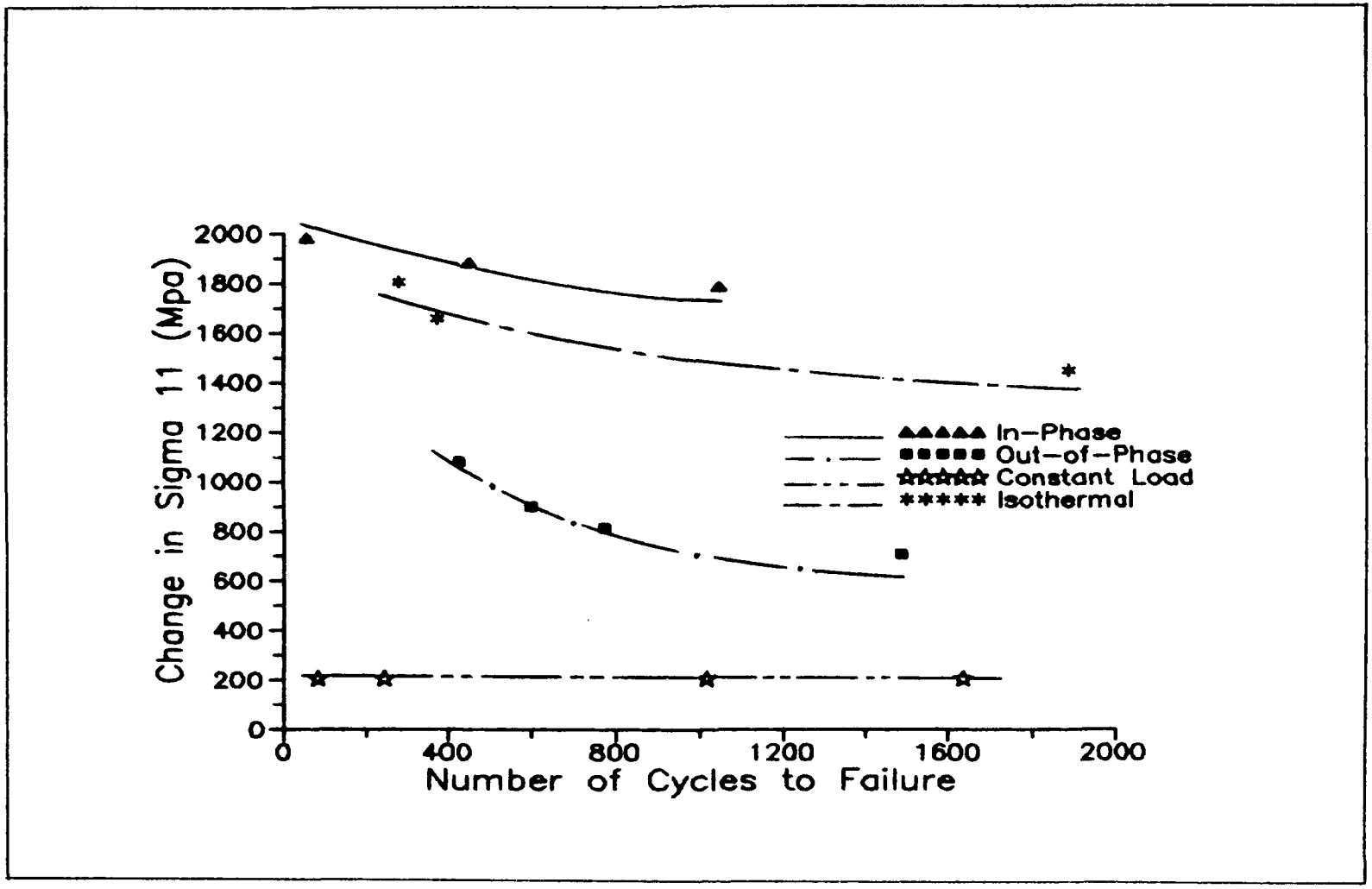

Figure 40A Change in Sigma 11 (in fiber) Versus Number of Cycles to Failure from Various Test Conditions

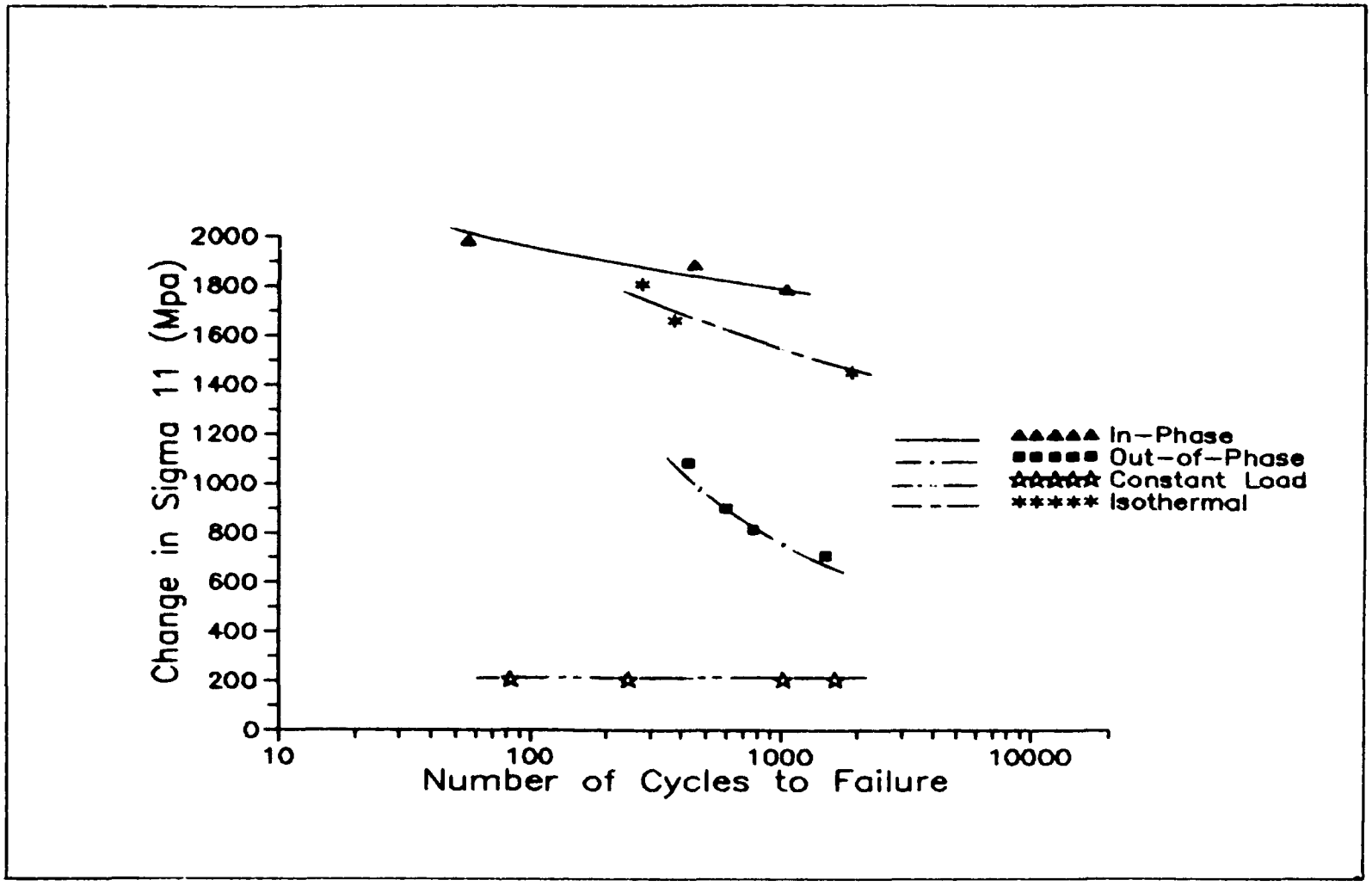

Figure 40B Change in Sigma 11 (in fiber) Versus Number of Cycles to Failure from Various Test Conditions

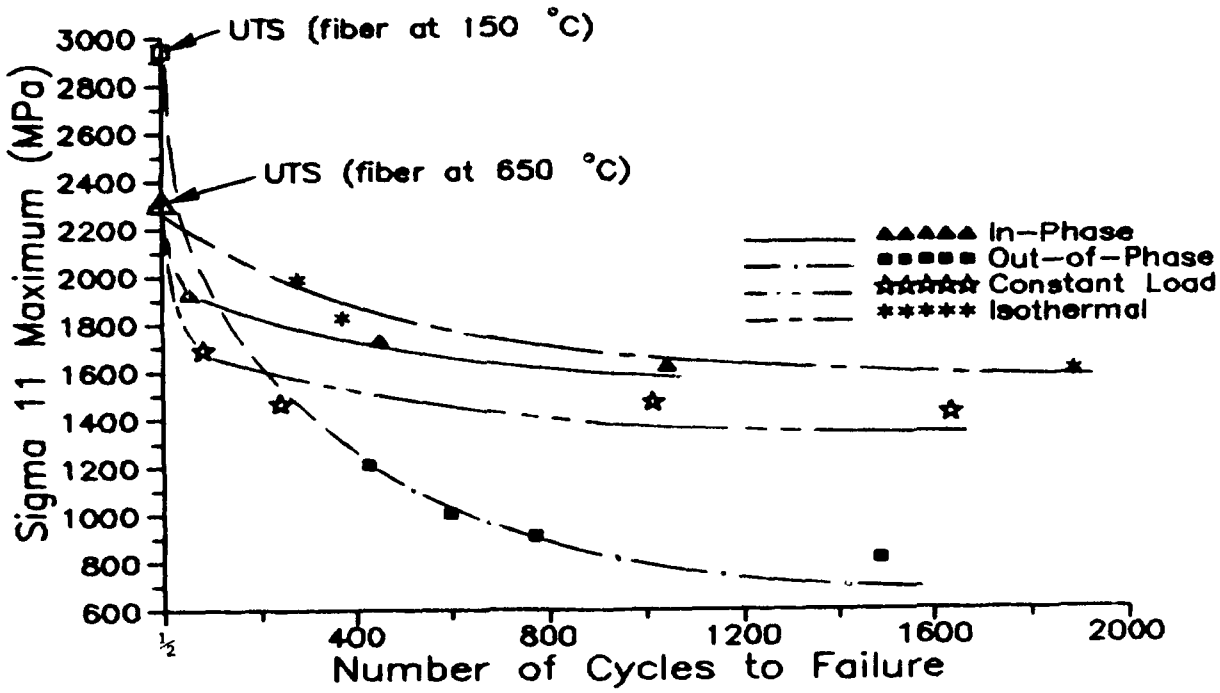

Figure 41A Possible Fiber Dominated Region for Various Test Conditions

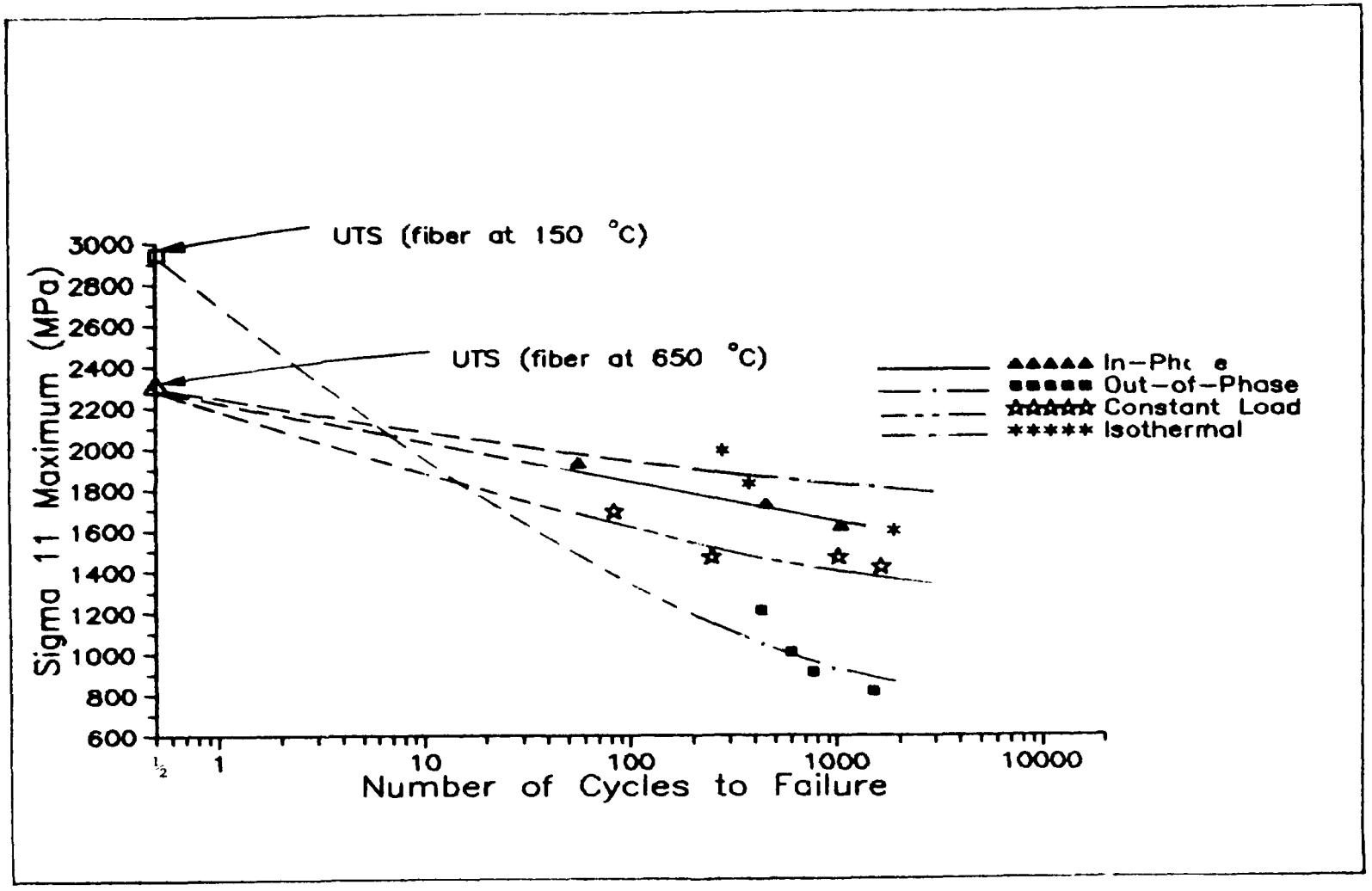

Figure 41B Possible Fiber Dominated Region for Various Test Conditions

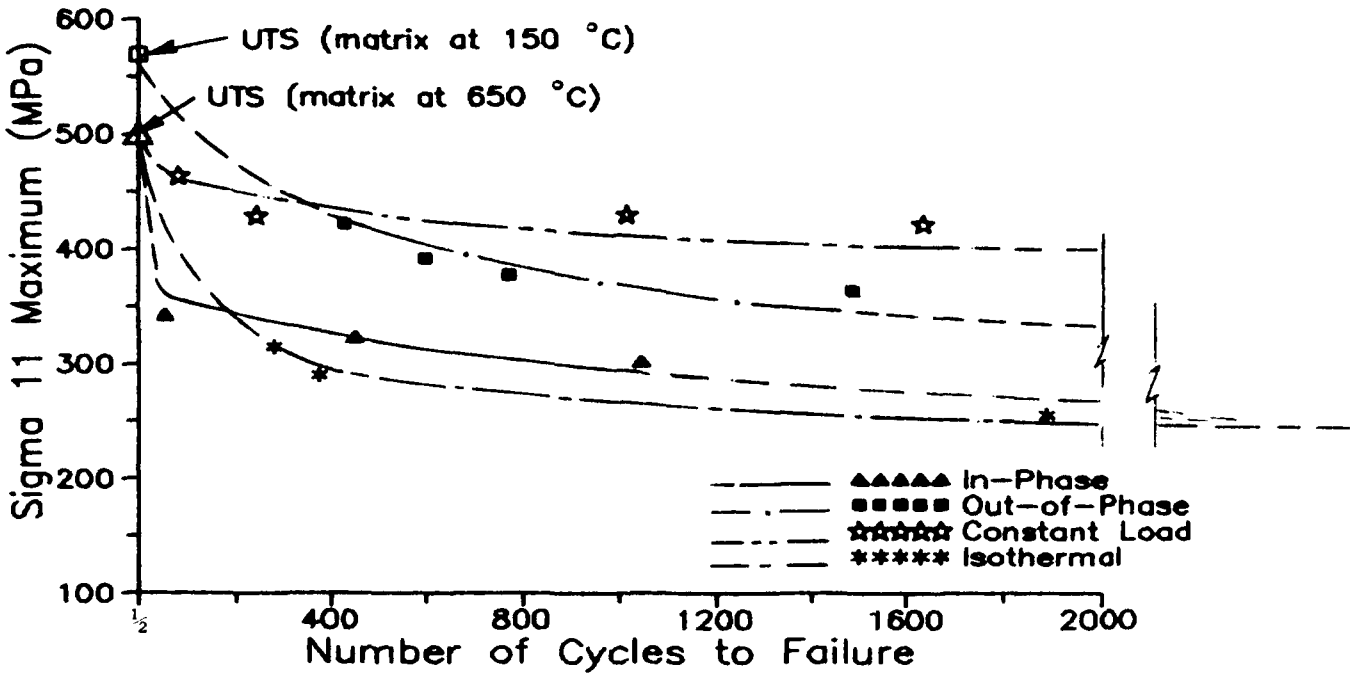

Figure 42A Possible Matrix Dominated Region for Various Test Conditions

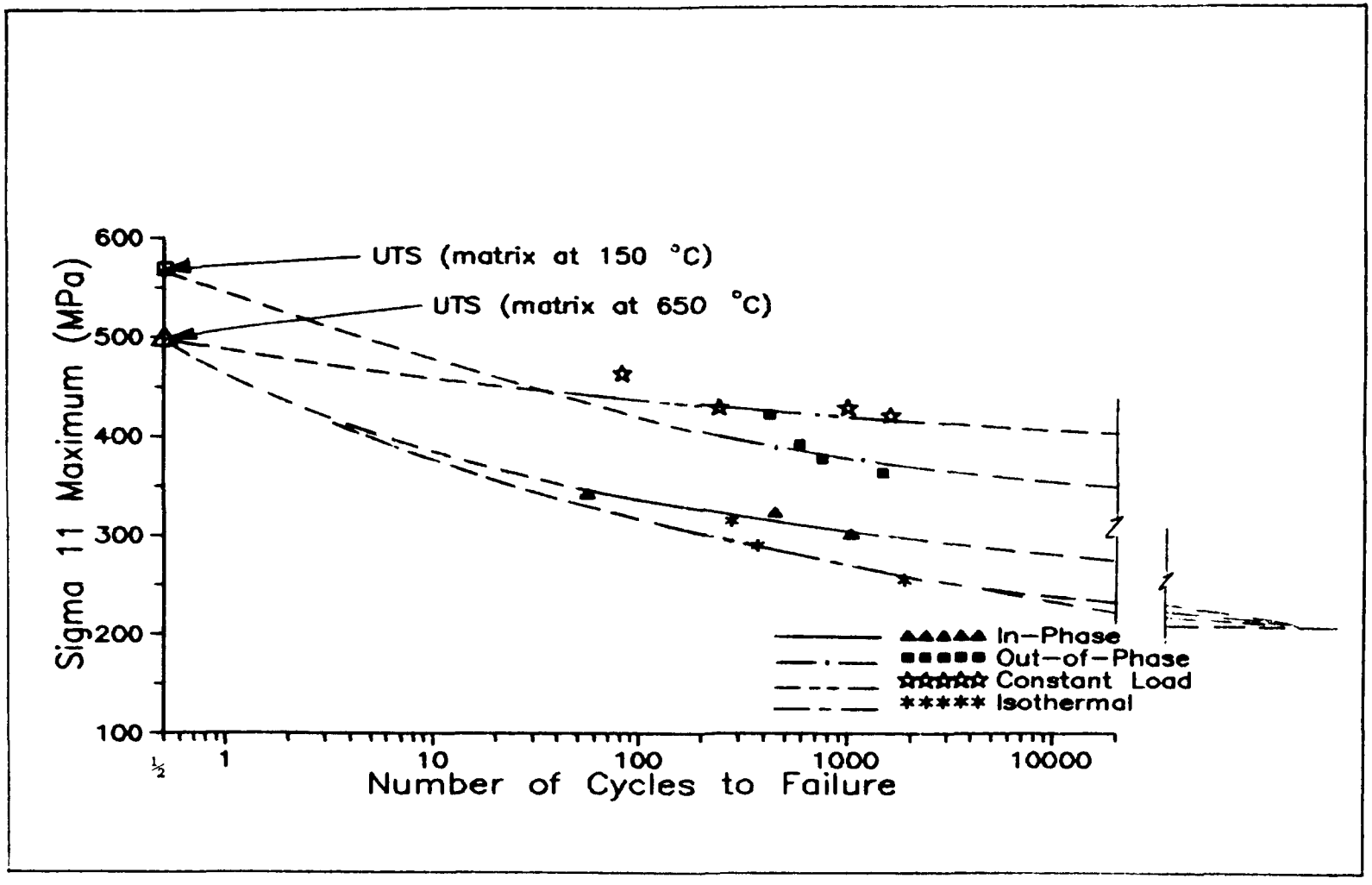

Figure 42B Possible Matrix Dominated Region for Various Test Conditions

IV. Conclusions and Recommendations

Conclusions:

The fatigue characteristics of SCS-6/Ti-24Al-11Nb subjected to in-phase and out-of-phase thermo-mechanical cycling were investigated. The fracture surfaces from both test conditions were studied using a scanning electron microscope and were compared. The fatigue damage was also investigated in regions located away from the fracture surface using a high power optical microscope and metallography. The stresses that occurred during the test cycles were analyzed and related to the observed fatigue damage. Additionally, the results from the in-phase and the out-of-phase testing were compared to test results from isothermal and constant load fatigue tests. Based upon analysis, the following conclusions are made.

1. Test specimens subjected to the out-of-phase test conditions failed sooner than their respective in-phase counterparts.

2. Scanning electron microscope fractographs revealed that there were no fatigue cracks on the in-phase test specimen fracture surfaces. This indicates that the in-phase test specimens were unable to support a crack.

3. Scanning electron microscope fractographs of the out-of-phase test specimen fracture surfaces revealed that damage initiated in the form of cracking in the matrix

perpendicular to the fibers at the fiber/matrix interface. These cracks initiated and progressed around the fiber in circular rings in the outer laminas. As damage progressed further these cracks coalesced to form a single macrocrack which surrounded a static tensile failure region located in the center of the test specimen's crossection.

4. Longitudinal and transverse sections taken from regions located in areas away from the fracture surfaces were observed under a high power optical microscope. These sections revealed that test specimens from both the in-phase and out-of-phase tests had the same fatigue damage in regions located away from the fracture surface. This damage consisted of broken fibers and cracks in the matrix perpendicular to the fiber located at the fiber/matrix interface.

5. The surfaces of test specimens from both in-phase and out-of-phase testing were oxidized due to the thermal cycle. The in-phase test specimens showed no additional surface damage and the out-of-phase specimens had surface cracks.

6. All of the test specimens failed without warning with the exception of one (Figure 21). The approach of the failure was indicated by changes in the secant modulus. This was probably due to the brittleness of the test material and the high mechanical test loads.

7. The average total strain increased slightly throughout in-phase testing due to creep.

8. The average total strain decreased early in out-of-phase testing and then stabilized for all tests with the exception of Figure 21. This decrease and stabilization may have been caused by work hardening of the matrix. In Figure 21 the average total strain increases throughout the test. This was due to crack initiation and progression in the interface reaction zone in the matrix.

9. Stress analysis indicates that during out-of-phase test conditions the longitudinal stress is high in the matrix and low in the fiber.

10. Stress analysis also indicates that during in-phase test conditions the longitudinal stress is low in the fiber and high in the matrix.

11. Stress analysis also indicates that neither the longitudinal stress in the matrix or in the fiber alone is governing the changes in fatigue life observed. It is, therefore, suggested that a complex interaction of the longitudinal stresses in both the fiber and matrix control the fatigue.

12. The results of the stress analysis from the in-phase and the out-of-phase test conditions were compared to the stress analysis from isothermal and constant load fatigue tests. Again, the comparison indicates that the

longitudinal stresses in both the fiber and the matrix govern the fatigue life in some unknown complex interaction.

Recommendations

The following suggestions are made for follow-on testing.

1. The fatigue life range (58-1634 cycles) in this investigation was narrow. Testing should be continued for much longer fatigue lives out to 10000 cycles.

2. Very short tests at high stress levels approaching zero cycles should be conducted in order to verify if a fiber dominated stress region exists. If it does exist, it would be at high stress levels and the longitudinal stresses in the fiber from the various test conditions should be on the same fatigue life curve.

3. Ideally, tests should be run to verify if no fatigue failures occur in the composite at stress levels below the endurance limit of the matrix. This would prove that damage is initiated in the matrix. This may be impractical because of the long cycle (six minutes) and the unknown large number of cycles that would be required.

Appendix A

Computer Program

METCAN2 (METal Matrix Composite ANalyzer), a computer code developed by the NASA Lewis Research Center, was used to analyze the stresses in the composite's fiber and matrix. This particular program has been described and compared to various other micromechanics models by Bigelow, Johnson, and Naik (2:21-31) and will be discussed here. According to Bigelow, et al, the program was developed primarily to do analysis of fiber-reinforced metal matrix composites for large structural applications. The standard output was formatted to interface with NASTRAN and the program uses a multi-cell model to predict mechanical properties, thermal properties, stresses, stress-strain relationships, failure modes, etc. (2:23-24).

The multi-cell model used in METCAN2 was designed to calculate laminate properties and stress-strain behavior in an average sense. For the purposes of this study a square unit cell divided into the two subregions (A and C) previously shown in Figure 22 on page 58 was used. The subregions were used to model the variations in stress throughout the individual laminas.

METCAN2 used micromechanics equations to calculate the ply mechanical properties, thermal properties, and the constituent stresses due to thermal and mechanical loading

in each of the regions previously shown in Figure 22. The micromechanics equations used in the model (2:23-24) are given below:

Ply longitudinal modulus:

$$E_{L11} = v_m E_{m11} + v_f E_{f11}$$

Ply longitudinal coefficient of thermal expansion:

$$\alpha_{L11} = v_m (E_{m11}/E_{L11}) \alpha_{m11} + v_f (E_{f11}/E_{L11}) \alpha_{f11}$$

Longitudinal fiber stress:

$$\sigma_{f11} = [\sigma_{L11}/E_{L11} + \Delta T(\alpha_{L11} - \alpha_{f11})] E_{f11}$$

Longitudinal matrix stress:

$$\sigma_{m11} = [\sigma_{L11}/E_{L11} + \Delta T(\alpha_{L11} - \alpha_{m11})] E_{m11}$$

where

E	is the modulus
v	denotes the volume fraction
α	is the coefficient of thermal expansion
ΔT	represents the temperature change

and the subscripts L, m, and f stand for the lamina, matrix, and fiber, respectively. The subscript 11 indicates the longitudinal direction.

The input data for METCAN2 was specified in different "card" groups of information. The various "card" groups contained information pertaining to the number of plies,

material, thickness, volume fraction, fiber orientation, loading, and program output reporting. METCAN2 used a resident data bank of constituent properties for the fiber and matrix which was modified to incorporate the material properties for SCS-6/Ti-24Al-11Nb. The reference properties were stored in the data bank and incorporated into the program by using the respective code names for the fiber and matrix on the appropriate data "cards". Loading was input into the program in tabular form representing discrete points on the loading profile.

Bibliography

1. Bartolotta, P. A., Castelli, M. G., and Ellis, J. R. "Thermomechanical Testing Techniques For High Temperature Composites: TMF Behavior Of SiC(SCS-6)/Ti-15-3," E-5543. National Aeronautics and Aerospace Administration, Lewis Research Center, Cleveland, Ohio.

2. Bigelow, C. A., Johnson, W. S., and Naik, R. A. "A Comparison Of Various Micromechanics Models For Metal Matrix Composites," The American Society of Mechanical Engineers Reprinted From Mechanics of Composite Materials and Structures, Book No. HOO464, 1989.

3. Broek, D., Elementary Engineering Fracture Mechanics (Fourth Revised Edition). Martinus Nijhoff Publishers, 1987.

4. Gabb, T. P., Gayda, J., and MacKay, R. A. "Isothermal And Nonisothermal Behavior Of A Metal Matrix Composite," Submitted to The Journal of Composite Materials.

5. Gambone, M. L. "Fatigue And Fracture Of Titanium Aluminides" EDR 14249. Allison Gas Turbine Division, General Motors Corporation, Indianapolis, Indiana, 1989.

6. Johnson, W. S., Lubowinski, S. J., and Highsmith, A. L. "Mechanical Characterization Of Unnotched SCS6/Ti-15-3 Metal Matrix Composites At Room Temperature," to appear in Thermal And Mechanical Behavior Of Ceramic And Metal Matrix Composites, ASTM STP 1080, Kennedy, Moeller, and Johnson, Ed., 1990.

7. Majumdar, B. S., and Newaz, G. M. "Thermo-mechanical Response And Damage In An Angle-Ply Metal Matrix Composite" submitted to The Journal of Engineering Materials and Technology - ASME, October, 1989.

8. Murthy, P. L. N., Hopkins D. A., Chamis C. C. "Metal Matrix Composite Micromechanics: In-Situ Behavior Influence on Composite Properties" NASA Technical Memorandum 102302. National Aeronautics and Space Administration, Lewis Research Center, Cleveland, Ohio.

9. Russ, S. M., Wright Research and Development Center/(WRDC/ MLLN), Wright Patterson Air Force Base, OH.